NTNU
Norwegian University of
Science and Technology

Weather-Optimal Positioning Control for Underactuated USVs

Øivind Kåre Kjerstad

Master of Science in Engineering Cybernetics
Submission date: June 2010
Supervisor: Thor Inge Fossen, ITK
Co-supervisor: Morten Breivik, CeSOS

Norwegian University of Science and Technology
Department of Engineering Cybernetics

Problem Description

Unmanned surface vehicles (USVs) are typically small, boat-like vehicles which are able to perform a large number of operations at sea. Some of these operations require the capability of dynamic positioning (DP), including the ability to keep station in some area of interest. In particular, DP functionality for USVs can be interesting for surveillance and reconnaissance purposes. For such applications, it is relevant to maximize operational time by minimizing fuel consumption, for instance by employing a weather-optimal DP scheme. In addition, most USVs do not have the possibility to independently actuate their lateral degree of freedom (DOF), which means that they are underactuated. The candidate will thus consider the problem of weather-optimal positioning control (WOPC) for underactuated USVs. Specifically, the thesis work will involve the following tasks:

1. Develop a 6 DOF dynamic model of the Viknes USV operated by Maritime Robotics and implement it in Matlab/Simulink.
2. Suggest suitable WOPC algorithms for the developed USV model.
3. Examine and illustrate the behavior of the suggested algorithms through numerical simulations in Matlab/Simulink.
4. Perform full-scale experiments with the actual Viknes USV in the Trondheimsfjord.
5. Evaluate the stability properties of the WOPC concept.
6. Suggest recommendations for future work regarding the proposed USV WOPC functionality.

Assignment given: 25. January 2010
Supervisor: Thor Inge Fossen, ITK

Preface

"Everything should be made as simple as possible, but not simpler."

- Albert Einstein

This thesis concludes my five years at the Norwegian University of Science and Technology. It has been an amazing journey where I have learned much more than I could have ever imagined, and it is with great satisfaction I now seek new adventures. Working with this thesis has been motivating, frustrating and very rewarding. Seeing the system functioning on a real vessel, doing what it was intended to do, made it all worth while.

I wish to express my gratitude to my supervisors and the others who made this work possible, my supervisors Morten Breivik for his superior help, advice and experience in writing such documents and Thor Inge Fossen for help with the hydrodynamic computations, Viknes Båt og Service AS for making the necessary vessel data available and the guys at Maritime Robotics, especially Arild Hepsø for assistance, and generously offering their Viknes 830 vessel for experimental uses. I would also thank my fellow students for a fun and enlightened work environment and my girlfriend for her patience. At last I would like to thank my father for helping me read through the thesis and correct errors.

I hope my work will be useful to others embarking on similar tasks and that someday the system might be implemented in a real world application.

Øivind Kåre Kjerstad
Trondheim, June 28, 2010

Summary

This thesis considers the design and development of a weather optimal positioning control system which is implemented on a developed 6 degrees of freedom vessel model of a Viknes 830 augmented with actuator and environmental models.

The intuitive pendulum principle provides a geometrical approach which gives a fuel-efficient weather optimal dynamic positioning controller. The convergence to the weather optimal heading is found to be related to the virtual pendulum length. Based on this a virtual anchoring function, and a positioning function was developed. Positioning control is achieved through moving the suspension point of the pendulum. Both functions subject to environmental disturbances were functionality tested using computer simulations and full scale experiments.

The Viknes 830, initially developed for combined pleasure and light fishing purposes was used in the tests. This vessel had lots of lacks, and was far from what can be characterized as an ideal design, both regarding heading stability and propulsion configuration. Despite this, the full scale test system implementation has proven that weather optimal and course independent positioning has the necessary versatility to sufficiently fit a wide range of crafts and purposes.

Contents

List of Figures

List of Tables

Chapter 1

Introduction

1.1 Motivation

Robotics and embedded systems are rapidly advancing and being developed for numerous tasks. In most cases such systems relieve humans of hard repetitive work but sometimes they are made to extend human capabilities to do tasks which humans are unsuited for. This might be high profile projects such as exploring Mars using small vehicles on the surface or simple tasks like persistent surveillance. Computers never get bored, tired or have opinions about their work. Humans would often be relieved to have machines do what they consider to be dirty, dull or dangerous assignments [Singer, 2009]. One branch of this development concerns unmanned surface vehicles (USVs), operating on or in the very near vicinity of the ocean surface. Today there are vast amounts of experimental vessels covering ground towards the vision of completely autonomous vessels capable of taking and executing simple high-level human orders in a safe and environmentally friendly manner. Intentionally these systems will aid and enhance marine operations in the near future. The most industrialized USVs are military, but there are development projects getting close such as the Mariner seen in Figure 1.1. There are many areas of application for such vessels but the first are envisioned among others to be seabed mapping, intelligence, surveillance and reconnaissance (ISR) missions and rescue operations. Today most advanced USVs still rely heavily on human input to operate safely but autonomisation is increasing.

The difference between an ordinary vessel and a USV is the USV's capability to autonomously collect data and perform an action without human intervention. To be able to do this the vessel needs a wide range of applications interconnected by a decision making system. If a new position is decided for, it must be able to collect information on the surroundings and maneuver there according to the rules applying at sea. If the operation requires the USV to hold its position, it should do so using minimal energy.

Globally, USV development programs are numerous where most vessels are designed as

Figure 1.1: The Mariner USV is a commercial USV system currently being developed. Courtesy of Maritime Robotics.

sensor platforms that can perform missions autonomously in a safe manner. For a more thorough discussion of USV development see [Bertram, 2008] which presents and discusses several interesting USV development projects.

This thesis considers the dynamic positioning (DP) system which keeps the vessel in a predetermined position. Environmental forces will always try to push the vessel away from its original position. The removal of this deviation tendency begins with detecting through the USV's sensor system and then calculation of thrust direction and magnitude. When it comes to endurance or operational range, ability to do so at minimal or very low energy has several advantageous economical and environmental aspects. By developing a system delivering station keeping capabilities through using the most common thruster configurations also opens the door to cheap leisure vessel applications.

1.2 Background

1.2.1 DP introduction

Holvik [1998] defines DP of a vessel as

"A means of holding a vessel in relatively fixed position with respect to the ocean floor, without using anchors accomplished by two or more propulsive devices controlled by inputs from sonic instruments on the sea bottom and on the vessel, by gyrocompass, by satellite navigation or by other means."

The dawn of DP started around 1953 when the first operations using a moored vessels were undertaken. A wide range of problems using tedious cumbersome anchor systems clearly demonstrated needs for more feasible alternatives. Further manual control proved very difficult which opened the door to electronic systems.

In the early days there were considerable difficulties in obtaining reliable and accurate real-time position measurements. Several solutions were proposed and for some time a combination of radar and taut-wire sufficed the purpose. The first generation of DP systems were relatively simple analogue installations which lacked means of redundancy [Bray, 2003]. When launched in 1961 Shell Oil Company's Eureka was a milestone in DP being the first vessel equipped with a heading and positioning controller. Throughout the 70s and 80s DP gained momentum in the industry and by 1985 150 vessels where equipped with DP capabilities [Bray, 2003]. Today thousands of vessels have different DP systems ranging from cruise vessels to highly specialized vessel in the oil industry. Today there are two distinctive different DP control methods available on the marked, PID control and model based schemes.

To achieve DP capabilities vessels needs to be fully actuated allowing for individual movement in surge, sway and yaw simultaneously. Thruster configurations in smaller vessels and USVs often limits these capabilities as system capacity only allows for movement in surge and sometimes yaw only. To avoid confusion when discussing actuation level on vessels and control systems, the following definitions are necessary.

Definition 1 *A fully actuated control scheme can be defined as control of n independent states with m inputs, where $m \geq n$. If this does not hold the scheme is regarded as underactuated.*

Definition 2 *An underactuated vessel can be defined as the lack of ability to independently control surge, sway and yaw simultaneously.*

Thus, an underactuated vessel can be positioned while using the heading as an additional control input. However, this solution does not represent an underactuated control problem since one of the DOFs is left uncontrolled. Nominally, the main purpose of DP is to keep vessels influenced by wave, wind and current loads in a specific position, at a given heading. Crucial components of a conventional DP system is featured in the block diagram in Figure 1.2 and each block will be discussed in the following.

Navigation system

The plant in any DP system is a vessel moving on the ocean surface. The ability to compensate for movements induced by environmental forces requires continuous measurements. Measurements concerning the vessel state and position are obtained through a wide range of sensor systems. The major systems for position measuremets are listed in Table 1.1. Most advanced vessels have GSP and INS systems installed as these are applicable without deployment of extra equipment world-wide.

Before the sensor data can be used in the control system it must be processed by a signal processing system, where erroneous signals from faulty sensors are handled in the appropriate way. For some signals as for instance velocities a reference frame transformation

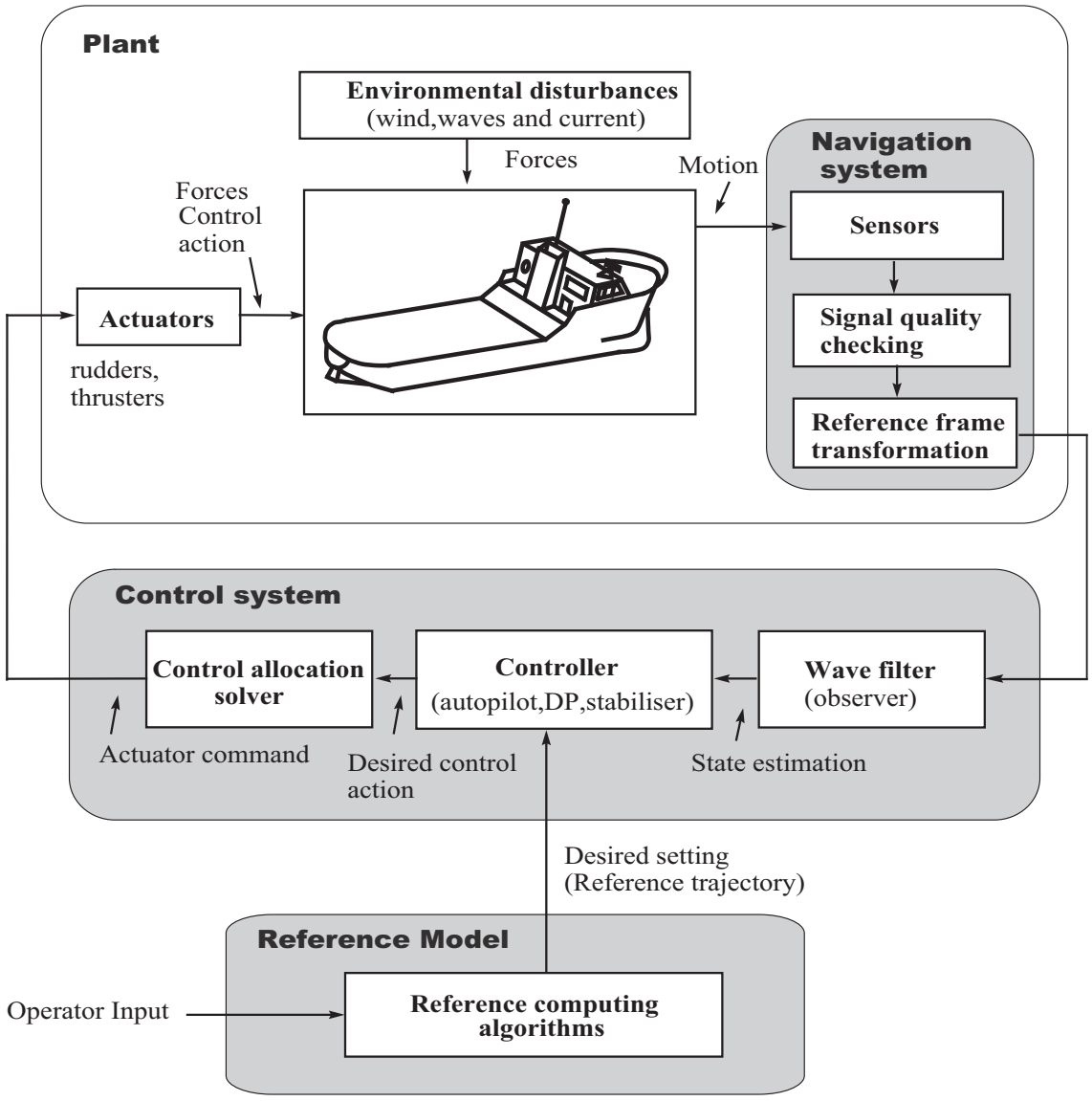

Figure 1.2: A block diagram representation of a conventional DP system. Adapted from Perez [2005].

GPS	The GPS system uses satellites to calculate the position. Fixed base stations calculate error measurements and broadcasted as differential corrections, hence GPS is extended to DGPS or Carrier DGPS (CDGPS) which further improves the measurements. GPS gives position measurements in the ECEF frame, discussed in Chapter 3 as either Cartesian coordinates or in latitude and longitude.
INS	Inertial navigation system (INS) measures the vessel movement in the body-frame using sensors described in Table 1.2.
Hydroacoustic positioning	Transmitters or transponders placed on the ocean floor sends or reflects signals which is used to calculate the position relative to the transponder.
Taut-wire	Using the angle measurement of a wire fixed to the ocean floor, the position can be calculated relative to a fixed position.
Other	Several other position reference systems based on Laser, Microwave and mechanical devices exists, all systems have advantages and disadvantages tied to accuracy, cost and reliability.

Table 1.1: Position reference systems.

Accelerometer	An accelerometer measures accelerations in one DOF.
Gyroscope	A gyroscope is a device for measuring angular velocities.

Table 1.2: ISA sensors.

is necessary as these become more intuitive seen from the vessel than from a north-fixed reference frame. For a more detailed discussion of different position measurement systems, and DP systems in general, see Bray [2003] and Holvik [1998].

Control system and reference model

The vessel observer is the first instance in the control system and it combines different sensor data to a noise filtered measurement vector consisting of vessel position, linear and angular velocities. The observer also provides estimation of states that are hard to measure, such as the linear velocities, it also offers dead-reckoning capabilities when a GPS dropout occurs. This means that the observer will continue to estimate the position and velocities even though the most important signal is removed. However, the signal the accuracy rapidly becomes poorer with time.

To avoid large steps in commanded thrust to the propulsion system, a position reference model delivers a smooth trajectory towards the position set point, hence deviation between the desired and actual position is kept small. This trajectory along with the vessel motion is fed into a controller calculating the body-frame thrust necessary to follow the trajectory. The thrust needed to follow the trajectory can be obtained through a variety of ways, from using simple PID controllers to advanced nonlinear optimization schemes. The thrust allocation calculates thruster set-points which is dependent on the configuration of the vessel actuators. A commercial DP system also offers a wide range of operational possibilities and features to improve feasibility and meet market trends. Some of these features are listed in Table 1.3. Other features can be selection of arbitrary rotation point and automatic or manual sea state selection for improved performance.

Selectable wind feed-forward	Wind speed and direction measured with anemometers can be added to the controller in a feed-forward term, which will improve the performance.
Gain adjustment	A DP system may have selectable low, medium and high gain in all operational modes. The gain refers to how hard the controller should try to maintain position and heading. Low gain gives lower system wear-and-tear, but reduced precision.
Operational mode option	A DP system may have manual, semi-auto and automatic operational modes, which defines the degree of computer control.

Table 1.3: Some commercial DP system features.

It is important to notice that the different control levels of a DP system have various bandwidth demands. Figure 1.3 displays the motion control hierarchy of typical marine surface vessels. On top is the strategic control level which is also is called the kinematic control level, issuing commands based on geometric aspects to achieve the control objective. The tactical level deals with the kinetics to generate the forces and moments necessary for the adequate vessel movement and further distribute the appropriate set-point to the thrusters making up the execution level which is responsible for making the movement ordered from the kinematic control level.

Simple DP systems may function as good as highly sophisticated ones when subject to low environmental loads. However subject to more harsh weather when the nonlinearities become more notable. As the coupling between the DOFs increase and thruster losses become important, then the difference in sophistication level will surface.

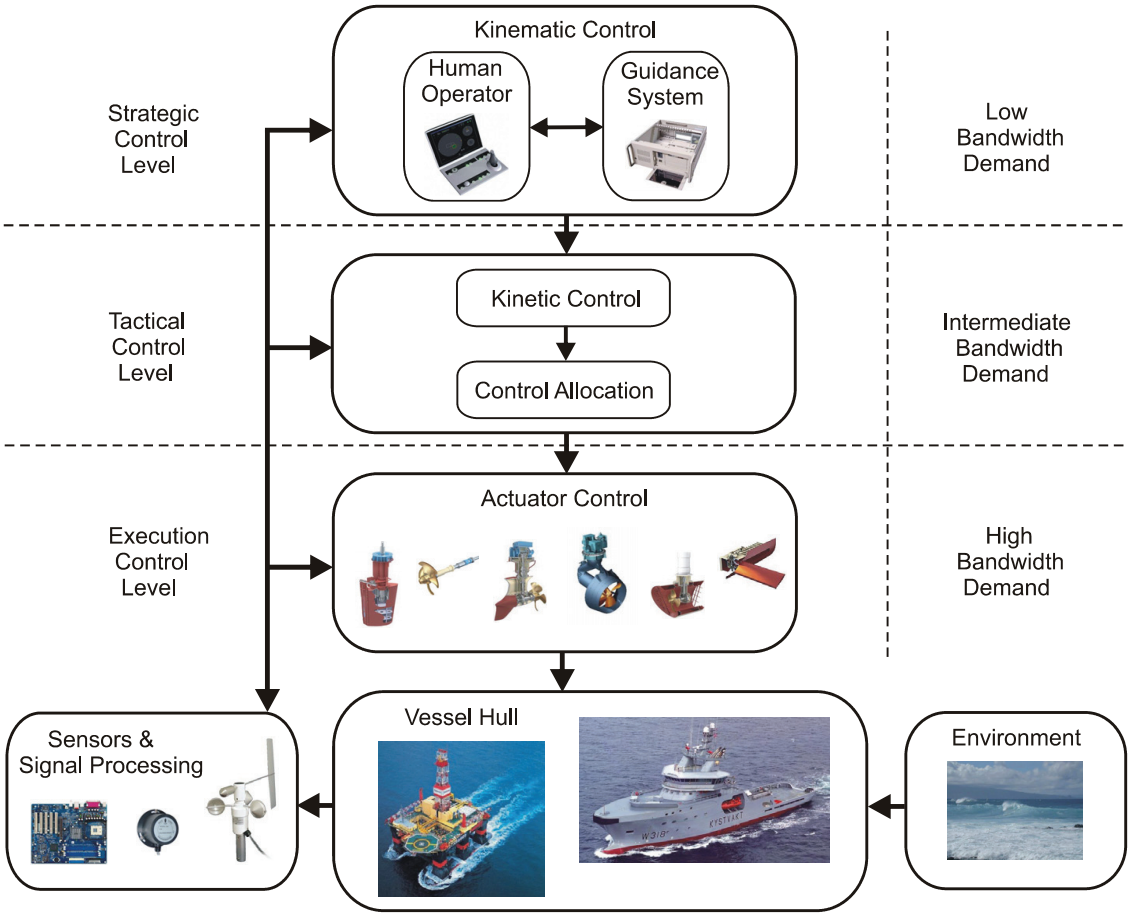

Figure 1.3: The motion control hierarchy of a marine surface vessel. Courtesy of Breivik et al. [2008].

1.2.2 Small vessel DP developments

Applying this technology on small vessels has not until recent years, been subject to few attempts. Reasons might be rooted in lack of industrial demand and position measurement inaccuracy in older systems and early GPS generations and the economical aspect of sufficient computational capacity. However as both risk assessment respective to health, safety and environment, navigational and computer issues have dramatically changed over the two last decades, time has seemingly matured especially for USVs which are now being considered for numerous tasks and applications. As technology has pushed the borders for small platform feasibility, DP systems will most certainly constitute crucial parts of both future USV concepts and operations. The last decade of research and development work on this subject also tends to underpin these allegations respective to both fully- and underactuated vessels. In Halvorsen [2008], a fully actuated DP system was successfully implemented and HIL tested, using a Linear-quadratic regulator (LQR) approach.

A handful of vendors offers to the market expensive high-end systems installed in luxury leisure vessels and super yachts. They operate by using at least two turnable pods much like azimuth thrusters fitted under the vessel. By having two or more independent turnable pods full DP functionality can be gained. These systems rely all on human operators entering set-points. Figure 1.4 features the Cummins MerCruiser Diesel [2010] Zeus system with two turnable pods suitable for DP operations. Both Volvo Penta [2010] and HamiltonJet [2010] also delivers a similar system based on slightly different actuator designs.

Figure 1.4: The Cummins MerCruiser Diesel Zeus double pod system. Courtesy of Cummins MerCruiser Diesel [2010].

Many development projects are considering underactuated DP on small USVs, and the major problem is controlling three DOFs by two independent inputs, which removes the possibility to move the vessel independently in surge, sway and yaw. Having no external environmental forces, gives the problem a resemblance to positioning a car. To move the

car sideways, surge force and yaw movement are required. Considerable environmental forces will always be present at sea.

A wide range of articles deal with control of underactuated small vessels, but few if any where the DP problem has been redefined to a fully actuated control problem:

- In Pettersen and Fossen [2000], a dynamic positioning scheme including a time-varying feedback control law with integral action was developed and proved to exponentially stabilize both the North and East positions and the orientation. Experimental results suggest that the vessel will obtain the desired position and heading, but struggles to maintain it due to the environmental disturbances.
- In Greytak and Hover [2007], a LQR in addition to a Manifold Convergence Controller (MCC) was implemented on a kayak using one azimuth thruster as propulsion. A hysteresis element to switch the MCC on and off based on the deviation from the desired position.
- In Matos and Cruz [2008], the ZARCO autonomous surface vehicle (ASV), a underactuated vessel, is provided with a feedback loop that stabilizes the vessel. The controller on-board the ZARCO relies on data provided by the navigation system, and does not rely on estimation of the environmental disturbances only.

1.3 Weather optimal positioning control

In a conventional dynamic positioning (DP) system surge, sway and yaw are controlled to a certain state, however this is not always optimal since another state could lead to better performance. In the context of weather optimal position control (WOPC) the lowest fuel consumption is the better performance whom is achieved through vessel positioning minimizing the environmental forces acting on the rigid ship.

Figure 1.5 illustrates the principle of WOPC which is to create a virtual pendulum where the vessel is the mass attached to the end. The pendulum system is influenced by a resultant force consisting of wind, wave and current forces which can be treated as a force field. By moving the virtual pendulum suspension point the vessel position may coincide with any desired position in the plane. The downside to WOPC is that heading control is lost due to using heading actively to turn up against the resultant environmental force. A simplification of WOPC is weather optimal heading control (WOHC) where the suspension point is fixed and the vessel will position itself somewhere on a circle surrounding it. Such a functionality is also known as virtual anchoring. WOHC and WOPC was first treated by Fossen and Strand [2001]. In Chapter 4 control laws for both WOHC and WOPC are derived.

An alternative approach which also obtains weather optimal positioning is described in Pinkster and Nienhuis [1986] where a large fully actuated tanker is controlled by leaving

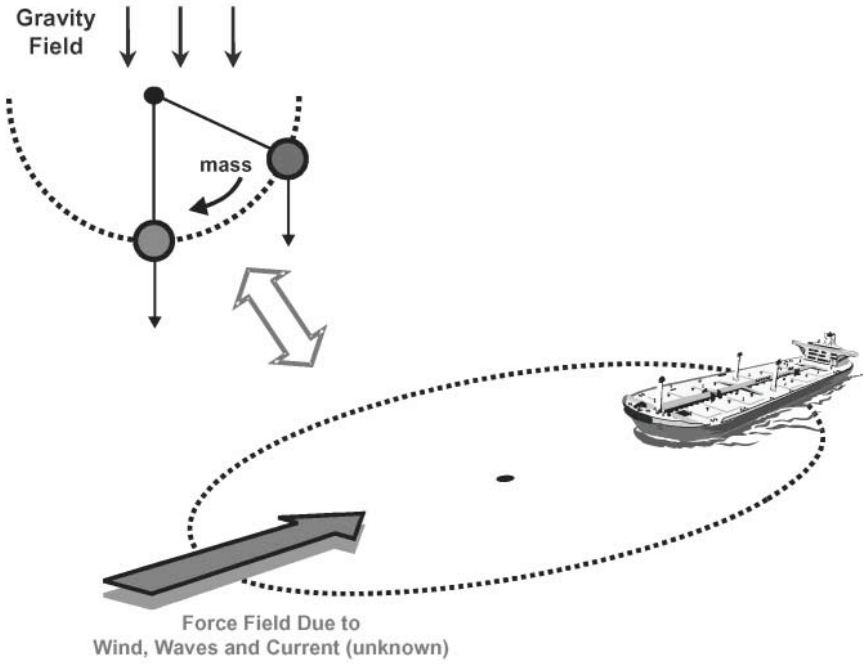

Figure 1.5: Illustration of a vessel suspended in a virtual pendulum influenced by the weather. Courtesy of Fossen and Strand [2001].

the heading open loop and surge and sway are used to correct the position deviation. The resultant environmental force turns the vessel like a weather vane minimizing the projected area enabling for better fuel consumption.

1.4 Small vessel aspects

When considering DP on small vessels several aspects separate these from their conventional counterparts, all details which require special attention. Small vessels as USVs will due to lower inertia , and their relative size difference compared to the waves, behave differently on the ocean surface. Negligible weather conditions to larger vessels have potential to induce violent motions in all DOFs to smaller USVs. On larger vessels these motions will be damped by the size and inertia of the vessel and the remains treated as noise and removed by filtering. On a small vessel the high frequency wave contribution cannot be treated as noise and the position deviation imposed by such forces must be counteracted using the actuators. Heavy sea states might impose acceleration and motion problems and Figure 1.6 features some issues concerning small vessels in big waves. However, as long as the hull and on-board systems are intact, a USV should be able to operate in almost any wave condition. Correcting huge and rapid disturbances calls for high-precision responsive actuators, subsequently increasing vessel costs, wear-and-tear in addition to increased

Figure 1.6: Small vessels in surf conditions may get problems. Courtesy of Mike Baird.

fuel consumption. Reducing the environmental forces by using intelligent systems to increase the operational space of small vessels such as USVs will be important. Improved performance and an increased in the operational space could be obtained through a wave management system determining the optimal angle through the waves. The SPARTAN USV has such a wave management system implemented, this is described in Doucy and Ghozlan [2008].

Several highly sophisticated DP systems are commercially available, however all intended for vessels much larger than small USVs. Classification society rules require high redundancy, subsequently leading to increased size and complexity. A large part of these systems are highly sophisticated user interfaces and advanced joystick solutions. A typical configuration is seen in Figure 1.7, which is the Rolls-Royce Marine DP chair from their Icon DP system. The chair is based on ergonomic principles to be a good human machine interface (HMI), with focus on keeping the important controls to run the DP operation is within arms reach.

High precision redundant commercial DP systems is often seen in the oil industry. Kongsberg Maritime and Rolls-Royce Marine are two of many vendors developing and delivering DP systems for larger vessels. DP systems are also used for other purposes, such as virtual anchor. This particular feature is often seen on new cruise ships, often used to avoid damage on the coral reefs. Similarly this functionality is emerging on some high end leisure boats.

Another difference between fully actuated offshore supply vessels (OSV) equipped with DP systems and small USV-like like vessels are the number of actuators. Small vessel limitations as space, weight and economical issues remove the possibility for independent movement in surge, sway and yaw. To avoid extra actuators it might be necessary to redefine the DP problem to disregard the heading and just keep the position. By doing this, two

Figure 1.7: Rolls-Royce Marine DP chair with touch screen. Courtesy of Rolls-Royce Marine.

independent states are controlled with two independent inputs, thus the control problem is fully actuated. This simplification is introduced due to the fact that an underactuated control scheme is very hard, if not impossible, to solve for a vessel subject to environmental forces on the ocean surface. Redefining the DP problem this way, will give the vessel some DP functionality, using a conventional underactuated surge and yaw propulsion system. This DP format will be beneficial to USVs whose main goal is not heading defined station keeping, or where the vessel heading is not crucial. A scheme utilizing the optimal heading towards the environment forces will be highly beneficial, both in terms of fuel consumption and system lifetime issues.

1.5 Scope

The scope of this thesis is to develop a WOPC scheme for the Viknes USV owned by Maritime Robotics and perform system verifying sea trial tests. This work implies development of a 6 DOF simulator model with actuators and environmental disturbances, used to verify and enhance the control design. After a simulation study the system will be implemented on-board the Viknes and full scale verification experiments will be carried out in the Trondheimsfjord. Using Lyapunov theory, a derived mathematical proof of the DP control concept will also be presented.

- Chapter 2 introduces the Viknes 830 USV vessel owned by Maritime Robotics and

sums up its characteristics and equipment.

- Chapter 3 explains fundamental concepts which are important to the derivation of the WOPC system and the mathematics of the different components used to build the simulator.
- Chapter 4 derives and describes the control design based on the pendulum principle and presents a mathematical proof of the stability of this.
- Chapter 5 explains the thrust allocation system which converts the controller forces to actual thruster set-points and discusses difficulties tied to the Viknes vessel.
- Chapter 6 presents and discusses the simulator and a study of the vessel behavior using both WOHC and WOPC under influence of the environment.
- Chapter 7 presents and discusses the actual Viknes implementation and displays the full scale results.
- Chapter 8 concludes the thesis and presents possible future work on the subject.

1.6 Abbreviations

ASV - Autonomous Surface Vehicle
CDGPS - Carrier Differential Global Positioning System
CG - Center of Gravity
DGPS - Differential Global Positioning System
DOF - Degree Of Freedom
DP - Dynamic Positioning
ECEF - Earth Centered Earth Fixed
ECI - Earth Centered Inertial
FPP - Fixed Pitch Propeller
GPS - Global Positioning System
HMI - Human Machine Interface
IMU - Inertial Measurement Unit
ISR - Intelligence, Surveillance and Reconnaissance
LQR - Linear Quadratic Regulator
MCC - Manifold Convergence Controller
MPC - Model Predictive Control
NED - North-East-Down
OSV - Offshore Supply Vessel
USV - Unmanned Surface Vehicle
WOHC - Weather-Optimal Heading Control
WOPC - Weather-Optimal Positioning Control

Chapter 2

Viknes 830

Figure 2.1: The Viknes 830 at cruising speed. Courtesy of Viknes.

Figure 2.1 features the Viknes 830 which is a semi-planing fibreglass hull, built for a variety of employment and tasks in Nordic conditions. It is manufactured by Viknes Båt og Service AS in Kleppestø, Norway under the slogan "Built for the North Sea". The prime mover is an inboard engine shafted to a conventional fixed pitch propeller, while a traditional rudder in combination with a electrical tunnel thruster are the means of manoeuvring. The vessel considered in this thesis is owned by Maritime Robotics, a small Trondheim based company, and is additionally equipped with an on-board computer (OBC) and an extended sensor package. This enables the vessel to operate as a versatile USV application development platform, and accommodates room for the developer to participate in full scale experiments inside the vessel. The spacious wheelhouse offers an adequate overview of the surroundings, and aids deeper understanding and enhanced feeling of the application under development. Even though modified to operate as a USV nothing except the possibility for computer control separates it from an ordinary multi-purpose vessel.

2.1 Hull

According to available information in [Viknes, 2010] the vessel displacement is approximately 3.300 kg with standard equipment and fully bunkered. Due to equipment installed by Maritime Robotics, a slight weight increase is assumed. Compared to similar vessels without keel the Viknes keeled hull has better directional stability and increased roll damping. Figure 2.2 displays the Viknes longitudinal dimensions. The vessel has a relatively large area above the water-line compared to the area below which makes the vessel highly susceptible to influence of wind forces, subsequently causing drift.

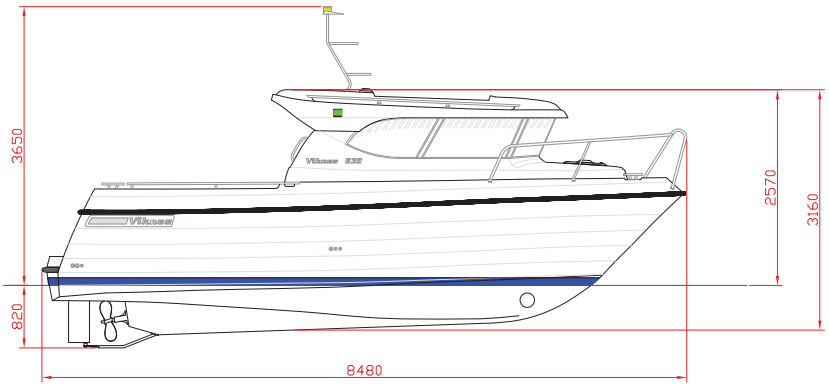

Figure 2.2: The Viknes 830 lateral dimensions. Courtesy of Viknes.

2.2 Actuators

2.2.1 Engine and gear

The 135.6 kW Yanmar 4LHA-DTP diesel engine is connected to a 1:2.03 ratio gear equipped with trolling capability. The trolling function, which normally is available at low RPM only enables the propeller shaft to rotate with a controlled slip relative to the fixed gear ratio. In principle this is achieved by utilizing the "link" created by viscosity of oil between two physically separated rotating discs. In trolling mode the propeller rpm is controlled by adjusting the gap between the two discs.

2.2.2 Propeller

A Sleipner S-8 skew-back propeller is fitted to the propeller shaft. Skew-back propellers have asymmetrical propeller blade contours which are swept backwards, (viewed from fore

to aft). This is a usual property for medium to high speed propellers and is said to create less vibrations, higher top speed and reduced fuel consumption. The propeller is displayed in Figure 2.3. The propeller blade area is 74% of the disc area.

Figure 2.3: The Viknes 830 S8 Skew-back propeller. Courtesy of Sleipner.

2.2.3 Rudder

As seen in Figure 2.2 a conventional balanced rudder is installed directly behind the propeller. With an area of 0,15 m^2 it provides for good manoeuvring capabilities even at low speeds. The rudder is controlled by a servo enabling a maximum rudder angle of $\pm 27°$.

2.2.4 Tunnel thruster

The Viknes's electrical bow tunnel thruster is delivered by Sleipner AS, and is featured in Figure 2.4. From [Sleipner Motor AS Product Specifications SP 55 Si] it is found to be a fixed transverse directional on-off thruster producing approximately 670 N of thrust when enabled. It is designed to operate continuously for maximum 2 minutes and 40 seconds in each sequence. During long time usage the thruster should not be left running for more than 8% of time. The thruster location relative to the hull is viewed in Figure 2.2 where the thruster is mounted in the tunnel pipe seen just below the waterline at the bow.

2.3 Custom equipment and interface

The Viknes has a custom extended equipment package enabling it to become a USV development platform. At the center of the system the OBC inputs position, yaw angle, velocity and yaw-rate from a Furuno SC-50 3-antenna GPS compass and outputs commands through a digital to analog converter to the electromechanical devices electronically manipulating throttle, rudder and tunnel thruster. The OBC runs an industrial control platform on top of a Linux operating system. In order to manipulate the output UDP data

Figure 2.4: The Viknes 830 SP 55 Si tunnel thruster arrangement. Cortesy of Sleipner.

packages containing set-points are sent to the OBC from another computer running the control system. For easy development a laptop is usually used, but completed functioning systems should be implemented on the OBC. The underlying control system offers several modes of operation. In this thesis the interface considered consists of a $\pm 0 - 100\%$ throttle wire setting, a -15 to 15 degree rudder setting and a -1, 0 or +1 tunnel thruster setting, where thrust direction is determined by the sign +/-. A Matlab/Simulink environment is used to read and send commands to and from the vessel. The system receives vessel data sent by the OBC via UDP packages and returns commands to the vessel in the same way. The WOPC system implementation is further discussed in Chapter 6.

2.4 DP considerations

Being a multi-purpose vessel, built for Nordic conditions, and due to both design and thruster configuration, the Viknes is not optimized for DP operation performance. The vessel profile above the water line is proportionally bigger than its opposite below the water line, causing vulnerability to drift due to wind influence. In low velocity operations such as DP, the rudder will not create sufficient yaw moment, subsequently this leads to requirements for use of the electrical tunnel thruster, imposing further technical challenges. The wheelhouse location in front of the center of gravity will strive to rotate the stern towards the wind. This is an instability in a weather optimal control scheme, which must be compensated either by active or passive measures. Active compensation could be use of the tunnel thruster, whilst passive compensation is achieved by changing the point of attack of the wind forces, for instance through adding a canopy or spanker sail. Both passive options are seen in Figure 2.5 and will enable the vessel to become stable whilst

headed into the wind.

Figure 2.5: Viknes 1030 with canopy and spanker sail. Courtesy of Viknes.

To design and implement a robust WOPC scheme into the Maritime Robotics Viknes, several practical issues have to be addressed. The first problem to overcome is the highly nonlinear throttle response in close to zero velocities, probably caused by a dead-band around zero throttle, and trolling gear dynamics. Any low velocity application will operate in the trolling gear load zone, mainly around $\pm 30\%$ throttle. Another issue is the electrical on-off tunnel thruster, which has limitations regarding operational sequence lengths, and further rapidly drains battery power, ultimately resulting in degraded performance. Additionally, before changing thrust direction, the tunnel thruster must be turned completely off for a short period of time.

Considering conventional DP on the Maritime Robotics Viknes is out of the question, due to the fact that the vessel is not fully actuated. On the other hand, a WOPC scheme, requiring only surge and yaw capabilities, could be implemented.

Chapter 3

Modeling fundamentals

3.1 Reference frames

ECI frame

The Earth-centered inertial (ECI) frame is an inertial frame where Newton's laws of motion apply. The origin is located at the center of the Earth but does not follow the planet's rotation. As the Earth orbits the Sun accelerations occur, thus the frame is not truly inertial, however the error introduced by neglecting these is for most applications assumed to be negligible.

ECEF frame

The Earth centered Earth fixed (ECEF) frame is located at the Earth center and synchronically rotates along with it. When placing the NED frame it is intuitively convenient to relate it to this frame, rather than the more abstract ECI frame.

North-East-Down frame

In Fossen [2002] the North-East-Down (NED) coordinate system is defined as $\{\mathrm{n}\}=(x_n, y_n, z_n)$ with origin o_n, and normally defined as the tangent plane on the surface of the Earth, fixed to the vessel movements. This coordinate system where N points towards true north, E points east, and D points, down normal to the Earth's surface is what commonly referred to in daily life. DP operations have approximately constant longitude and latitude, hence using the NED frame for navigation is appropriate and this is often referred to as flat-Earth navigation. The NED frame is assumed to be inertial, thus Newton's laws are applicable. The ECI, ECEF and NED frames are illustrated in Figure 3.1.

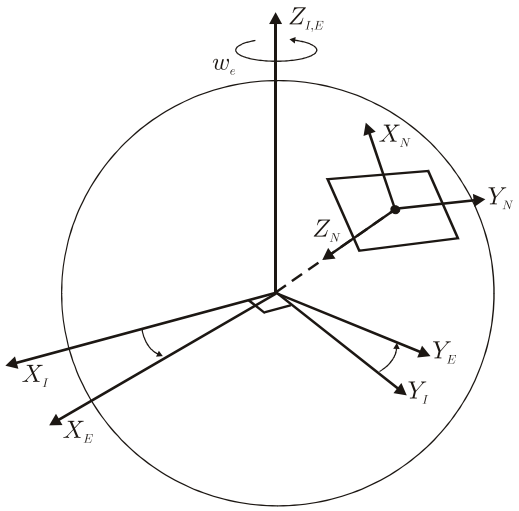

Figure 3.1: Illustration of the ECI, ECEF and NED reference frames. Courtesy of Breivik [2003].

Body frame

The body-fixed reference frame {b}=(x_b, y_b, z_b) with origin o_b is a moving vessel fixed coordinate frame, see Figure 3.2. The origin is usually chosen to coincide with a point amidships in the water line. The body axes, often chosen to coincide with the principal axes of inertia is usually defined as shown in Table 3.1.

x_b	Longitudinal axis (directed from aft to fore)
y_b	Transversal axis (directed to starboard)
z_b	Normal axis (directed from top to bottom)

Table 3.1: Definition of body axes.

The body frame is used to relate the vessel position and orientation to an inertial frame. The linear and angular vessel velocities are expressed in the body frame, which also is the most intuitive. For more thorough description of reference frames, and their mathematical relations, see Fossen [2002].

3.2 Response amplitude operators

When developing a DP control system it is important to understand the vessel kinetics describing how forces act on the vessel and the motions these produce. In Perez et al. [2004]

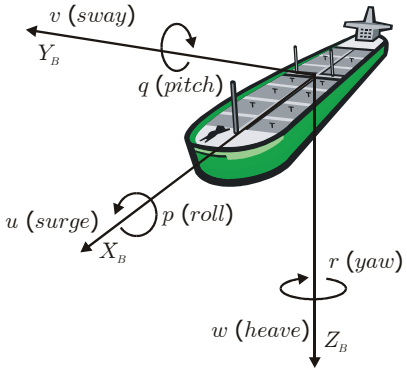

Figure 3.2: DOF illustration on oil tanker in body-fixed frame. Courtesy of Breivik [2003].

it is stated that force or motion superposition is commonly used in development of mathematical vessel models. The forces/motion acting on the vessel is often divided into three classes consisting of: first-order wave-induced forces/motion, slowly-varying disturbance force/motion and control-induced force/motion. For determination of wave force/motion influencing the vessel, response amplitude operators (RAO) are often used. These are transfer functions mapping the wave elevation or wave slope into force/motion.

Perez [2005] states that motion superposition as seen in Figure 3.3 is the most commonly adopted model for control system design. This model outputs the total motion as a sum of independent motion contributions. Sea keeping theory is the study of surface vessel motion in waves and manoeuvring is the study of vessel movement in calm water. Motion superposition has two shortcomings, the first is that it might not be used for multi-body system interaction, and secondly that the manoeuvring part does not incorporate fluid memory effects associated with the wave-frequency induced motion. Fluid memory is explained in [Fossen, 2002] to be the dependencies between dissipative forces and past velocities in addition to the velocity at time t. The shortcomings might result in miss-modelled dynamics related to changes in added mass and damping which is dependent on wave excitation frequency. By using the force superposition alternative the fluid memory effects associated with the wave-frequency is incorporated using a time-domain representation. Figure 3.4 displays this approach which has proven to produce high-accuracy vessel models. Environmental and control forces that act on the vessel is calculated before it is filtered by the vessel to produce the resulting motion. This is a more realistic approach which gives a model that might be used for slow maneuvering.

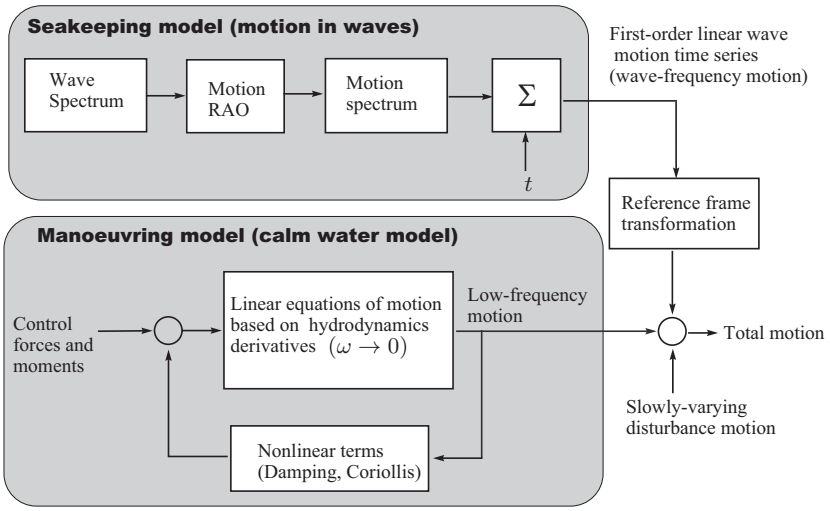

Figure 3.3: Motion response amplitude operator principle illustration. Courtesy of Perez [2005].

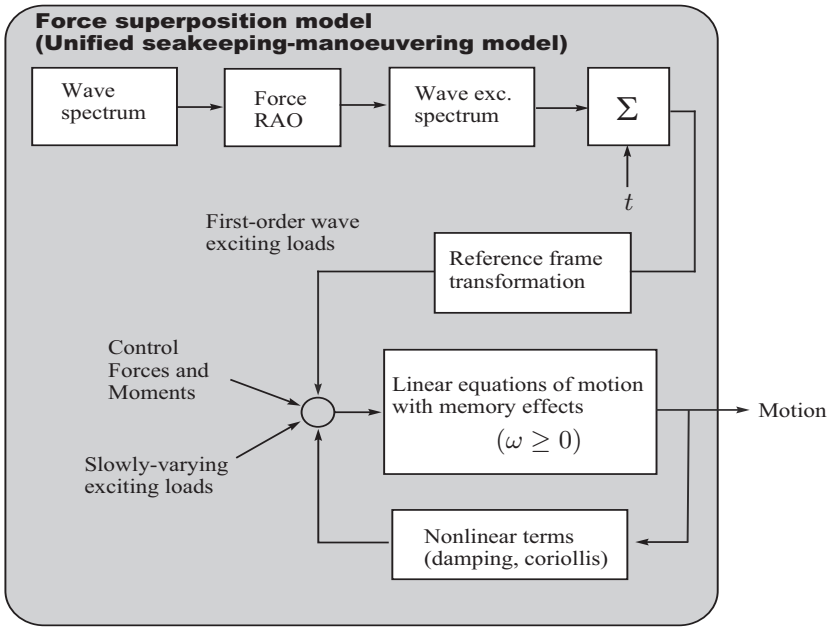

Figure 3.4: Force response amplitude operator principle. Courtesy of Perez [2005].

3.3 Mathematical modeling

When developing control systems interacting with real world dynamics, it is helpful and potentially cost reducing to use mathematical models which are approximated descriptions of the physical phenomena. This enables simulations of various and unlikely scenarios, where system performance can be tested to the extreme. This methodology opens for development of more advanced and better systems with proven performance in complex and challenging operational scenarios.

Sophisticated mathematical models also allow for development leaps, (compared, but not contradictive to normal generic developments) in creating more detailed, fine-tuned and robust control systems. To simplify the system migration into the physical vessel (in this thesis), a full 6 DOF mathematical model of the Viknes 830 vessel is derived and augmented with actuator dynamics and actual real world interface.

The data received from the hydrodynamical software ShipX is used in the unified 6 DOF seakeeping and maneuvering model derived by

$$\dot{\boldsymbol{\eta}} = \mathbf{J}(\boldsymbol{\eta})\boldsymbol{\nu} \tag{3.1}$$

$$\mathbf{M}\dot{\boldsymbol{\nu}} + \mathbf{C_{RB}}(\boldsymbol{\nu})\boldsymbol{\nu} + \mathbf{C_A}(\boldsymbol{\nu}_r)\boldsymbol{\nu}_r + \mathbf{D}(\boldsymbol{\nu}_r)\boldsymbol{\nu}_r + \boldsymbol{\mu} + \mathbf{G}\boldsymbol{\eta} = \boldsymbol{\tau}_{waves} + \boldsymbol{\tau}_{wind} + \boldsymbol{\tau} \tag{3.2}$$

3.3.1 Vectors η and ν

The vectors $\boldsymbol{\eta}$ and $\boldsymbol{\nu}$ describe the vessel position, orientation and velocity in the NED and body frames.

$$\boldsymbol{\eta} = [x, y, z, \phi, \theta, \psi]^\top \tag{3.3}$$

$$\boldsymbol{\nu} = [u, v, w, p, q, r]^\top \tag{3.4}$$

Where Table 3.2 shows the relation between the two vectors. $\boldsymbol{\eta}$ is given in the NED reference frame and $\boldsymbol{\nu}$ is given in the body frame.

DOF		Forces and moments	Linear and angular velocities	Positions and Euler angles
1	Motion in the x-direction (surge)	X	u	x
2	Motion in the y-direction (sway)	Y	v	y
3	Motion in the z-direction (heave)	Z	w	z
4	Rotation about the x-axis (roll,heel)	K	p	ϕ
5	Rotation about the y-axis (pitch,trim)	M	q	θ
6	Rotation about the z-axis (yaw)	N	r	ψ

Table 3.2: The notation of SNAME (1950) for marine vessels.

3.3.2 Inertia

The mass matrix consist of two separate terms

$$\mathbf{M} = \mathbf{M}_{RB} + \mathbf{M}_A \tag{3.5}$$

where $\mathbf{M}_{RB}$ is the contribution of the rigid physical structure of the vessel and $\mathbf{M}_A$ is the contribution from the hydrodynamically added mass which can be seen as a virtual mass added to the system due to an acceleration or deacceleration of the vessel which imposes an acceleration or deacceleration of some of the surrounding fluid. The fluid movement adds virtual mass to the vessel. The rigid body matrix $\mathbf{M}_{RB}$ is composed as

$$\mathbf{M}_{RB} = \begin{bmatrix} m\mathbf{I}_{3\times 3} & -m\mathbf{S}(\mathbf{r}_g^b) \\ m\mathbf{S}(\mathbf{r}_g^b) & \mathbf{I}_b \end{bmatrix} \tag{3.6}$$

$$= \begin{bmatrix} m & 0 & 0 & 0 & mz_g & -my_g \\ 0 & m & 0 & -mz_g & 0 & mx_g \\ 0 & 0 & m & my_g & -mx_g & 0 \\ 0 & -mz_g & my_g & I_x & -I_{xy} & -I_{xz} \\ mz_g & 0 & -mx_g & -I_{yx} & I_y & -I_{yz} \\ -my_g & mx_g & 0 & -I_{zx} & -I_{zy} & I_z \end{bmatrix} \tag{3.7}$$

where m is the vessel mass and $\mathbf{S}(\mathbf{r}_g^b)$ is a skew symmetric matrix of the distance vector between the buoyancy center of the vessel and its center of gravity. $\mathbf{I}_b$ is the inertia matrix about the vessel' center of buoyancy.

In general, the hydrodynamically added mass matrix $\mathbf{A}(\omega)$ depends on the frequency of motion due to water surface effects, but as stated in Fossen [2002] the added mass can be approximated to a constant frequency independent matrix based on the assumption that the surge motion is decoupled and that the vessel is port-starboard symmetric. This gives a hydrodynamically added mass matrix $\mathbf{M}_A$ the following form

$$\mathbf{M}_A = -\begin{bmatrix} X_{\dot{u}} & 0 & 0 & 0 & 0 & 0 \\ 0 & Y_{\dot{v}} & 0 & Y_{\dot{p}} & 0 & Y_{\dot{r}} \\ 0 & 0 & Z_{\dot{w}} & 0 & Z_{\dot{q}} & 0 \\ 0 & K_{\dot{v}} & 0 & K_{\dot{p}} & 0 & K_{\dot{r}} \\ 0 & 0 & M_{\dot{w}} & 0 & K_{\dot{q}} & 0 \\ 0 & N_{\dot{v}} & 0 & N_{\dot{p}} & 0 & K_{\dot{r}} \end{bmatrix} \tag{3.8}$$

3.3.3 Coriolis and centripetal forces

The Coriolis-centripetal matrix contains nonlinear terms due to Coriolis and centripetal effects, which appears due to the dynamics are stated in the non-inertial body frame.

Coriolis and centripetal forces are work-less forces in the sense that they neither introduce nor dissipate energy. The Coriolis and centripetal terms are as follows

$$\mathbf{C}(\boldsymbol{\nu}, \boldsymbol{\nu_r}) = \mathbf{C_{RB}}(\boldsymbol{\nu})\boldsymbol{\nu} + \mathbf{C_A}(\boldsymbol{\nu_r})\boldsymbol{\nu_r}. \tag{3.9}$$

$\mathbf{C_{RB}}(\boldsymbol{\nu})$ relates to the contribution generated by the rigid body and $\mathbf{C_A}(\boldsymbol{\nu_r})$ to the added mass. In Fossen [2002] it is stated that both terms can be linearized around the forward velocity of the vessel $\boldsymbol{\nu_0} = [U \;\; 0 \;\; 0 \;\; 0 \;\; 0 \;\; 0]^\top$, which is stated to become

$$\mathbf{C}^*_{RB} = U\mathbf{M}_{RB}\mathbf{L} \tag{3.10}$$

$$\mathbf{C}^*_{A} = U\mathbf{M}_{A}\mathbf{L}, \tag{3.11}$$

where U is the relative water speed. The selection matrix $\mathbf{L}$ used to select the appropriate columns in either $\mathbf{M}_{RB}$ or $\mathbf{M}_A$ is defined as

$$\mathbf{L} = \begin{bmatrix} 0 & 0 & 0 & 0 & 0 & 0 \\ 0 & 0 & 0 & 0 & 0 & 1 \\ 0 & 0 & 0 & 0 & -1 & 0 \\ 0 & 0 & 0 & 0 & 0 & 0 \\ 0 & 0 & 0 & 0 & 0 & 0 \\ 0 & 0 & 0 & 0 & 0 & 0 \end{bmatrix}. \tag{3.12}$$

3.3.4 Damping forces

Hydrodynamical damping affects all marine vessels which displaces water and is mainly caused by potential damping, skin friction, wave drift damping, lifting forces and damping due to vortex shedding. The damping term of equation (3.2) is $\mathbf{D}(\boldsymbol{\nu}_r)\boldsymbol{\nu}_r$. This dissipative force is usually modeled as

$$\mathbf{D}(\boldsymbol{\nu}_r) = \mathbf{D}_L + \mathbf{D}(\boldsymbol{\nu}_r) \tag{3.13}$$

where $\boldsymbol{\nu}_r$ is the velocity relative to the water. This means that the vessel might have velocity over ground without being affected by damping forces. Free drift is such a scenario. Due to symmetry around the xz-plane it is possible to assume decoupled surge dynamics which gives the linear matrix as

$$\mathbf{D}_L = -\begin{bmatrix} X_u & 0 & 0 & 0 & 0 & 0 \\ 0 & Y_v & 0 & Y_p & 0 & Y_r \\ 0 & 0 & Z_w & 0 & Z_q & 0 \\ 0 & K_v & 0 & K_p & 0 & K_r \\ 0 & 0 & M_w & 0 & M_q & 0 \\ 0 & N_v & 0 & N_p & 0 & N_r \end{bmatrix}. \tag{3.14}$$

This is the linear contribution to the dissipative force and is the dominating force at low velocities. The nonlinear contribution $\mathbf{D}(\boldsymbol{\nu}_r)$ is treated as two independent phenomenas nonlinear surge damping and cross-flow drag.

Nonlinear surge damping

The nonlinear surge damping is the prevailing surge damping when the velocity reaches a certain level. In [Fossen, 2002] the surge damping coefficient is modeled as

$$C_X = \frac{S}{A_x} C_f, \tag{3.15}$$

where S is the wetted surface of the hull, A_x is the frontal projected area and C_f is the friction modelled as

$$C_f(u_r) = \frac{0.075}{(log_{10} R_n - 2)^2} + \Delta C_f, \tag{3.16}$$

where ΔC_f represents additional friction due to hull roughness, wave resistance etc. The surge damping then becomes

$$X = X_{|u|u} \left| u_r \right| u_r \tag{3.17}$$

where

$$X_{|u|u} = \frac{1}{2} \rho A_x C_X \tag{3.18}$$

The nonlinear term is intuitively a quadratic damping force but this model is only applicable as long as the vessel does not lift itself out of the water due to increasing velocity. When that happens the equations are no longer valid.

Cross flow drag

To compute the nonlinear damping effects in Y and N the cross-flow drag principle seen in [Faltinsen, 1993] is applied. The nonlinear sway and yaw terms then become

$$Y = -\frac{1}{2} \rho \int_{\frac{-L_{pp}}{2}}^{\frac{L_{pp}}{2}} T(x) C_d^{2D}(x) \left| v_r + xr \right| (v_r + xr) \, dx \tag{3.19}$$

$$N = -\frac{1}{2} \rho \int_{\frac{-L_{pp}}{2}}^{\frac{L_{pp}}{2}} T(x) C_d^{2D}(x) x \left| v_r + xr \right| (v_r + xr) \, dx \tag{3.20}$$

where C_d^{2D} is the 2D-drag coefficient found in Hoerner's curve using the beam and length of the vessel. $T(x)$ is the vessel draft and v_r is the relative sway velocity.

3.3.5 Restoring forces

Restoring forces are usually referred to as metacentric stability for surface vessels. It can be regarded as a spring in a mass-damper-spring system trying to push the vessel to its equilibrium points in heave, roll and pitch. The stabilizing effect is created by the restoring forces gravity and buoyancy which affect the vessel differently. Figure 3.5

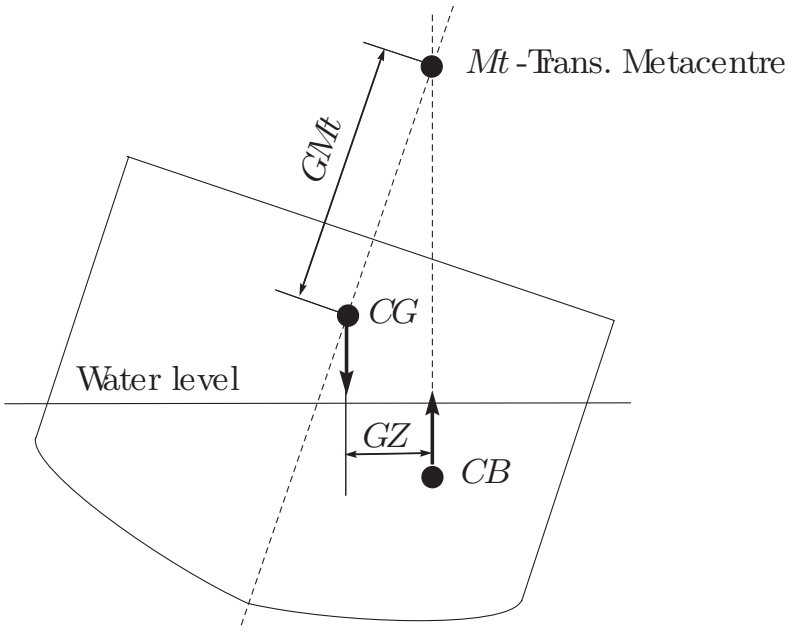

Figure 3.5: Restoring forces acting on a rolling vessel. Courtesy of Perez [2005].

displays a illustrating scenario which explains the concept. When a vessel rolls the center of buoyancy (CB) moves due to the changed distribution of volume beneath the surface whereas the center of gravity (CG) is always fixed in the same point. This creates a transverse righting arm (GZ) which in this case tries to restore the roll equilibrium.

The GMt length is the transversal metacentric height which is an important measure of stability. Large GMt gives a stiff spring which is highly stabilizing but it will be uncomfortable for passengers. A similar value applies for the longitudinal case and the principle is the same for restoring the pitch equilibrium.

The restoring term $\mathbf{G}\boldsymbol{\eta}$ seen in (3.2) is a linear approximation of the restoring forces which is convenient for surface vessels. Due to asymmetry about the yz-plane [Fossen, 2002] states that $\mathbf{G}$ is defined as

$$\mathbf{G} = \begin{bmatrix} 0 & 0 & 0 & 0 & 0 & 0 \\ 0 & 0 & 0 & 0 & 0 & 0 \\ 0 & 0 & -Z_z & 0 & -Z_\theta & 0 \\ 0 & 0 & 0 & -K_\phi & 0 & 0 \\ 0 & 0 & -M_z & 0 & -M_\phi & 0 \\ 0 & 0 & 0 & 0 & 0 & 0 \end{bmatrix} > 0. \tag{3.21}$$

3.3.6 Fluid memory effects

Due to the motion of the vessel, waves are generated which in turn will affect the vessel and this is known as the fluid memory effect. The fluid memory effect is a phenomenon affecting the linear dissipative forces in the system. The term $\boldsymbol{\mu}$ in (3.2) has the following dynamics

$$\dot{\mathbf{x}} = \mathbf{A}_\mathbf{r}\mathbf{x} + \mathbf{B}_\mathbf{r}\delta\boldsymbol{\nu} \tag{3.22}$$

$$\boldsymbol{\mu} = \mathbf{C}_\mathbf{r}\mathbf{x}. \tag{3.23}$$

This model behaves as a low-pass filtered damper when the vessel changes the momentum of the fluid which will affect the forces in the future. This means that the radiation forces depend on the history of the velocity of the vessel.

3.3.7 Driving forces

The vectors $\boldsymbol{\tau}$, $\boldsymbol{\tau}_{wind}$ and $\boldsymbol{\tau}_{waves}$ are driving forces of the system. $\boldsymbol{\tau}_{wind}$ and $\boldsymbol{\tau}_{waves}$ are environmental forces while $\boldsymbol{\tau}$ are the control forces allocated by the vessel itself.

3.3.8 Actuator models

Main propulsion

The vessel main propulsion consists of a diesel engine with a trolling gear connected to the propeller via a shaft. As mentioned in Chapter 2 the interface to the main propulsion is a $\pm$ 100 % throttle value. It is assumed that each throttle step corresponds to a given rpm which enables the simplification of regarding the engine as a low pass filter of the desired throttle value. The engine model then becomes

$$\dot{\omega} = k_\omega \left(-\omega + \omega_d(\vartheta)\right). \tag{3.24}$$

where ω is the actual rpm and $\omega_d(\vartheta)$ is the desired rpm which is a function of the throttle input to the interface ϑ. The function $\omega_d(\vartheta)$ incorporates the trolling gear functionality. This model is not highly accurate due to several reasons. On the real vessel the engine cannot achieve rpms lower than a certain threshold since the engine would stop. The trolling gear enables propeller shaft rpm lower than the crankshaft of the vessel but it is assumed to have different dynamics. From physical investigation of the vessel it is assumed that even though different dynamics apply to different rpm regions the whole system can be regarded as a low pass filter of the desired input. The propeller shaft rpm is geared down compared to the crankshaft with a given gear ratio

$$\omega_p = k_{gr}\omega, \tag{3.25}$$

where ω_p is the propeller shaft rpm and k_{gr} is the gear ratio. In [Fossen, 2002] it is stated that the propeller thrust might be modeled as

$$X_p = T_{n|n|} n\,|n| - T_{|n|u_a}\,|n|\,u_a, \tag{3.26}$$

where

$$T_{n|n|} = \rho D^4 \alpha_2 \tag{3.27}$$
$$T_{|n|u_a} = \rho D^3 \alpha_1 \tag{3.28}$$
$$u_a = (1-w)u \tag{3.29}$$

In (3.27)-(3.29) the parameters are defined as, α_1 and α_2 are constants, D is the propeller diameter, ρ is the density of water and w is the wake friction number generated by the movement of the water along with the vessel. Since ω_p is defined as propeller shaft rpm it needs to be converted to $\left[\frac{1}{s}\right]$ by

$$n = \frac{\omega}{60}. \tag{3.30}$$

This is a general propeller model that might not account for all of the characteristics of the vessel propeller due to having a somewhat different design than an ordinary propeller. It is possible to assume that the propeller would generate a pitch angle, but since this is a low speed maneuvering model, the pitch contribution would be minimal and is therefore omitted. The vessel would also have a small heading rate due to the rotation of the propeller shaft but this effect is also disregarded.

Rudder

The rudder system consists of a rudder servo, some mechanics and the rudder itself. The rudder servo is connected to the OBC which inputs the desired angle defined through the interface. The rudder servo system is regarded as a low pass filtering of the desired angle δ_d

$$\dot{\delta} = k_\delta \left(-\delta + \delta_d\right), \tag{3.31}$$

where δ is the actual rudder angle and k_δ is a adjustment of the system time constant to fit the real world system. The rudder generates forces in 4 DOFs where the parameters are dependent on the size and shape of the rudder. These are

$$X_r = \frac{1}{2} v_r^2 \rho A \left(\frac{(\frac{\delta C_L}{\delta \alpha_e}\delta)^2}{0.9\pi a_r} + C_{D0} \right) \tag{3.32}$$
$$Y_r = \frac{1}{2} v_r^2 \rho A \frac{\delta C_L}{\delta \alpha_e}\delta \tag{3.33}$$
$$K_r = -\left(VCG - \frac{1}{2}s_p \right) \frac{1}{2} v_r^2 \rho A \frac{\delta C_L}{\delta \alpha_e}\delta \tag{3.34}$$
$$N_r = -LCG \frac{1}{2} v_r^2 \rho A \frac{\delta C_L}{\delta \alpha_e}\delta \tag{3.35}$$

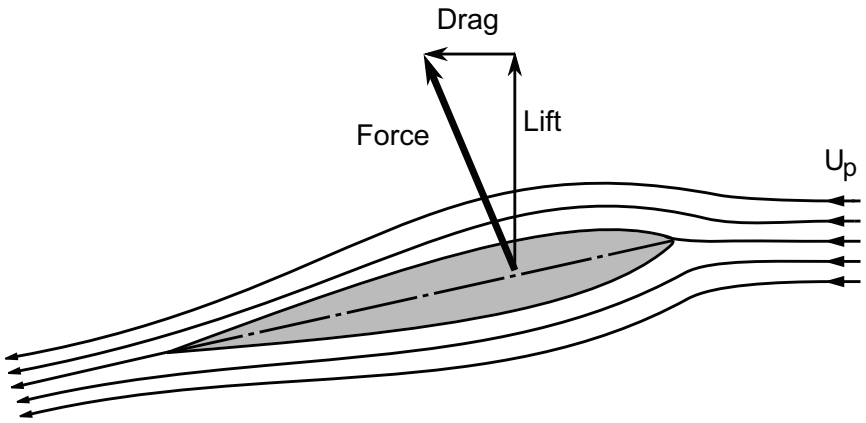

Figure 3.6: Rudder lift and drag.

where Table 3.3 explains the parameters of the force equations. The physical interpretation of (3.32)-(3.35) is that X_r is drag, Y_r is lift, K_r is roll moment and N_r is yaw moment imposed by the rudder. The lift and drag is displayed in Figure 3.6. The aspect ratio α_r

δ	Rudder angle
$\frac{\delta C_L}{\delta \alpha_e}$	Rudder lift coefficient
ρ	Water density
v_r	Relative water speed
A	Rudder area
a_r	Aspect ratio
C_{D0}	Drag coefficient at zero angle of attack
s_p	Rudder span
VCG	Vertical distance to center of gravity
LCG	Lateral distance to center of gravity

Table 3.3: Rudder equation parameters.

of the rudder is a measure of the proportion of the rudder defined as

$$a_r = \frac{\text{Height}}{\text{Width}}. \tag{3.36}$$

This is an important measure when designing a rudder since a low aspect ratio imposes more drag.

As long as the vessel is moving, drag will be imposed by the rudder even when no lift is generated. To account for this a zero angle of attack constant is determined as

$$C_{D0} = 2.5\frac{0.075}{(\log_{10} R_n - 2)^2} \tag{3.37}$$

where R_n is the Reynolds number

$$R_n = \frac{Vc}{\nu} \tag{3.38}$$

consisting of the water inflow velocity V, the mean cord length c and the kinematic viscosity of water ν. If the rudder is turned too much a phenomena called stall might occur. This causes the rudder to loose lift instead of gaining it when increasing the rudder angle. This effect is unfortunately not incorporated in the model even though it might be of interest.

Tunnel Thruster

The tunnel thruster system on the Viknes seen in Figure 2.4 consists of an electric motor and a small propeller. In contrast to the two other actuators this is an on-off thruster governed by the direction control signal defined as

$$C_{TT} = \begin{cases} 1 & \text{Starboard rotation} \\ 0 & \text{Thruster off} \\ -1 & \text{Port rotation} \end{cases} \tag{3.39}$$

The actuator dynamics is modeled as a first order process with an adjusted time constant

$$\dot{\alpha} = k_\alpha \left(-\alpha + \alpha_d \left(C_{TT}\right)\right). \tag{3.40}$$

Based on the input signal, α_d can be defined as

$$\alpha_d \left(C_{TT}\right) = k_{kg} C_{TT} \tag{3.41}$$

where k_{kg} is the constant thrust in kg described in the manufacturer's data-sheet. The produced yaw moment of the tunnel thruster can then be written as

$$N_{TT} = 9.81 LCG\alpha \tag{3.42}$$

The tunnel thruster would also generate a roll force due to the moment arm from CG. This could be incorporated, but it would be of minimal influence on the vessel dynamics and is therefore neglected.

Total control forces

The vessel model is affected by the actuators and the environment. The forces and moments generated by the actuators are listed below.

$$X_c = X_p + X_r \tag{3.43}$$
$$Y_c = Y_r \tag{3.44}$$
$$Z_c = 0 \tag{3.45}$$
$$K_c = K_r \tag{3.46}$$
$$M_c = 0 \tag{3.47}$$
$$N_c = N_{TT} + N_r \tag{3.48}$$

3.4 Environmental modeling

As mentioned above, the main goal of a DP system is to keep the vessel in a preset position at a given heading, independent of environmental disturbances. When designing a DP system, developing a system model without disturbances would have little purpose. The main environmental forces to consider are sea current, wind and waves. These can be modeled as three independent phenomena, or as a combined disturbance. Due to rigidity of the vessel it will experience one force which is the the sum of the environmental force vectors.

3.4.1 Sea current

Currents are fluid movement caused by several forces such as celestial gravitational and temperature difference based forces, basically induced respectively by the Moon and the Sun. These forces act on huge areas and shift the equilibrium of the oceans, generating massive movements of water. In small or local areas such as DP system operating zones the current may be regarded as a constant uniform movement of the fluid surrounding the vessel. By augmenting (3.1) a simple current disturbance can be introduced, and become

$$\dot{\boldsymbol{\eta}} = \mathbf{R}(\psi)\,\boldsymbol{\nu} + \mathbf{v}_c. \tag{3.49}$$

As a current approximation by itself, this is not very sophisticated, but catches the most significant effect of adding not propulsion generated velocities to the vessel. The current velocities have predefined direction and magnitude,

$$\mathbf{v}_c = \begin{bmatrix} V_c\cos(\beta_c) & V_c\sin(\beta_c) & 0 \end{bmatrix}^\top, \tag{3.50}$$

where V_c is the magnitude and β_c is the direction in the NED frame. The current force is assumed not to influence the vessel heading. The current could also be approximated as a constant force acting on the system.

3.4.2 Waves

Waves are a wind generated complex phenomena occurring on the ocean surface. Ocean surface waves are considered to be irregular, which in this case introducing randomness in both time and space. A common assumption is that local sea level can be considered as realization of a stationary stochastic process. A wave spectrum is used to describe the energy distribution in the frequency domain of the ocean surface. Due to variations in the wave frequency distribution, the wave spectrum will be dependent on location of operation. The chosen wave spectrum is used to deliver the wave frequencies, which excite the RAOs, returning either force, or motion response, as demonstrated in the top of both Figure 3.3 and 3.4.

The wave impact on the vessel is dependent on how they hit the vessel. Figure 3.7 describes the definition of how the waves are encountering the vessel, and the naming for this. The

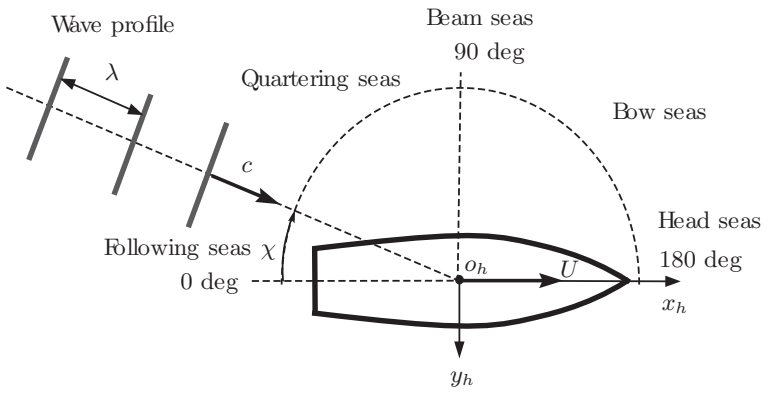

Figure 3.7: Wave encounter angle definition. Adapted from Perez [2005].

encounter angle is described by χ, the speed of the waves is described by c and λ describes the wave length period. Waves forces are referred to the hydrodynamic origin o_h of the vessel.

An important measure of waves is the significant wave height which is the mean wave height of the one-third largest waves in the sea state. This means that if a sea state has a significant wave height of 2 [m] the common waves are smaller. However larger waves will also occur.

Looking at vessel interaction, waves are often divided into first-order and second-order wave excitation forces. First-order wave excitation forces are the zero-mean oscillatory forces. Second-order wave excitation forces include mean wave-drift loads, slowly varying and rapidly varying wave loads. For a more thorough description of environmental disturbances see Perez [2005].

3.4.3 Wind

Wind is defined as air movement relative to the Earth's surface. Similar to waves it will affect the vessel depending on angle of attack. Wind usually consists of several components, but normally modeled as a mean wind with a random fluctuating component labeled as gust. Practically this could be implemented as a random walk process added to a constant term. As for the other environmental forces the projected area towards the disturbance is crucial to minimize the effect. In this case the important environmental disturbance of consideration is a resultant wind force, constantly trying to push the vessel away from its desired position. The wind model described in [Fossen, 2002] is

$$\boldsymbol{\tau}_{wind} = \frac{1}{2}\rho_a V_{rw}^2 \begin{bmatrix} C_X(\gamma_{\omega_{rw}})A_{Fw} \\ C_Y(\gamma_{\omega_{rw}})A_{Lw} \\ C_Z(\gamma_{\omega_{rw}})A_{Fw} \\ C_K(\gamma_{\omega_{rw}})A_{Lw}H_{Lw} \\ C_M(\gamma_{\omega_{rw}})A_{Fw}H_{Fw} \\ C_N(\gamma_{\omega})\rho_a V_r^2 A_{Lw}L_{oa} \end{bmatrix}, \tag{3.51}$$

where the parameters are explained in Table 3.4 and

$$V_{rw} = \sqrt{u_{rw}^2 + v_{rw}^2} \tag{3.52}$$

$$\gamma_{rw} = -atan2(v_{rw}, u_{rw}) \tag{3.53}$$

which is the relative wind speed and the angle of attack. This model accounts for an asymmetric vessel through the wind coefficients.

γ_ω	Relative wind angle
C_i	Wind coefficient
A_{Fw}	Frontal projected area
A_{Lw}	Lateral projected area
H_{Fw}	Frontal centroid above the water line
H_{Lw}	Lateral centroid above the water line
L_{oa}	Vessel overall length

Table 3.4: Wind forces and moment parameters used in (3.51).

Wind coefficients can be found in several ways, one option is through experiments physically measuring the forces, wind velocity and angle of attack and derive the them by curve fitting or other methods. Alternatively, it is possible to estimate the coefficients using an approximate exterior model of the vessel in conjunction with vessel dimensions.

3.5 Beaufort wind force scale

There are several measurement systems describing the environmental conditions at sea. The Beaufort wind force scale is one widely accepted system. It describes the wind and wave magnitude at open seas. Even though inaccurate for shore conditions the system provides a good measure of the operational space of small vessels. The Beaufort wind force scale is displayed in Table 3.5 and further described in [Oliver, 2005].

Beaufort no.	Description	Wind speed	Wave height	Sea conditions
0	Calm	< 0.3 m/s	0 m	Calm (glassy).
1	Light air	0.3-1.5 m/s	0-0.2 m	Calm (rippled).
2	Light breeze	1.6-3.4 m/s	0.2-0.5 m	Smooth (wavelets).
3	Gentle breeze	3.4-5.4 m/s	0.5-1 m	Slight.
4	Moderate breeze	5.5-7.9 m/s	1-2 m	Slight-Moderate.
5	Fresh breeze	8.0-10.7 m/s	2-3 m	Moderate.
6	Strong breeze	10.8-13.8 m/s	3-4 m	Rough.
7	Near gale	13.9-17.1 m/s	4-5.5 m	Rough-Very rough.
8	Gale	17.2-20.7 m/s	5.5-7.5 m	Very rough-High.
9	Severe gale	20.8-24.4 m/s	7-10 m	High.
10	Storm	24.5-28.4 m/s	9-12.5 m	Very High.
11	Violent storm	28.5-32.6 m/s	11.5-16 m	Very High.
12	Hurricane	> 32.6 m/s	> 14 m	Phenomenal.

Table 3.5: The Beaufort wind force scale. Wind is measured at 10 m reference height.

The wind-speeds featured in the Beaufort wind scale are measured at a height of 10 m above the surface. Due to friction along the surface the actual wind speed affecting small vessels will be lower. To compensate for this a formula described in [Kaltschmitt et al., 2007] can be used

$$v_w(h) = v_{10} \left(\frac{h}{h_{10}} \right)^a , \tag{3.54}$$

where $v_w(h)$ is the wind-speed at a give height h, v_{10} is the wind-speed at 10 meters, $h_1 0 = 10$ and a is the Hellman exponent which is found to be 0.4 for stable air above flat open coast.

3.6 Model discussion

When building a mathematical vessel model, many approaches and aspects of concern have to be considered. Sørensen [2005] defines the concepts process plant model and control plant

model. A process plant model is a comprehensive model of the actual process whose main purpose is to simulate the real plant dynamics. The control plant model is a simplified model, describing the main physical properties. Normally a process plant model is used to test the robustness and performance of the control system, while the control plant model is used during the system development.

An implementation of the above described model would result in a process plant model which describes the vessel and the environment. The downside of using such model for controller development is the complexity and the simulation time. Using the process plant model, stability is hard to prove mathematically. Such a model also demands more computing time than a control plant model.

In general, when developing DP models and controllers, to reduce model complexity, and design controllers counteracting the important dynamics, several DOFs are left out. Normally, and due to negligible DP disturbance contributions, heave and pitch are removed. In systems not striving to reduce roll dynamics, roll is removed also.

A mathematical model of the vessel, actuators and environment will never describe the real world perfectly, however, if the right parameters are found, a very good approximation can be obtained. In the case of the Viknes, better models of the actuators could be derived through further studies on each individual device.

Chapter 4

Control design

4.1 Scheme selection

To enable the Viknes 830 to do station keeping using its current thruster configuration, a sway independent scheme must be considered, which in turn disqualify ordinary DP schemes. By redefining the station keeping problem, as mentioned in Chapter 1, this might be accomplished using a vessel capable of performing independent surge and yaw movement. However, this will not suffice the purpose, as the vessel is affected by environmental forces of unknown magnitude and direction. By utilizing the environment as a force field, a scheme where the vessel keeps a distance and heading towards a given point can be created, using the rudder and tunnel thruster for heading management and propeller and engine for the distance control. Station keeping, is by this, defined as any position on a circle around a given point, and known as weather optimal heading control (WOHC). WOPC is obtained by moving the pendulum suspension point, yielding coincidence between vessel and desired position.

The approach downsides are the convergence time dependency from environmental forces and the inability of heading predetermination. If the environmental forces are strong then convergence is rapid, whereas weak force yields slow convergence. The vessel heading will be the opposite of the environmental force field direction. The upside is the ability of underactuated vessels to perform station keeping.

The whole scheme is analogous to a pendulum in a force field. This property is derived in the following and utilized in the control design.

4.2 Control design

4.2.1 Pendulum analogy

Dynamics

In Figure 4.1, a line connects a mass and a suspension point, where the mass is influenced by a homogeneous force field. This pendulum scheme is analogous to the environment acting on a vessel tided to a pole. The weather constantly acts on the vessel and moves it to a weather optimal position where the angle between the environmental resultant force F_e and the line is 180 [deg]. In the real world the force field acting on the vessel is a resultant force of current, wind and waves.

The differential equation for a pendulum without damping is as follows

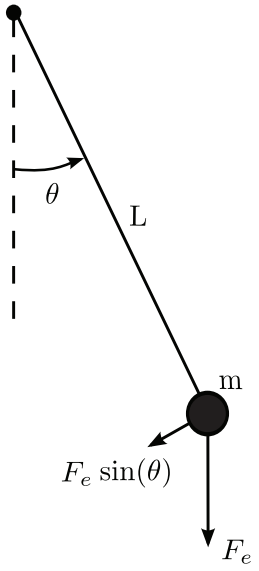

Figure 4.1: The pendulum principle is the foundation of WOPC.

$$mL\ddot{\theta} + F_e \sin(\theta) = 0. \tag{4.1}$$

This however is not correct for a marine vessel, due to a significant damping force in the system. Damping of a pendulum in air is low, but for a vessel in water, damping will significantly affect the system. Introducing damping in (4.1) as follows

$$mL\ddot{\theta} + d\dot{\theta} + F_e \sin(\theta) = 0, \tag{4.2}$$

which is equal to

$$\ddot{\theta} + \frac{d}{mL}\dot{\theta} + \frac{F_e}{mL}\sin(\theta) = 0. \tag{4.3}$$

4.2.2 Convergence rate

Some simplifications have to be made due to the complexity of finding the analytical solution of (4.3). Looking at dynamics where the simplification of small angles $\sin(\theta) \approx \theta$ holds, an analytical solution of the dynamics can be derived. Using this it is possible to determine to what extent the pendulum length affects the convergence to a weather optimal heading. Using the assumption of small angles, (4.3) can be written as

$$\ddot{\theta} + \frac{d}{mL}\dot{\theta} + \frac{F_e}{mL}\theta = 0. \tag{4.4}$$

This differential equation can be written on the form

$$\ddot{\theta} + 2\zeta\omega_0\dot{\theta} + \omega_0^2\theta = 0, \tag{4.5}$$

where

$$\omega_0 = \sqrt{\frac{F_e}{mL}} \tag{4.6}$$

$$\zeta = \frac{d}{2mL\omega_0}. \tag{4.7}$$

The roots are determined to be

$$\lambda_+ = -\zeta\omega_0 + \sqrt{(\zeta\omega_0)^2 - \omega_0^2} \tag{4.8}$$

$$\lambda_- = -\zeta\omega_0 - \sqrt{(\zeta\omega_0)^2 - \omega_0^2}. \tag{4.9}$$

From investigation of the root expressions, the length of the pendulum cannot exceed the limit determined by (4.10) if the system is to be over-damped

$$L < \frac{d^2}{4mF_e}. \tag{4.10}$$

It is assumed that this inequality is true and that the system is over-damped, which gives the following solution

$$\theta(t) = c_1 e^{\lambda_+ t} + c_2 e^{\lambda_- t}. \tag{4.11}$$

The constants c_1 and c_2 in (4.11) will be dependent on the initial conditions of the system, and is found to be

$$c_1 = \theta(0) + \frac{\lambda_+\theta(0) - \dot{\theta}(0)}{\lambda_- - \lambda_+} \tag{4.12}$$

$$c_2 = -\frac{\lambda_+\theta(0) - \dot{\theta}(0)}{\lambda_- - \lambda_+}. \tag{4.13}$$

These constants will determine which of the exponential terms in (4.11) are dominant. By using this, a boundary on the time constant can be found to be

$$\frac{1}{-\lambda_-} \leq T \leq \frac{1}{-\lambda_+}. \tag{4.14}$$

Both exponential terms in (4.11) are directly influenced by the pendulum length, which enables the possibility to actively use it in a control scheme. Since m, d and F_e is given by the vessel and the environment, L will be the only adjustable variable. From computer simulations it is found that the energy used to correct the heading angle decreases when the length of the pendulum increases. This is reasonable since the angle related to correcting a deviation from the desired position decreases as the pendulum length increases. This means that the vessel will turn less to correct the error than with a shorter pendulum. The trade-off for a longer, more energy efficient pendulum is that the system dynamics become slower, allowing larger and longer deviations from the desired position.

This property can be used to optimize the length of the pendulum to the sea state such that the vessel does not use unnecessary fuel. For a sensor platform buoy, the WOPC system can increase operational time by improving the fuel efficiency.

4.3 Weather optimal heading control

Assuming the vessel acts like a pendulum in the environmental resultant force field, a weather optimal heading controller can be derived. The pendulum length directly relates to the radius of the circle seen in Figure 4.2, which in the following will be denoted r_c. Depending on the resultant force direction the vessel will position itself on the circle arc directing its heading towards the suspension point $\mathbf{p_c} \triangleq [x_c, y_c]^\top$. Defining deviations from the suspension point $\mathbf{p_c}$ as follows:

$$\tilde{x} \triangleq x_c - x \tag{4.15}$$

$$\tilde{y} \triangleq y_c - y, \tag{4.16}$$

The pendulum scheme has one stable and one unstable equilibrium point, which comes from the fact that two positions on the circle arc correspond to alignment with the resultant force, physically explained as an inverted pendulum and a normal pendulum. Subject to an ideal uniform force field it is possible for the vessel to end up in the unstable inverted pendulum equilibrium. For a pendulum in the real world this is impossible. In the real world, small disturbances will always act and push the vessel away from the unstable equilibrium point, and the system will converge to the stable equilibrium where the heading is 180 [deg] opposite of the resultant force. Using a surge and yaw controller, a virtual pendulum line can be created.

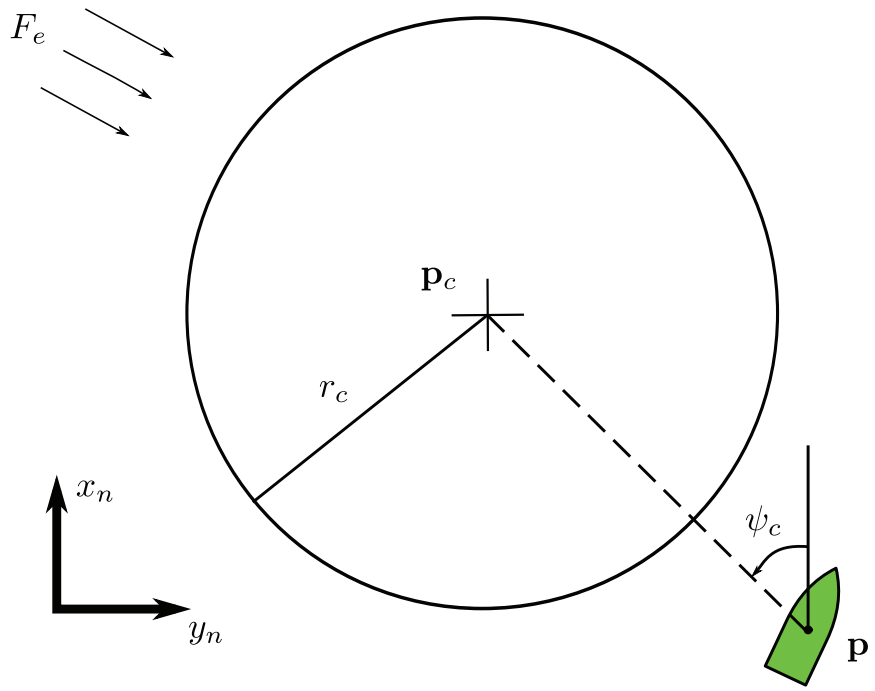

Figure 4.2: Illustration of a vessel suspended as a virtual pendulum influenced by the weather. The circle describes all possible positions.

4.3.1 Surge control

The surge controller aims to control the body-fixed surge deviation to become r_c, which in the pendulum analogy corresponds to the length of the line. The body-fixed deviations towards the suspension point $\mathbf{p_c}$ is as follows

$$\mathbf{e}_b = \mathbf{R}^\top(\psi) \begin{bmatrix} \left(\sqrt{\tilde{x}^2 + \tilde{y}^2} - r_c\right) \cos\psi_c \\ \left(\sqrt{\tilde{x}^2 + \tilde{y}^2} - r_c\right) \sin\psi_c \\ 0 \end{bmatrix} \tag{4.17}$$

such that the body-fixed surge deviation element becomes

$$\begin{aligned} e_{b,surge} = &\left(\sqrt{\tilde{x}^2 + \tilde{y}^2} - r_c\right) \cos\psi_c \cos\psi \\ &- \left(\sqrt{\tilde{x}^2 + \tilde{y}^2} - r_c\right) \sin\psi_c \sin\psi, \end{aligned} \tag{4.18}$$

where ψ_c is defined as

$$\psi_c \triangleq atan2(\tilde{y}, \tilde{x}), \tag{4.19}$$

the heading towards $\mathbf{p_c}$ defined in the NED frame. The control law τ_{surge} is chosen as

$$\tau_{surge} = K_{d_s}(\tilde{u}) + K_{i_s} \int \kappa_i e_{b,surge} d\tau, \tag{4.20}$$

where

$$\tilde{u} \triangleq u_d - u. \tag{4.21}$$

The desired velocity u_d is derived from (4.22), which is a mathematical function utilizing properties of the sigmoid hyperbolic tangent function to define a velocity profile dependent on the vessel deviation from $\mathbf{p_c}$:

$$u_d \triangleq u_{d,max} \tanh\left(\frac{e_{b,surge}}{u_{d,max}\Delta u}\right). \tag{4.22}$$

The velocity profile above is made scale independent which means that changing the maximum velocity does not affect the profile, which is important when it comes to tuning since if not scale independent set-point overshoot might easily occur if desired velocity is increased.

$$\kappa_i \triangleq 1 - \left| K_{\alpha,s} \tanh\left(\frac{e_{b,surge}}{K_{\beta,s}}\right)\right|. \tag{4.23}$$

Since u_d is calculated using the position of the vessel, the first term of (4.20) implies a bounded proportional and derivate gain, which removes the need for a reference filter. This is useful since a conventional reference filter relies on tuning and not feedback. An illustrative velocity profile can be seen in Figure 4.3 inspired by a similar approach also using sigmoid functions can be seen in [Breivik et al., 2008].

Integral buildups might be a problem when the vessel initial condition places it away from the circle around $\mathbf{p_c}$. Avoiding this can be done by defining an area where the integral term of (4.20) is active. An illustrative integral adjustment graph is seen in Figure 4.3.

4.3.2 Yaw control

The yaw controller purpose is to direct the heading towards the circle center, in accordance with the pendulum line analogy. Due to the two distinctive different yaw actuators it is switched between two controllers.

Switching algorithm

A relay scheme is used to switch between the rudder and tunnel thruster controller where the relative water-speed estimate u_p is the switching argument. Due to the inefficiency of the rudder at low velocity and the tunnel thruster at high only use of one of the actuators at a time are feasible. This is done to utilize the best of each actuator. Figure 4.4 displays the scenario. The benefit of using a hysteresis scheme is that it if adjusted correctly removes the possibility to end up in the point where both controllers are turned on and off due to small perturbations. It ensures that one of the controllers always are enabled and if a switch occurs the switch back will not happen before the water-speed over the rudder either has increased or decreased considerably.

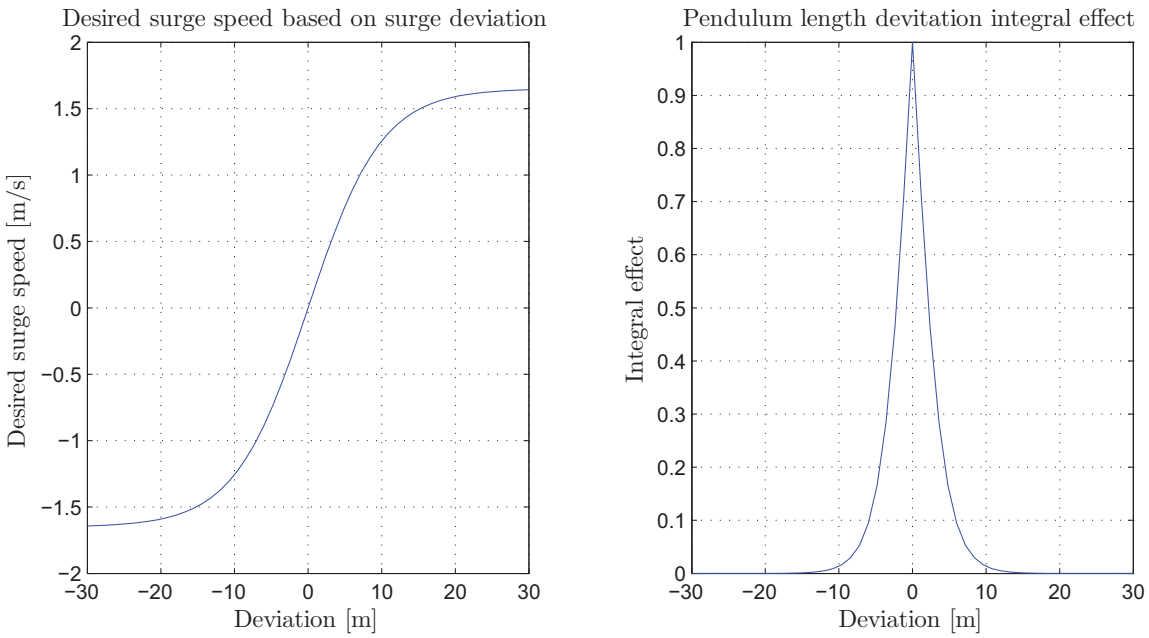

Figure 4.3: Desired velocity profile.

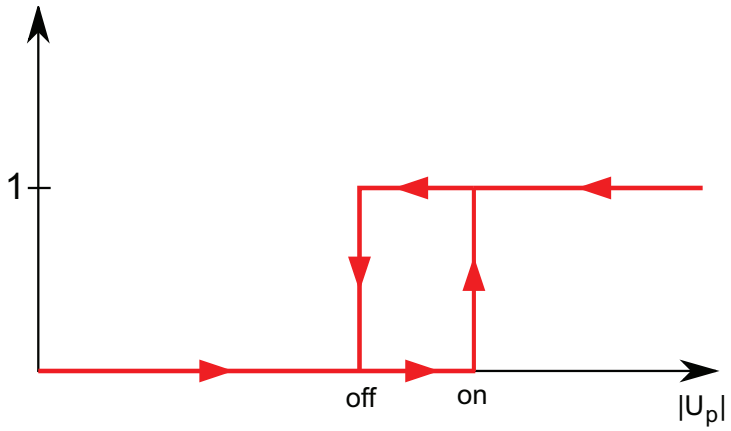

Figure 4.4: Yaw controller hysteresis switching law.

Yaw controller

The rudder and tunnel thruster controllers both have the same structure consisting of a scale independent angular velocity profile using the ψ deviation as input. The structure is as follows

$$\tau_\psi = K_{d_\psi}(\tilde{r}), \tag{4.24}$$

$$\tilde{r} \triangleq r_d - r \tag{4.25}$$

where

$$r_d = r_{max} \tanh\left(\frac{\tilde{\psi}}{r_{max}\Delta r}\right), \tag{4.26}$$

$$\tilde{\psi} \triangleq \psi_c - \psi \tag{4.27}$$

and where the desired heading ψ_c is defined by (4.19). Both controllers use the same strategy of following a velocity trajectory to correct the deviation from the desired heading. The difference between the controllers are the tuning of the angular velocity profile and the proportional gain. It is desirable to set $K_{d_\psi} = 1$ when using the tunnel thruster. This gives a more intuitive thrust allocation due to working with the actual yaw rate deviation.

4.3.3 Control vector

The control vector responsible for making the vessel emulate a pendulum becomes

$$\boldsymbol{\tau} = \begin{bmatrix} K_{d_s}(\tilde{u}) + K_{i_s}\int_0^t \kappa_i e_{b,surge} d\tau \\ 0 \\ K_{d_\psi}(\tilde{r}) \end{bmatrix}, \tag{4.28}$$

where K_{d_s},K_i and K_{d_ψ} are gains in the PD controller design. It should be noted that since the sway force is set to 0 the vessel becomes underactuated. The vessel will pursue the suspension point $\mathbf{p_c}$ by a pure pursuit guidance law if placed away from the circle. In Breivik et al. [2008], pure pursuit and other guidance laws are derived and discussed.

4.4 Weather optimal positioning control

4.4.1 Suspension point controller

Controlling the position of the vessel can be done by controlling the suspension point $\mathbf{p_c}$. Figure 4.5 demonstrates the principle of the circle center controller, where a virtual pendulum suspended in $\mathbf{p_c}$ is created by the surge and yaw controllers. Environmental influence creates a force field enabling the pendulum analogy. Minimizing the angular

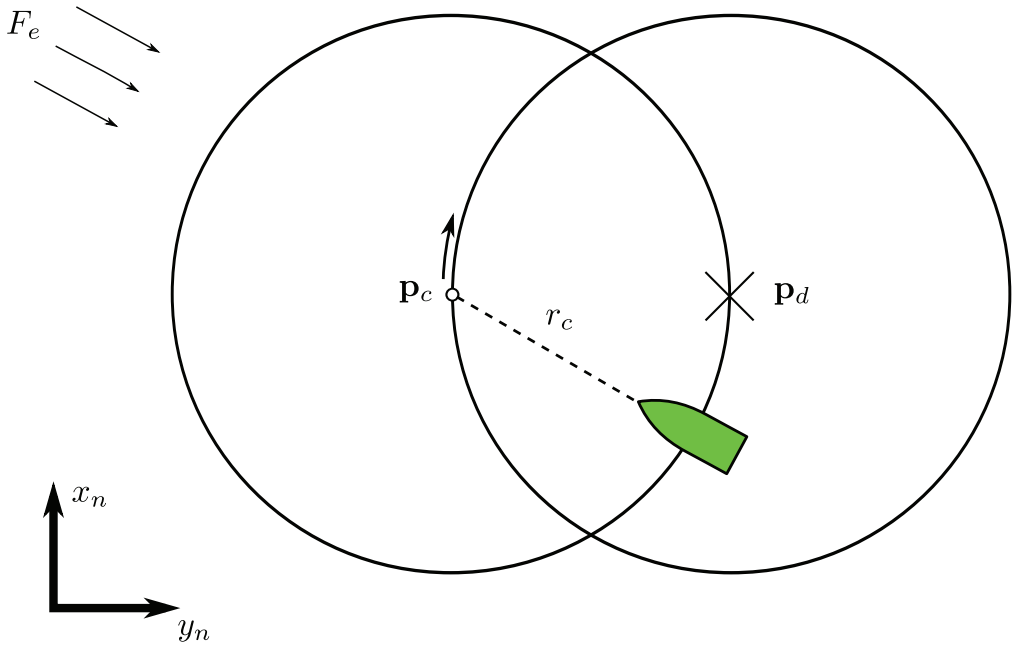

Figure 4.5: By moving the suspension point $\mathbf{p_c}$, the vessel may be positioned so that it coincides with the desired position $\mathbf{p_d}$.

deviation between the vectors seen in Figure 4.6 by controlling $\mathbf{p_c}$ on the circle of the desired point $\mathbf{p_d}$, it is possible to position the vessel in $\mathbf{p_d}$.

Drawing circles around $\mathbf{p_c}$ and $\mathbf{p_d}$ with radius r_c, and identifying that $\mathbf{p_c}$ must lie on the circle arc of $\mathbf{p_d}$ to be able to provide convergence of the vessel to $\mathbf{p_d}$. Modeling the movement of $\mathbf{p_c}$ as a first order system enables a simple control law moving $\mathbf{p_c}$. The controller objective is to remove angular deviation between ψ and ψ_d. Figure 4.6 illustrates the principle. Vessel deviation from the suspension point $\mathbf{p_c}$ is defined in (4.15) and (4.16), and the deviation between $\mathbf{p_d}$ and $\mathbf{p_c}$ is defined as follows

$$\tilde{x}_{cd} = x_c - x_d \tag{4.29}$$

$$\tilde{y}_{cd} = y_c - y_d. \tag{4.30}$$

The angle between $\mathbf{p_d}$ and $\mathbf{p_c}$ is defined as

$$\psi_d = atan2(\tilde{y}_{cd}, \tilde{x}_{cd}). \tag{4.31}$$

The deviation to minimize is

$$\tilde{\psi}_{cd} = \psi_c - \psi_d. \tag{4.32}$$

Problems might arise if the placement of $\mathbf{p_c}$ is based on the deviation from the desired position alone, since this moves $\mathbf{p_c}$ with infinite velocity, which could lead to stability issues. Due to the cascade of the controllers it is identified that the inner virtual pendulum line controller must be faster than the outer suspension point controller. Applying low

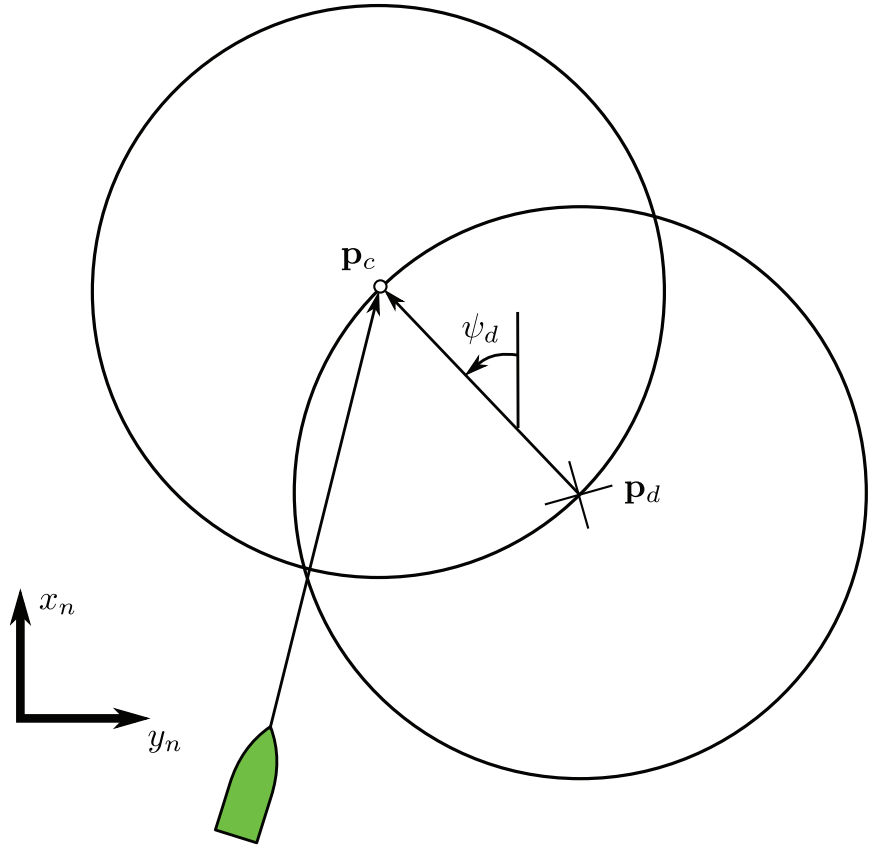

Figure 4.6: By making the vector from the vessel to the suspension point coincide with the vector from the desired point to the suspension point, the vessel will be positioned at the desired position.

pass properties to the movement of $\mathbf{p_c}$ will solve the problem, and this is done indirectly by modeling ψ_d as a first order system

$$\dot{\psi}_d = k(\epsilon)\tilde{\psi}_{cd}, \tag{4.33}$$

where $k(\epsilon)$ is a adaptive gain defined as

$$k(\epsilon) = \epsilon + \xi, \tag{4.34}$$

where ξ is a constant to ensure a minimum of movement and the dynamics of ϵ is

$$\dot{\epsilon} = k_\epsilon \left(-\epsilon + \left| \dot{\psi}_c \right| \right). \tag{4.35}$$

The idea of the adaptive gain is to enable the system to move $\mathbf{p_c}$ with a angular velocity proportional to the strength of the environmental force field. The force field is measured indirectly through the derivative of ψ_c. If $\dot{\psi}_c$ is large it indicates a strong force field which enables more movement of $\mathbf{p_c}$. If $\dot{\psi}_c$ is small a weather optimal heading is relatively close or the force field is weak. In both cases the movement of $\mathbf{p_c}$ must be low. Due to the low pass properties of the dynamics of ϵ and the definition of ψ_c seen in (4.19) this will create a adaptive gain which adjusts the angular movement of $\mathbf{p_c}$. ϵ is saturated between 0 and a upper limit. k_ϵ should be adjusted to not become to large which will lead to low performance or to low which will impose unnecessary long time away from the desired position.

The angle in the circle around the desired point where the vessel should point to converge to the desired position is now defined, and thus the position becomes

$$x_c = r_c \cos(\psi_d) + x_d \tag{4.36}$$

$$y_c = r_c \sin(\psi_d) + y_d. \tag{4.37}$$

The suspension point controller moves $\mathbf{p_c}$, which is the set point of the virtual pendulum controller, so that the pendulum analogy is complete. The virtual pendulum WOHC scheme creates the virtual pendulum line so that it tries to point towards $\mathbf{p_c}$ with distance r_c. The circle controller moves $\mathbf{p_c}$ on the circle around the desired point, which makes the vessel position coincide with the desired position. WOPC will be obtained given that the bandwidth of the virtual pendulum WOHC is relatively higher than the suspension point controller.

4.4.2 Initialization

Initialization of the suspension point can be done by either using a fixed angular value and let the system converge or make an assumption. If the initialization is done at the opposite angle between the vessel and desired point the vessel will travel towards the desired position. At this position the suspension point controller has obtained its objective which is to minimize the deviation between ψ_c and ψ_d. It is assumed that this makes the convergence faster as the vessel pursues both the circle center and the desired position.

4.5 Control design discussion

Many aspects of this control design might cause problems in a real implementation. By using a limited integral area in the surge controller, possibilities of having a stationary deviation and ending up outside the defined area is always present. By detecting the stationary deviation state, and increasing integral area, or proportional gain, until the integral part area envelope the vessel position, the offset position problem could be solved.

Using WOPC, another major concern which might cause several problems, is the movement of the suspension point. If the suspension point movement is too slow the convergence time will be long, where the vessel will perform unnecessary work and have unnecessary long periods of deviations exceeding desired magnitude. If moved to fast, the vessel will not be able to follow the suspension point resulting in a state where the total movement is dominated by the self induced vessel movement, ending up circling around the desired position. The idea behind the adaptivity in the suspension point controller is to consider the movement of the vessel, which is an indicator of the environmental force, and move the suspension point accordingly. The performance might be further enhanced through design of an estimator which includes the vessel dynamics and predicts new weather direction and force used for inputs to the suspension point controller update calculations. Using an estimator in the position update of the suspension point might improve convergence time. On the other hand an estimator needs more vessel characteristics data on mass and damping, thus the system becomes less adequate to the average leisure craft. A system independent of hull design which only needs to be tuned is easy to retrofit to the wide range of leisure vessels.

4.6 Mathematical proof

Lyapunov analysis is used when dynamical systems are investigated enables for a proof of convergence to a equilibrium. The proof will also give a clue to the behavior of the convergence and for which areas it is defined. A storing function is chosen and the derivative of this is used to determine the stability of the system. For a thorough discussion of Lyapunov theory see [Khalil, 2001].

4.6.1 Lyapunov analysis

Investigating the stability properties of the pendulum scheme, where the system model is as follows

$$mL\ddot{\theta} + d\dot{\theta} + F_e \sin(\theta) = 0. \tag{4.38}$$

This might be rewritten to become two connected first order system as

$$\dot{x_1} = x_2 \tag{4.39}$$

$$mL\dot{x_2} + dx_2 = -F_e \sin(x_1), \tag{4.40}$$

where

$$x_1 = \theta \tag{4.41}$$

$$x_2 = \dot{\theta}. \tag{4.42}$$

For a pendulum with a fixed rigid line between the suspension point and the mass bulb there are multiplum of equilibrium points. These points are identified by setting $\dot{x_1} = 0$ and $\dot{x_2} = 0$, which gives equilibrium points in ($\pm n\pi$,0), for integer n. By considering only the domain $0 \leq \theta < 2\pi$ there are equilibrium points in (0,0) and (π,0). To analyze the stability properties of each the system is linearized around the point in question.

The Jacobian matrix is given by

$$\frac{\delta f}{\delta x} = \begin{bmatrix} \frac{\delta f_1}{\delta x_1} & \frac{\delta f_1}{\delta x_2} \\ \frac{\delta f_2}{\delta x_1} & \frac{\delta f_2}{\delta x_2} \end{bmatrix} = \begin{bmatrix} 0 & 1 \\ \frac{-F_e}{mL}\cos(x_1) & -\frac{d}{mL} \end{bmatrix} \tag{4.43}$$

This is evaluated in each equilibrium point to be

$$A_{(0,0)} = \begin{bmatrix} 0 & 1 \\ \frac{-F_e}{mL} & -\frac{d}{mL} \end{bmatrix} \tag{4.44}$$

$$A_{(\pi,0)} = \begin{bmatrix} 0 & 1 \\ \frac{F_e}{mL} & -\frac{d}{mL} \end{bmatrix}. \tag{4.45}$$

$$\tag{4.46}$$

The eigenvalues in both cases are found to be

$$\lambda_{(0,0),1,2} = -\frac{d}{2mL} \pm \sqrt{\left(\frac{d}{2mL}\right) - \frac{4F_e}{mL}} \tag{4.47}$$

$$\lambda_{(\pi,0),1,2} = -\frac{d}{2mL} \pm \sqrt{\left(\frac{d}{2mL}\right) + \frac{4F_e}{mL}} \tag{4.48}$$

Given $d, F_e > 0$, the eigenvalues of $\lambda_{(0,0)}$ are both in the left half plane and thus the point is stable. One of the eigenvalues of $\lambda_{(\pi,0)}$ will reside in the right half plane which makes the point unstable. This result is in accordance with the physical understanding of a pendulum system with a rigid line. There will be a stable equilibrium point on the opposite side from where the weather force is coming from. Since there are multiple equilibrium point the system cannot be globally asymptotically stable. To analyze the system stability properties of the system in general a Lyapunov function candidate is proposed

$$V = p\,(1 - cos(x_1)) + \frac{1}{2}x_2^2 \tag{4.49}$$

V is positive definite in the domain $0 \leq x_1 < 2\pi$ and $V(0) = 0$. The next step is to look at the time derivative of V which must be negative definite for the system to be asymptotically stable. This condition states that the system cannot gain energy, only dissipate what it already has to be stable.

$$\dot{V} = p\dot{x}_1 \sin(x_1) + x_2\dot{x}_2 \tag{4.50}$$

$$= p\sin(x_1)x_2 + x_2\frac{1}{mL}\left(-dx_2 - F_e\sin(x_1)\right). \tag{4.51}$$

By choosing $p = \frac{F_e}{mL}$ the time derivative of the Lyapunov function candidate becomes

$$\dot{V} = -\frac{F_e}{mL}x_2^2. \tag{4.52}$$

V is clearly negative semidefinite since it only contains one of the state variables. To determine the properties of the system LaSalle's invariance principle must be applied. For the system to maintain $\dot{V}(x) = 0$ the trajectory of the system must be confined to $x_2 = 0$. If $x_2(t) = 0$, then $\dot{x}_2(t) = 0$ which by investigation of the system equations gives that $\sin(x_1(t)) = 0$. The only point where $\dot{V} = 0$ can be maintained is in the origin (0,0). This means that $V(x(t))$ will decrease towards 0 which in turn gives that $x(t) \to 0$ as $t \to \infty$. This is in accordance with how the system works since the energy is lost in the hydrodynamical damping.

Above is the first part of the stability proof and the rest could be done by considering each component by itself starting with the surge and yaw controllers providing stability proofs of each subsystem. By using the available information about each subsystem the total system could be proved stable. This approach is described in [Khalil, 2001] as the stability analysis of interconnected systems.

Chapter 5

Thrust allocation

5.1 Interface and vessel challenges

Making a good thrust allocation on the Viknes USV implies several challenges, all related to the types of actuators and interfaces. The control interface to the vessel consists of three inputs; throttle and rudder angle in addition to tunnel thruster enabling. Each of the interface elements are further discussed below.

5.1.1 Throttle

The interface to propel the vessel forward is a value between -100% and 100%. This is an input to the engine and trolling gear control cable, controlling the trolling gear and engine rpm, hence it is actually indirect propeller thrust control only. The trolling gear function purpose is to enable propeller revolutions below engine idle rpm, without having to use higher gear ratio which is less ideal respective to cruising speed and propeller choice. The trolling functionality is actually a controlled slip in a viscosity based sliding disc coupling, comparable to a slipping clutch in a car. As oil is a non-ideal fluid it creates a viscous connection where the output shaft revolution is dependent on and controlled by the distance between the rotating disc surfaces. Hence in the trolling rpm range it becomes a variable ratio gear. At engine rpm above the trolling, the engine crankshaft connected to the propeller via a gear with a fixed ratio achieved by collapsing the span in the viscous trolling disc coupling. The mechanical arrangement connected to the throttle wire makes for a highly nonlinear mapping between throttle input and propeller output. There are no direct feedbacks from either the engine or propeller shaft rpm and the only measure of input is the vessel velocity.

5.1.2 Rudder angle

The interface to the rudder angle is a reference between -15 and 15 to a servo control system, able to output between approximately $\pm$ 27 [deg]. At present there is no rudder angle feedback, hence a short convergence period has to be assumed for the rudder to arrive at its set-point.

5.1.3 Tunnel thruster

The interface to the electrical powered tunnel thruster is an integer on-off signal between -1 and 1, where the thrust direction is designated to the sign. In the data sheet, max continuous operation time is set to 2 minutes and 40 seconds. During long time operation the intermittent usage should not exceed 8% of total time. Further investigation surfaced the inability of thrust direction direct switching. The tunnel thruster does not deliver any feedback. The actual interface implementation on the Viknes 830 USV does not consider the constraint of the average run-time and the continuous run-time is constrained to 25 seconds.

5.2 Surge allocation

From the overlaying controllers a force set-point will be calculated, and to work with the input specified on the vessel, this must be converted to a throttle set-point. This is done by estimating the propeller rpm corresponding to the set-point force and subsequently applying a mapping between rpm and throttle. Rudder usage impose a drag, leading to desired surge output will be too low. To compensate for this, a drag estimate is calculated. When the rudder is idle at $\delta = 0$ [deg] it imposes minimal drag. It is assumed that

$$X = X_c + X_r, \tag{5.1}$$

where X_c is the controller set-point and X_r is the rudder drag described by

$$X_r = \frac{1}{2}\hat{u}_r^2 \rho A \left(\frac{(\frac{\delta C_L}{\delta \alpha_e}\delta)^2}{0.9\pi a_r} + C_{D0} \right). \tag{5.2}$$

The rudder drag is dependent on the rudder angle and the relative water-speed passing it. The rudder angle set-point is known and the relative water speed is approximated using a water-speed model described in [Pivano, 2008]. This model is based on the idea that the propeller can be regarded as an infinitely thin disc of area A_0 in the mid-section of a Bernoulli tube. This scenario is displayed in Figure 5.1. By application of momentum

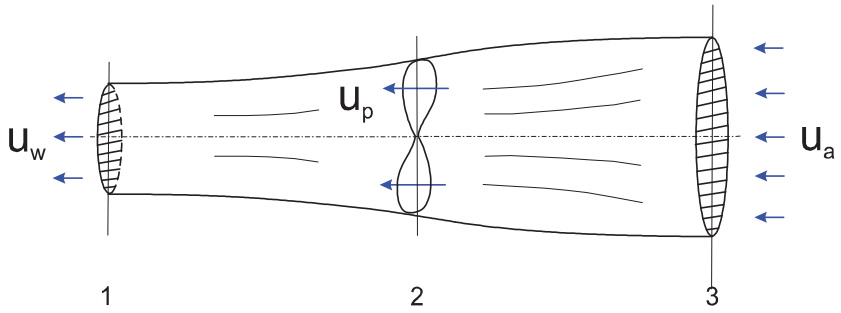

Figure 5.1: Cross-section 1: wake speed u_w, cross-section 2: velocity through the propeller disc and cross-section 3: advance speed u_a. Courtesy of [Pivano, 2008].

theory and the advance velocity a hydrodynamical model for the velocity through the propeller can be showed to be

$$m_f \dot{u}_p = -d_{f_1} |u_p| u_p + d_{f_2} |u_p| u_a + d_{f_3} |u_a| u_a + T_p, \tag{5.3}$$

where the parameters of the propeller water-speed model are displayed in Table 5.1. The

u_p	Relative water velocity from the propeller
u_a	Relative water velocity towards the propeller
A_0	Projected propeller disc area
a	Constant $0 < a < 1$
m_f	Water mass inside Bernoulli tube
d_{f_1}	$\frac{1}{2a^2}\rho A_0$
d_{f_2}	$\frac{1-a}{a^2}\rho A_0$
d_{f_3}	$\frac{2a-1}{2a^2}\rho A_0$
T_p	Propeller thrust

Table 5.1: Parameters of axial flow model seen in (5.3).

argument for using an estimate of the axial flow over the propeller is dualistic, it can be used to make a more sophisticated thrust allocation and further based on a better argument it enables selection of a yaw actuator. The propeller flow determines the rudder efficiency, this enables using the rudder in situations where the vessel has low speed, e.g. when relatively high throttle is commissioned but due to inertia the vessel speed is slowly building up.

On the Viknes USV the rudder is placed very close to the propeller, see Figure 2.2, therefore it might be possible to assume that the water speed over the propeller is approximately the same as the one passing the rudder. Figure 5.2 displays the propeller rudder scenario. When the vessel is reversing u_a is used as the water velocity over the rudder.

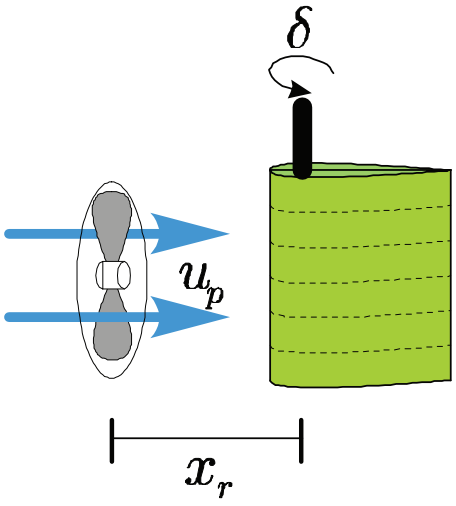

Figure 5.2: Propeller water velocity. Adapted from [Lindegaard, 2003]

5.2.1 Propeller rpm estimation

By solving the propeller model the ω corresponding to a given X and u might be determined

$$\rho d^4 \alpha_2 |\omega| \omega - \rho d^3 \alpha_1 u_a |\omega| = X \tag{5.4}$$

This could either be done by solving the equation numerically or analytically. It is most desirable to do the calculation analytically and find the correct corresponding ω. A solution defining different equations based on the quadrant of the input was tested, however this proved to be difficult to implement, hence a simplification is introduced. By looking at solving (5.4) as if $u_a = 0$ and then correcting the result by using the actual u_a,

$$\omega = \frac{X}{|X|}\sqrt{\frac{|X|}{\rho d^4 \alpha_2}} + k u_a \tag{5.5}$$

was found to be a good approximation. This simplification is possible and might be justified due to the bounded desired vessel velocity. The ω found is the propeller velocity and this is scaled by the gear ratio to achieve the engine rpm

$$rpm = k_{gr}\omega, \tag{5.6}$$

where $k_{gr} = 2.03$. The rpm found is used to look-up the corresponding throttle input from a table containing an rpm to throttle mapping.

5.3 Yaw allocation

To create a yaw moment there are two actuators available, but both have challenges related to the usage. The rudder needs enough water flow past it to be effective, which in practice

means that the vessel must move forward for it to be effective. Overheating, battery drainage and time limitations are the challenges when using the tunnel thruster. The efficiency of the tunnel thruster drops relatively to the surge speed of the vessel. Since each actuator works best under certain conditions an allocation is proposed below.

5.3.1 Tunnel thruster

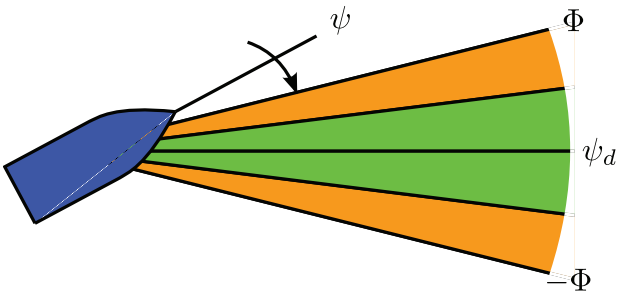

Figure 5.3: Tunnel thruster allocation principle where orange shows the relay zones and green the breaking zones.

From the overlaying tunnel thruster controller an angular velocity deviation is delivered. The idea of the allocation is to follow the yaw rate trajectory towards the desired heading by keeping the yaw rate magnitude above the trajectory. This is done by bursting the thruster much like a pulse-width modulated signal. When the heading enters a relay zone on its way towards the desired heading it continues as normal and enters the green breaking zone where the yaw rate is slowed down below the desired trajectory. The idea is that it must drift outside the relay zone to be pushed back in. This is done to avoid the heading being stuck on the transition between the breaking zone and the trajectory following zone. Figure 5.3 features this where the relay zones and breaking zones are drawn illustratively larger than in the implementation.

When the heading deviation is larger than the magnitude of the relay zones Φ the the tunnel thruster is used as

$$TT(\tilde{r})_{i+1} = \begin{cases} 1 & \text{if } \tilde{r} > 0 \text{ and } \psi_d - \psi > \Phi \text{ and } TT(\tilde{r})_i \,!= -1 \text{ and } s == 1 \\ -1 & \text{if } \tilde{r} < 0 \text{ and } \psi_d - \psi < -\Phi \text{ and } TT(\tilde{r})_i \,!= 1 \text{ and } s == 1 \\ 0 & \text{else } t_s + \Delta t > t_a \end{cases} \tag{5.7}$$

where Φ defines the angular magnitude of the breaking zone, t_s is the start time of the last burst, Δt defines the shortest burst time interval allowed, t_a is the system time and s is a flag which is low in a small time interval starting from when the output is 0 to protect the thruster from changing directions too fast. If the heading deviation is decreasing meaning

it has been outside the relay zone and is approaching the breaking zone it operates as Φ was set to the heading defining the start of the breaking zone. If the heading has been inside the breaking zone the relay zones act as an extended dead zone. This is done as a measure to decrease the amount of short burst that could arise if the weather pushes the heading to the edge of the breaking zone without a relay zone. Within the breaking zone the following is applied

$$TT(\tilde{r})_{i+1} = \begin{cases} 1 & \text{if } \tilde{r} > \Lambda \text{ and } TT(\tilde{r})_i \; ! = -1 \text{ and } s == 1 \\ -1 & \text{if } \tilde{r} > -\Lambda \text{ and } TT(\tilde{r})_i \; ! = 1 \text{ and } s == 1 \\ 0 & \text{if } t_s + \Delta t > t_a \end{cases} \tag{5.8}$$

where Λ is a angular rate. The idea of the breaking zone is to reduce the yaw rate just below the trajectory which should bring the heading to rest at approximately the correct heading. The implementation of this algorithm is done in software since it was necessary to time-constrain the lower boundary of each tunnel thruster run sequences and protect the signal from going directly from -1 to 1 or 1 to -1. This is done to always deliver an allocation that is possible for the actuator to follow. The output to the interface is as follows

$$TT_{on/off} = TT(\tilde{r})TT_{buffer}, \tag{5.9}$$

where TT_{buffer} is a finite size FIFO buffer with a constant sampling time at twice the rate of the shortest possible tunnel thruster usage. This buffer denies the tunnel thruster to exceed its allowed run time and average usage. It is defines as

$$TT_{buffer} = \begin{cases} 0 & \text{if cont. run-time} > 25s \\ 0 & \text{if mean usage } > 0.08 \\ 1 & \text{else} \end{cases} \tag{5.10}$$

5.3.2 Rudder

From the overlaying rudder controller a moment is delivered. This is converted to a rudder angle by

$$\delta = \frac{2N}{u_p^2 \rho A \frac{dC_L}{dA_e} LCG} \tag{5.11}$$

where the parameters are found in Table 3.3. The maximum rudder angle is saturated to be ± 27 [deg]. To enable a continuous signal δ_a which the rudder is able to follow the rudder machinery dynamics is used to filter the calculated value as

$$\dot{\delta}_a = \frac{-\delta_a + \delta}{t_c} \tag{5.12}$$

where $\dot{\delta}_a$ also is saturated. This is done to reduce wear-and-tear on the rudder servo. The interface of the vessel is defined to input a value between $-15 \leq \delta_a \leq 15$ [deg] which means

that the rudder angle δ_a must be scaled as

$$\delta_{a,interface} = \frac{15}{27}\delta_a, \tag{5.13}$$

before it is delivered to the interface.

5.4 Discussion

A high precision DP control system is useless if the thrust allocation does not meet the required standards. Deviations, poorly modeled and tuned allocation components will influence the precision of the entire system. However some deviations might be accounted for by integrators in overlying controllers but it is not desirable to base a thrust allocation system on this assumption. In this case the thrust allocation problem could have been solved in a more generic way as described in Fossen [2002] but due to the actual thruster configuration which have highly specialized actuators for surge and yaw this is not necessary.

Creating a thrust allocation system for the Viknes 830 USV poses many difficulties and uncertainties due to the lack of feedback from the actuators. The only actuator feedback available is through a mechanical gauge displaying engine rpm and indirectly through $\boldsymbol{\eta}$ and $\boldsymbol{\nu}$. Due to this it is not known if the actuators follows the set-points provided by the thrust allocation. Mounting sensors to measure the desired variables could be a solution but this is not in the scope of this thesis. However this would enable a more precise thrust allocation and better models of the system.

The thrust allocation system does not guarantee that the calculated control vector from the overlaying controllers is actually allocated to the vessel. As an example might be significant discrepancies between a given X and the calculated throttle input to the vessel. There are many reasons for this but since the model is a simplification of the real world and the parameters based on qualified guesses and empirical data, discrepancies are bound to appear. While using the tunnel thruster it is impossible to obtain the desired yaw moment exactly due to the nature of the actuator and the technical difficulties such as the time it needs to be on at each burst and the off time between direction changes. More precise bursts could be made if the rotational velocity of the thruster was available through feedback. By performing experimental tests better models of the actuators could be selected or derived and curve fitted to deliver a highly precise allocation. This however is time consuming work where the missing feedback would be necessary.

The tunnel thruster is not designed to be a part of a control system striving to keep a defined heading which represents a series of small bursts to correct deviations. Under normal WOPC conditions the main engine will be at approximately idle rpm which might cause problems if the average battery drain is higher than the charging. It is not implemented a system for the 8% limit in the vessel but the usage should be minimized to avoid depletion of

the battery pack. The performance of the system will be dependent on the heading stability when facing the environment. If a weather optimal heading stable vessel is used the need for the tunnel thruster would be minimal and the electrical tunnel thruster could be a desirable solution. If unstable the best solution would be to install a linear proportional tunnel thruster to continuously control the heading. If the instability is not severe an alternative solution could be to improve the tunnel thruster rudder cooperation by actively adjusting the rudder in advance of a throttle increase. If the tunnel thruster is disabled the rudder and propeller could be used in a burst strategy where the rudder is adjusted before a burst is commenced. Benefiting form the inertia of the vessel only small position deviations would occur. In total this would be a time-dependent control law where it is switched between correcting heading deviations and position deviations. This however demands a precise and accurate thrust allocation scheme using another implementation.

Chapter 6

Simulator implementation and results

6.1 Simulator implementation

The models of the vessel, actuators and environment as discussed in Chapter 3 were incorporated into Matlab/Simulink to form a simulator. This was done by editing the template *MAN_ForceRAO.mdl* incorporating (3.1) and (3.2) found in the hydro library in [Marine Systems Simulator, 2009]. The template also contained a force RAO wave model implementation. This was augmented by environmental models of wind and current, along with the control system and thrust allocation. In total, this forms an accurate and complex process plant model, comprising the most important environmental and hydrodynamic effects; It should however be kept in mind that the environmental and hydrodynamic model elements in their own nature, are not 100% eligible and will never mimic the real world perfectly. The purpose of the simulator was to determine the performance of the WOPC system and assist the building and further underpinning of an implementable system.

6.2 Parameter identification

One of the main problems with mathematical models, replicating the vessel and actuator dynamics, is to obtain the coefficients which determine the equations characteristics. Respective to a marine vessel, several methods are applicable, of which the most immediate and obvious is through series of experiments, and subsequently curve fitting the collected data to the equations. This is time-consuming work, requiring accurate measurements. It should further be noted that this method is exposed to several biases, and possibilities of environmental dynamics affecting the results which in turn might creates discrepancies between the model and the real world.

In determining a vessel's hydrodynamic characteristics, software is a very good alternative

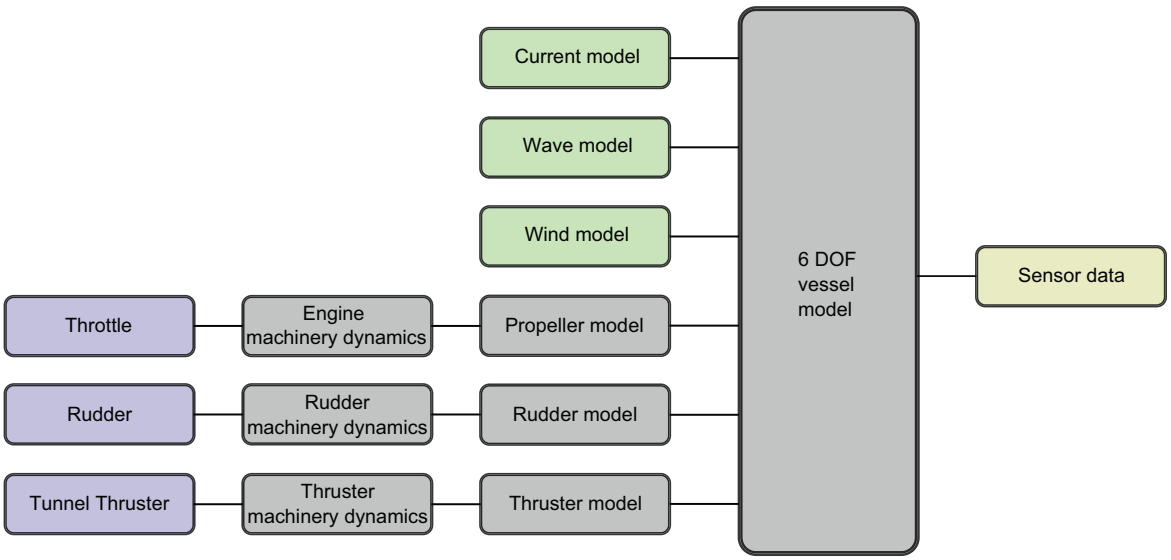

Figure 6.1: Viknes 830 simulator structure.

or supplement to expensive sea trials. From vessel's line drawings and weight information software can derive most of the information needed to build a conventional vessel model with wave disturbance. Such software is found in MARINTEK's Vessel Response program, (ShipX VERES). Based on the Viknes 830 drawings and information, a set of parameters for the vessel was calculated. Appendix A reviews some of the parameters used in the hydrodynamic software computation. ShipX VERES did not calculate wind coefficients and actuator parameters. These where found using the dimension drawings and experimental testing of the vessel. Each of the important parameters is presented as a part of the simulator description in the following.

6.3 Viknes vessel model

The simulator was structured as featured in Figure 6.1 where the blue boxes depicts the interfaces. The sensor data contains both $\boldsymbol{\eta}$ and $\boldsymbol{\nu}$.

6.3.1 Inertia

The rigid body matrix and added mass matrix was computed to be

$$\mathbf{M}_{RB} = \begin{bmatrix} 5002.6 & 0 & 0 & 0 & -1260.7 & 0 \\ 0 & 5002.6 & 0 & 1260.7 & 0 & 0 \\ 0 & 0 & 5002.6 & 0 & 0 & 0 \\ 0 & 1260.7 & 0 & 4280.2 & 0 & 0 \\ -1260.7 & 0 & 0 & 0 & 19535.6 & 0 \\ 0 & 0 & 0 & 0 & 0 & 19217.9 \end{bmatrix} \tag{6.1}$$

It is important to note that the hydrodynamic software computed the displacement to be approximately 5 tonnes, whilst the factory claims it to be approximately 3,5 tonnes, dry weight. A plausible reason for the large difference is probably related to the factory declaring vessel weight, based on weighing off assembly line, without any equipment, whilst the waterline, which for pleasure crafts often is based on factual measurements including equipment, is featured in the drawing documentation. Then when the vessel draught is entered into the hydrodynamic software, and applied in the computation as the deciding parameter the difference materialize. Weighing of the actual vessel would have solved the uncertainty and probably added knowledge to the software as well. The added mass matrix was computed to be

$$\mathbf{M}_{A} = \begin{bmatrix} 439.7 & 0 & 0 & 0 & 0 & 0 \\ 0 & 1774.3 & 0 & 1057.8 & 0 & 400.6 \\ 0 & 0 & 13722.8 & 0 & 3737.4 & 0 \\ 0 & 843.7 & 0 & 2131 & 0 & 198.7 \\ 0 & 0 & 7605.1 & 0 & 37153.1 & 0 \\ 0 & 361.5 & 0 & 106.8 & 0 & 5176.6 \end{bmatrix}. \tag{6.2}$$

The weight difference influence is actually unknown, it is, however, assumed to have significant impact. Since both $\mathbf{M}_{RB}$ and $\mathbf{M}_{A}$ are constant matrices, a constant total of the two components can be achieved as follows

$$\mathbf{M} = \begin{bmatrix} 5442.3 & 0 & 0 & 0 & -1260.7 & 0 \\ 0 & 6776.8 & 0 & 2318.5 & 0 & 400.6 \\ 0 & 0 & 18725.4 & 0 & 3737.4 & 0 \\ 0 & 2104.4 & 0 & 6411.3 & 0 & 198.7 \\ -1260.7 & 0 & 7605.1 & 0 & 56688.7 & 0 \\ 0 & 361.5 & 0 & 106.8 & 0 & 24394.5 \end{bmatrix}. \tag{6.3}$$

6.3.2 Coriolis and centripetal forces

By using the simplification proposed in Chapter 3 the coriolis and centripetal matrices becomes

$$\mathbf{C}^*_{RB} = U \begin{bmatrix} 0 & 0 & 0 & 0 & 0 & 0 \\ 0 & 0 & 0 & 0 & 0 & 5002.6 \\ 0 & 0 & 0 & 0 & -5002.6 & 0 \\ 0 & 0 & 0 & 0 & 0 & 1260.7 \\ 0 & 0 & 0 & 0 & 0 & 0 \\ 0 & 0 & 0 & 0 & 0 & 0 \end{bmatrix} \tag{6.4}$$

$$\mathbf{C}^*_{A} = U \begin{bmatrix} 0 & 0 & 0 & 0 & 0 & 0 \\ 0 & 0 & 0 & 0 & 0 & 0.17 \\ 0 & 0 & 0 & 0 & -1.37 & 0 \\ 0 & 0 & 0 & 0 & 0 & 0.08 \\ 0 & 0 & 0 & 0 & -0.76 & 0 \\ 0 & 0 & 0 & 0 & 0 & 0.03 \end{bmatrix} \tag{6.5}$$

where U is the relative water speed. The computation inconsistency impact on the coriolis and centripetal forces is unknown, but for practical and simplification reasons, as this being a low speed application, it is assumed to be negligible.

6.3.3 Damping forces

The linear damping matrix was found to be to be

$$\mathbf{D}_L = \begin{bmatrix} 268.09 & 0 & 0 & 0 & 0 & 0 \\ 0 & 1083.3 & 0 & 0 & 0 & 0 \\ 0 & 0 & 0 & 0 & 0 & 0 \\ 0 & 0 & 0 & 84.3 & 0 & 0 \\ 0 & 0 & 0 & 0 & 0 & 0 \\ 0 & 0 & 0 & 0 & 0 & 1274.2 \end{bmatrix}, \tag{6.6}$$

where the yaw damping has been adjusted when fitting the model to recorded data. It was computed to 3185.5 but this was adjusted to 1274.2 which is only 40 % of the original value. It can also be noted that this is a simplification of (3.14) which only contains the most important linear damping terms.

Nonlinear surge damping

By manual curve fitting to recorded data the nonlinear damping was found to be approximately

$$X \approx 11499 \left(\frac{0.075}{\left(log_{10} R_n - 2 \right)^2} + 0.0025 \right) |u_r| \, u_r, \tag{6.7}$$

where R_n is the Reynholds number and u_r the relative water velocity.

Cross flow drag

To calculate the nonlinear viscous current loads in sway and yaw the trapezoidal rule was used to solve (3.20) and (3.20), where the 2D-drag coefficient found in Hoerner [1965] curve, was adjusted to 60 % of its computed value when manually curve fitting the model to the recorded data. The integrals which was solved at each timestep was found to be

$$Y \approx 143.7 \int_{-\frac{L_{pp}}{2}}^{\frac{L_{pp}}{2}} |v_r + xr| \, (v_r + xr) \, dx \tag{6.8}$$

$$N \approx 143.7 \int_{-\frac{L_{pp}}{2}}^{\frac{L_{pp}}{2}} x \, |v_r + xr| \, (v_r + xr) \, dx. \tag{6.9}$$

$$\tag{6.10}$$

In the Simulink simulator a block from Marine Systems Simulator [2009] did the integration.

6.3.4 Restoring forces

The restoring forces were calculated by the hydrodynamical software using the linear approximation described in (3.21) to become

$$\mathbf{G} = \begin{bmatrix} 0 & 0 & 0 & 0 & 0 & 0 \\ 0 & 0 & 0 & 0 & 0 & 0 \\ 0 & 0 & 146197,67 & 0 & -9002,86 & 0 \\ 0 & 0 & 0 & 47648,48 & 0 & 0 \\ 0 & 0 & -9002,86 & 0 & 423188,66 & 0 \\ 0 & 0 & 0 & 0 & 0 & 0 \end{bmatrix}. \tag{6.11}$$

6.3.5 Fluid memory effects

Each of the 6 elements in

$$\boldsymbol{\mu} = \begin{bmatrix} \mu_u \\ \mu_v \\ \mu_w \\ \mu_p \\ \mu_q \\ \mu_r \end{bmatrix} \tag{6.12}$$

consist of a sum of the output of three independent linear systems. The **A**,**B**,**C** and **D** matrices creating these systems where computed by the hydrodynamical software. In total 18 independent linear systems make up the fluid memory effect. The input to these systems are

$$\delta\boldsymbol{\nu} = \boldsymbol{\nu} - \begin{bmatrix} u \\ 0 \\ 0 \\ 0 \\ 0 \\ 0 \end{bmatrix} \tag{6.13}$$

6.3.6 Actuators

The machinery and actuator models described in Chapter 3 was used. In the following these will be presented with the parameter tuning used during simulations.

Main propulsion

As previously mentioned the main propulsion consist of one engine tied to a gearbox with built-in trolling functionality shafted to the main propeller. As it would not be feasible to use 100 % during a DP operation, the throttle range was saturated to ± 60 %. This also helps keeping the model valid as the vessel operates in a low velocity range. The curve featured in Figure 6.2 was used for transforming throttle input to rpm. This was found by using the recorded data, and some qualified assumptions based on the trolling gear properties. In the mapping both engine- and trolling gear dynamics properties are incorporated. The engine dynamics was assumed to be be

$$\dot{\omega_a} = 2\left(-\omega_a + \omega_d\right), \tag{6.14}$$

where ω_a is actual engine RPM. The propeller shaft angular velocity is found by

$$n = \frac{2.03\omega_a}{60}, \tag{6.15}$$

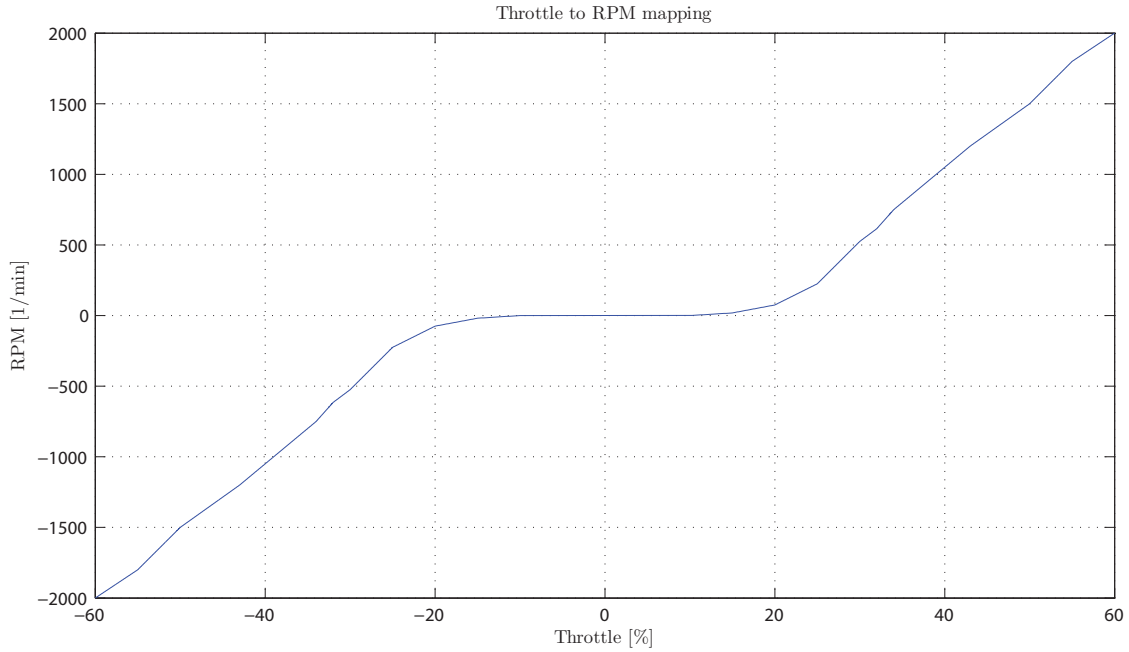

Figure 6.2: Throttle to RPM mapping in the range of ± 60 % throttle.

where 2.03 is the gear ratio and the division of 60 is to convert from [1/min] to [1/s]. The propeller model was found to be

$$X_p = 29.37n\,|n| - 6.12\,|n|\,u_a, \tag{6.16}$$

Rudder

The machinery consists of a linear servo manipulation the rudder angle by moving the rudder arm. The parameters of the low pass approximation of the linear servo were after inspecting the vessel found by trial and error along with qualified guesses to become

$$\dot{\delta}_a = 2\,(-\delta_a + \delta)\,, \tag{6.17}$$

where a rate saturation limits $\dot{\delta}_a$ to change less than 10 [deg/s]. Using the hydrodynamical calculated CG the rudder position was found to be

$$\begin{bmatrix} -3.5 \\ 0 \\ -1.17 \end{bmatrix} \tag{6.18}$$

relative this. The rudder span and cord where found to be 0.55 and 0.275 [m] respectively. By assuming 2 m/s and the rudder dimensions C_{D0} is approximated to be

$$C_{D0} \approx 0.0135 \tag{6.19}$$

Based on the rudder dimensions, the rudder aspect where found to be ≈ 2, declaring the rudder span to length ratio.

The derivative $\frac{\delta C_L}{\delta \alpha_e}$ of the lift coefficient C_L for a rudder with aspect ratio of 2 is found to be ≈ 2.65 in [Bertram, 2000]. The rudder model used is as follows

$$X_r = 77.5 v_r^2 \left(8.64 \frac{\delta^2}{\pi} + 0.0135 \right) \tag{6.20}$$

$$Y_r = 205 v_r^2 \ \delta \tag{6.21}$$

$$K_r = -183.5 v_r^2 \delta \tag{6.22}$$

$$N_r = -717.4 v_r^2 \delta \tag{6.23}$$

The rudder model from Marine Systems Simulator [2009] implementing the above equations was used in the simulator. The relative water-speed flowing past the rudder was estimated using (5.3). This is threated further in 6.3.8.

Tunnel Thruster

Due to being an electrical on-off thruster, the spin-up time was assumed to be short. Hence the dynamics was set to

$$\dot{\alpha} = 50 \left(-\alpha + \alpha_d \left(C_{TT} \right) \right). \tag{6.24}$$

Here, the magnitude of C_{TT} was, after manually curve fitting the model to recorded data, found to be ± 20. The tunnel thruster was approximated to have a longitudinal distance of 3 [m] forward of the CG, giving the following yaw moment contribution

$$N_{TT} = 29.43 \alpha \tag{6.25}$$

6.3.7 Model validation

To constitute robust results when validating mathematical models against real world systems, requires data comparisons from both sides. In this case several parts could be validated separately, however, due to time constraints and vessel usage/access limitations, the two most important are displayed. Figure 6.3 features the surge speed as a function of throttle, where both model and actual vessel response is plotted. Unfortunately a minor problem with the Simulink setup disabled the throttle set-points recordings and for this reason the time of each step is only assumed in the model response. The step throttle magnitudes used were [25 35 40 45] [%]. As seen on the plot which closely follows the recorded data, the figure shows good vessel model performance. If more data were recorded, and curve fitting alogrithms applied to obtain the parameters, the result could have been better.

For the system to work under physical conditions, the yaw dynamics are the most important to be correct. Figure 6.4 features the yaw rate response of the vessel and model using the

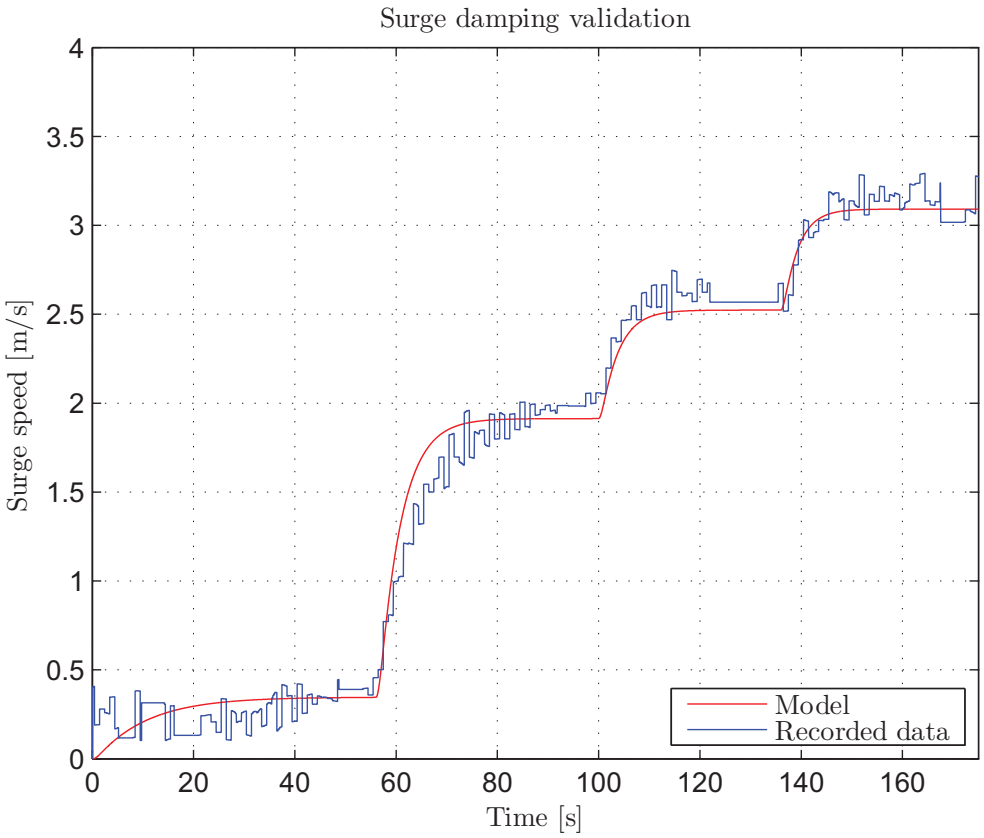

Figure 6.3: Surge speed validation using recorded vessel data.

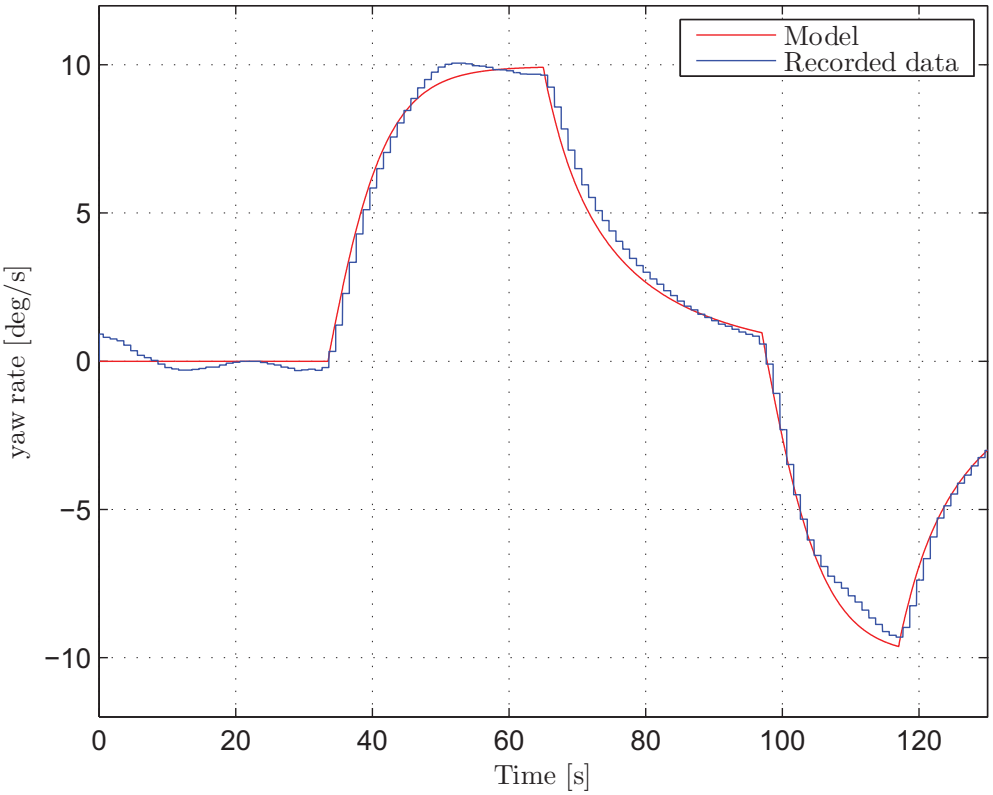

Figure 6.4: Yaw rate validation using recorded data.

approximate same input. When the data were recorded, due to lack of control interface implementation, the tunnel thruster was operated manually. Fortunately it was easy to identify the input which was 1 from 33.5 [s] to 65.5 [s], -1 from 97 [s] to 117 [s] and 0 elsewhere. It can be seen that the model follows the recorded data with high precision, both during thruster bursts and free movement.

Compared to the problem complexity and due to the low available data amount several sources of error are obvious and might cause deviations between the real vessel and model, in fact probably one of the root causes of the inconsistencies. In both cases the response is a function of two models. First the actuator interface input goes through the actuator model and is converted to a force or moment, acting on the vessel. Even though the response from interface to output velocity, or yaw rate, seems desirable, there might still be significant deviations between each of the models and its physical counterpart. The environmental disturbance on the recorded data is unknown, and might give a biased result, even the fact that the weather was calm when the tests were conducted, might constitute one such error. Another example is vessel response to reversing engine power. Dynamics which are not captured by the recorded data, will most certainly differ due to the structural vessel design

causing the damping to be different. To obtain a good model, high precision measurement devises must be used to record large amounts of data, subsequently used to obtain correct vessel parameters.

6.3.8 Estimation of propeller water-speed

The propeller area is 0.74 of the total disc area which have a diameter of 21". Using this and $\rho = 1025$ the parameters of (5.3) was found to be

$$10\dot{u}_p = -1963\,|u_p|\,u_p + 3140\,|u_p|\,u_a - 1177\,|u_a|\,u_a + T_p, \tag{6.26}$$

where the mass inside the Bernoulli tube was assumed to be 10 [kg]. The a constant was set to 0.2 after trial and error.

It is not highly important for the parameters in (6.26) to be correct. The main aim of this model is to provide a measurement that adds more information on the potential effect of the rudder, apart from the obvious forward velocity.

6.3.9 Environmental models

Current

The current model described in Chapter 3 was implemented as stated and current direction and magnitude were adjusted in each simulation study. In order to use the current in accordance with the vessel model, a rotation matrix was applied to translate the current from the NED to the BODY frame

$$\boldsymbol{\nu}_c = \begin{bmatrix} \cos\psi & \sin\psi & 0 \\ -\sin\psi & \cos\psi & 0 \\ 0 & 0 & 1 \end{bmatrix} \mathbf{v}_c, \tag{6.27}$$

where $\mathbf{v}_c$ is the same as in (3.50). This BODY fixed current vector was subtracted from $\boldsymbol{\nu}$ to form

$$\boldsymbol{\nu}_r = \boldsymbol{\nu} - \boldsymbol{\nu}_c \tag{6.28}$$

which is input to the centripetal and coreolis term and damping term of (3.2).

Waves

The wave model used was already implemented in the template. It is based on building blocks from [Marine Systems Simulator, 2009] and applies the force RAOs computed by the hydrodynamics software to calculate the forces acting on the vessel. Both high frequency

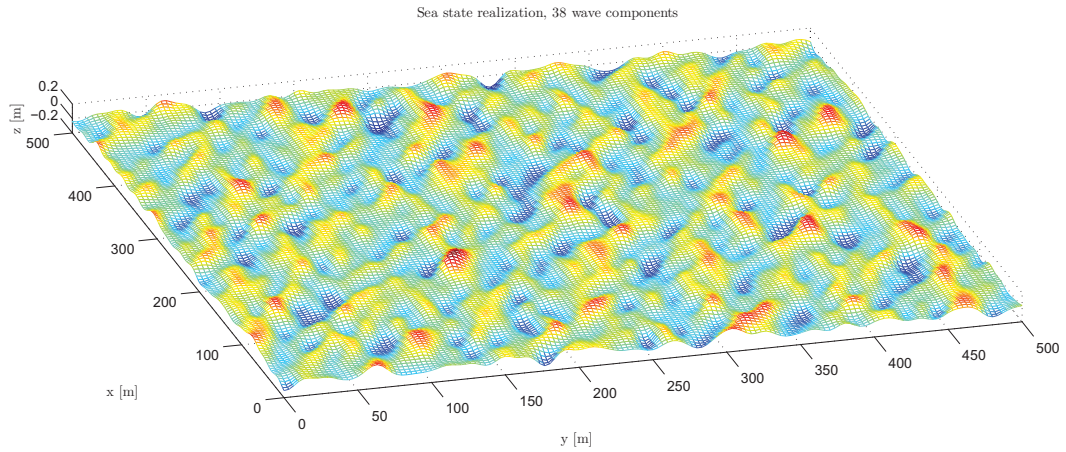

Figure 6.5: Sea state realization created by the wave Simulink wave block using 38 wave components, 90 [deg] direction and a significant wave height of 0.2 [m].

waves and drift forces are calculated in the wave model. It was set up using different significant wave heights in each simulation. The peak frequency was set to use north sea statistical data, the mean wave direction was different in each simulation, and a wave spreading factor of 2 was used. To simulate deep waters, the water dept was set to infinite. 20 frequencies and 10 directions in each grid was used, 50 wave components and using default frequency and direction cut-off factors.

Figure 6.5 features a visualization of a sea state based on the above settings along with 0.2 [m] significant wave height at 90 [deg]. This is an irregular short crested sea state realization for deep waters and open sea. Due to varying depths and obstacles affecting the wind-fetch, the sea states in sheltered waters are assumed to be different. Respective to this thesis, the significances of different sea state properties it is not highly important. The important issue to the model development is to have access to a wave disturbance, oscillating and creating yaw moment and drift forces, similarly to real world. In sheltered waters, partly due to wave propagation and reflections from surrounding landscape the number of wave components is assumed to be higher, resulting in a different frequency spectrum. This is also anticipated to results in other physical characteristics of each separate wave.

Wind

The simulator implements a wind disturbance in surge, sway and yaw as described in [Blendermann, 1994]. The procedure is similar to the equations described in Chapter 3. To calculate the approximate wind forces and corresponding moments, the vessel length, frontal and longitudinal projected areas above the waterline, and their respectice centroids, in addition to the vessel type are applied. The vessel type is used to determine a set of predefined parameters suitable for a certain vessel type. Figure 6.10 displays the assumed

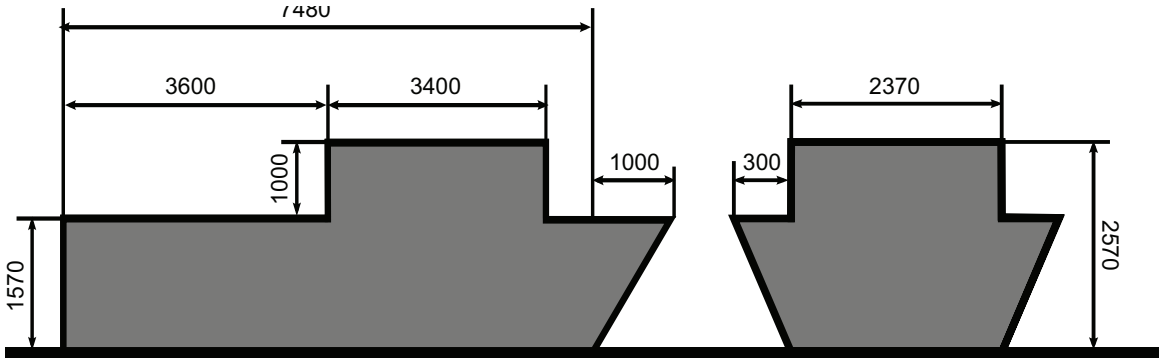

Figure 6.6: Approximate contour of the Viknes 830.

contour of the Viknes 830 which was used to calculate the following parameters

$$A_{Fw} = 6.56 \ \ [m^2] \tag{6.29}$$
$$A_{Lw} = 15.93 \ \ [m^2] \tag{6.30}$$
$$s_H = 0.03 \ \ [m] \tag{6.31}$$
$$s_L = 0.904 \ \ [m], \tag{6.32}$$

where A_{Fw} is the frontal projected area, A_{Lw} is the longitudinal projected area, s_H is the horizontal distance to the centroid of A_{Lw} from the main section of the vessel and s_L is the vertical distance to the centroid of A_{Lw} from the water-line. Due to having the wheelhouse in front, which gives approximately the same wind characteristics as an offshore supply vessel, this structure was chosen for vessel type, resulting in the following wind vector

$$\boldsymbol{\tau}_{wind} = \begin{bmatrix} \frac{1}{2} C_X \rho_a V_r^2 A_{Fw} \\ \frac{1}{2} C_Y \rho_a V_r^2 A_{Lw} \\ 0 \\ 0 \\ 0 \\ \frac{1}{2} C_N \rho_a V_r^2 A_{Lw} L_{oa} \end{bmatrix} \tag{6.33}$$

where the V_r is the relative wind speed, ρ_a is the air density at $15°C$ which is 1.224 $[kg/m^3]$ and L_{oa} is the overall length. The wind coefficients are determined by

$$C_X = \frac{-CDlAF\cos(\gamma_r)}{1 - \frac{1}{2}\delta\left(1 - \frac{CDl}{CDt}\right)\sin\left(2\gamma_r\right)^2} \tag{6.34}$$
$$C_Y = \frac{CDt\sin(\gamma_r)}{1 - \frac{1}{2}\delta\left(1 - \frac{CDl}{CDt}\right)\sin\left(2\gamma_r\right)^2} \tag{6.35}$$
$$C_N = \left(\frac{s_L}{L_{oa}} - 0.18\left(\gamma_r - \frac{\pi}{2}\right)\right) C_Y \tag{6.36}$$
$$\tag{6.37}$$

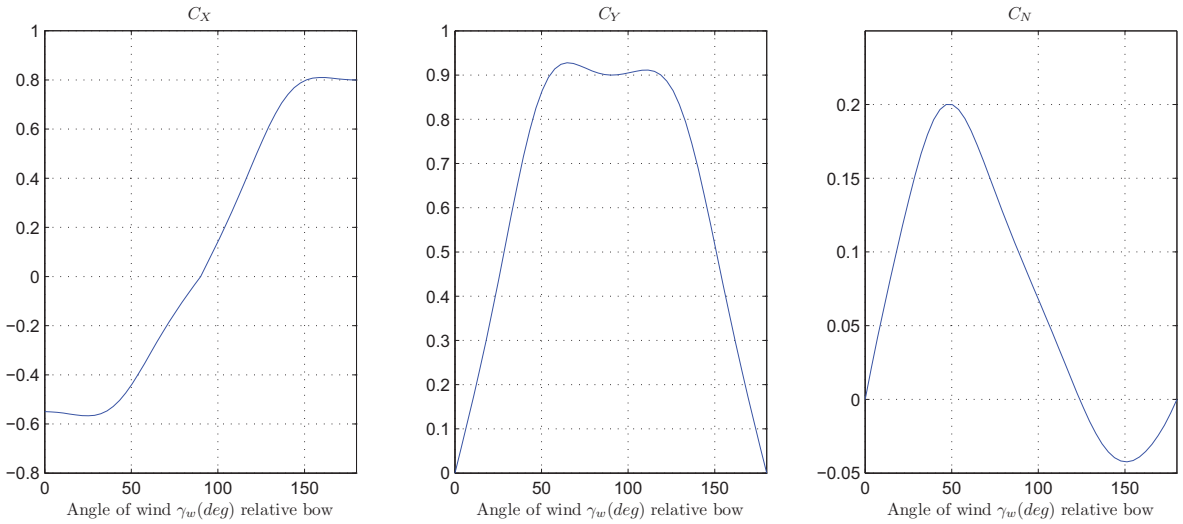

Figure 6.7: Wind coefficients based on Viknes data and offshore vessel type.

where $CDlAF$ is determined by the wind direction relative to the bow or stern to be either 0.55 or 0.80. δ and CDt is also a predetermined vessel type parameters which in the case of an offshore supply vessel is 0.55 and 0.90. CDl is determined by

$$CDl = CDlAF\frac{A_{Fw}}{A_{Lw}} \tag{6.38}$$

By using this equation, the above the wind coefficients where found and plotted in Figure 6.7. This is naturally an approximation of the real world and the coefficients are assumed to differ to some extent due to uncertainties in vessel parameters and discrepancies in the assumed vessel type contour. The most important effects of the wind are to induce a disturbance, heavily affecting the vessel heading and drift.

Wind is often composed by one mean and one gusty component. This was modelled as the integration of a band-limited white noise signal.

$$V_{wg} = \int w_V dt \tag{6.39}$$

$$\beta_{wg} = \int w_\beta dt, \tag{6.40}$$

$$\tag{6.41}$$

where w_V was set up with a noise power of 0.001 and w_β 0.1. In order to create a turning wind influence a first order process with time constant of 100 [s] was applied. The magnitude of the step input to the turning dynamics was specified in each simulation where it was used.

6.4 Parameter discussion

In the vessel model most parameters where found using the result from the hydrodynamic software. The exception is the nonlinear drag which was adjusted to fit recorded vessel data. The data where collected during testing the vessel for learning and understanding its capabilities and limitations, and consist mainly of velocity and position measurements in addition to system variables. As there are no measurements from the actuators, and very little information on the vessel characteristics, there are several unknowns creating a difficult parameter values determination. Due to this thesis time limitations the nonlinear drag was adjusted to fit the recorded data by trial and error.

The actuator parameters where found through vendor data-sheets, drawings and existing recorded data, if feedback had been available all the parameters could have been validated and adjusted. In case of the propeller, no characteristics could be released to this scientific work and the vendor supplied the dimension- and type information only. For this reason a standard propeller model was chosen, subsequently there are uncertainties whether this encompasses all of the dynamics of a skew-back propeller claiming to have better performance. Further in case of the rudder, the uncertainties are tied to the factual rudder angle and convergence time when set at maximum in the interface. Also the tunnel thruster lacks modelled effects, such as the ventilation possibility in waves and the dynamics of the battery depletion. The reduced efficiency as a function of forward velocity is neither modelled.

Despite several uncertainties tied to the model parameters it still reflects a good measurement of low velocity applications. The performance difference between real world vessel and model is small. Based on this it can be concluded that the model is applicable for performance tests. The model is valid for low speeds before the semi-planing dynamics occur.

Access to further experimental time feedback from the actuators could be mounted and experiments constructed to improve the model. In some cases extra sensor equipment should be mounted to capture all effects. By recording long data series of each actuator and the vessel in total a curve fit strategy could be applied to enhance parameter precision in the individual models. By doing so the environmental effects on the recorded data series could be minimized.

6.5 Controller and thrust allocation setup

The top-layer control system and thrust allocation is featured in Figure 6.8. Both during simulations and experimental tests this structure remained the same.

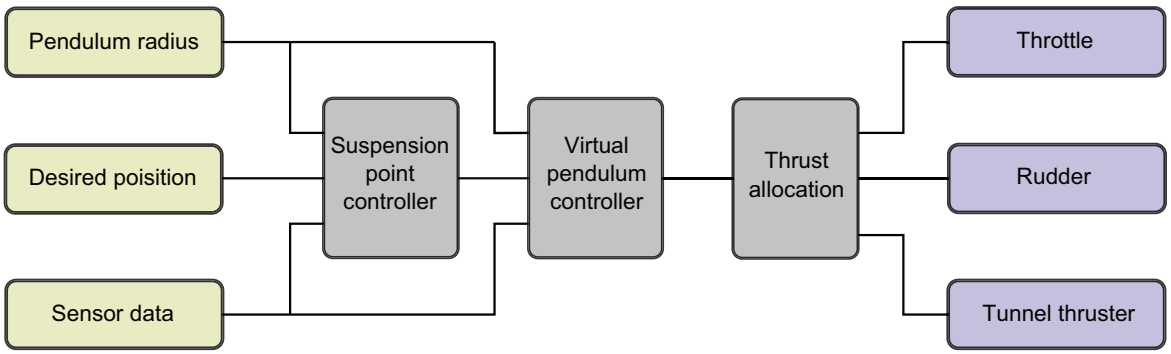

Figure 6.8: Control system and thrust allocation connected to vessel interface.

6.5.1 Suspension point controller

The suspension point movement dynamics where set up as described in Section 4.4applying the following parameters found by trial and error.

$$\dot{\psi}_d = k(\epsilon)(-\psi_d + \psi_c), \tag{6.42}$$

where $k(\epsilon)$ is a adaptive gain defined as

$$k(\epsilon) = \epsilon + 0.004, \tag{6.43}$$

and

$$\dot{\epsilon} = 0.05\left(-\epsilon + \left|\dot{\psi}_c\right|\right). \tag{6.44}$$

The $\left|\dot{\psi}_c\right|$ is found by using a derivative block in Simulink.

6.5.2 Virtual pendulum controller

The virtual pendulum controller which is responsible for the WOHC functionality was implemented as described in Chapter 4. It consists of three separate controllers calculating set-points for the vessel interface. To determine which of the two yaw controllers to be active, a switching law was applied.

Surge controller

The surge controller was set up with the following tuning

$$\tau_{surge} = K_{d_s}\left(u_d - u\right) + K_{i_s}\int \kappa_i e_{b,surge} d\tau \tag{6.45}$$

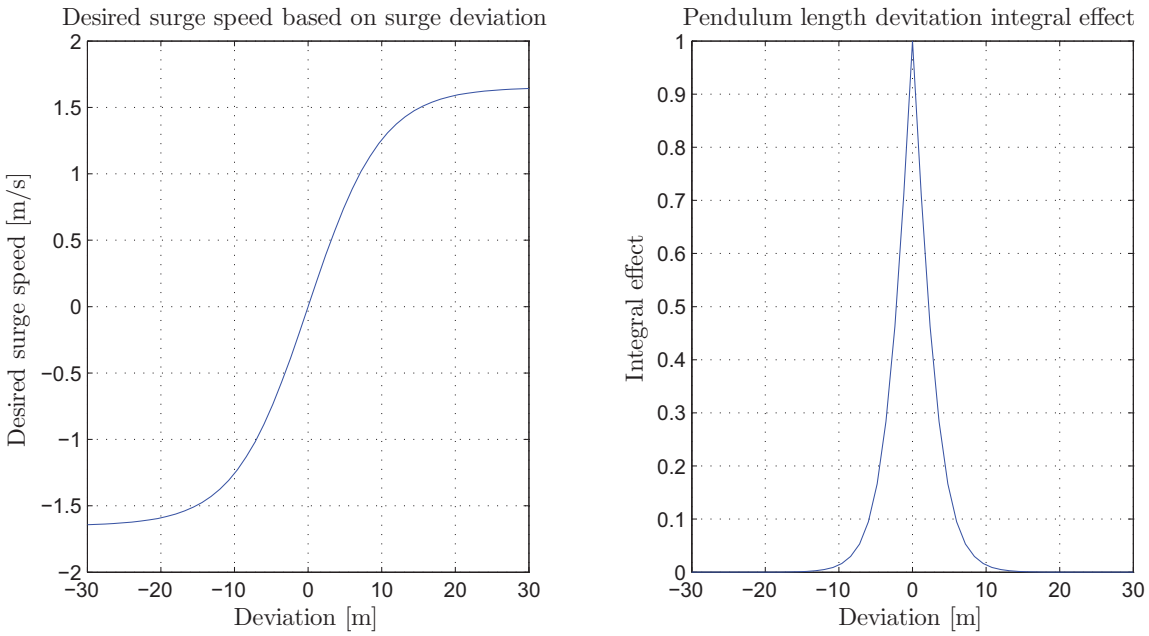

Figure 6.9: Desired surge speed and integral effect based on pendulum length deviation.

where

$$K_{d_s} = 1000 \tag{6.46}$$

$$K_{i_s} = 10 \tag{6.47}$$

A controlled approach towards the desired position was achieved by adjusting the sigmoid function describing the velocity profile to give a top speed of 1.65 [m/s].

$$u_d = 1.65 \tanh\left(\frac{e_{b,surge}}{10}\right). \tag{6.48}$$

where $e_{b,surge}$ is the body fixed deviation in surge to the desired position. The integral effect was tuned to become

$$\kappa_i = 1 - \left|\tanh\left(\frac{e_{b,surge}}{4}\right)\right|. \tag{6.49}$$

Figure 6.9 features both desired surge speed and integral effect based on the pendulum length deviation. If the vessel ends up in a state outside the limits of the integral effect this could be detected and the integral limits expanded to encompass the vessel correcting the pendulum length.

Yaw controller switch law

The switching law was implemented through a relay block in Simulink, which was set up to change from tunnel thruster to rudder control, if the estimated water-speed from

the propeller exceeded 1 [m/s] and from rudder to tunnel thruster at 0.9 [m/s]. Even though the switching values are quite close, this worked satisfactory without undetermined controller problems.

Rudder controller

The rudder controller was tuned to

$$\tau_{\psi_r} = 1000\,(r_d - r)\,, \tag{6.50}$$

where

$$r_{d_r} = \frac{6\pi}{180}\tanh\left(\frac{\psi_c - \psi}{0.2014}\right). \tag{6.51}$$

The maximum turning rate when using the rudder was set to 15 [deg/s]. The maximum turning rate is correlated with the water-speed past the rudder, hence an adaptivity could be used to calculate gains in (6.51) which considers this. In turn this might lead to increased precision and enhanced performance.

Tunnel thruster controller

The tunnel thruster controller was set to

$$\tau_{\psi_t t} = (r_{d_{tt}} - r)\,, \tag{6.52}$$

where

$$r_{d_{tt}} = \frac{8\pi}{180}\tanh\left(\frac{\psi_c - \psi}{1.4}\right). \tag{6.53}$$

The rationale behind this is to obtain a better intuitive thrust allocation scheme. The maximum desired rotation rate was set to 8 [deg/s] which is 2 [deg/s] lower than the maximum yaw rate when using the tunnel thruster. The idea of the controller is to use the on-off tunnel thruster as a pulse-width modulate signal to obtain the desired velocity, subsequently resulting in the desired heading. The conversion from $\tau_{\psi_t t}$ to pulses will be covered below when discussing thrust allocation setup.

6.5.3 Thrust allocation setup

Propeller water-velocity estimation

The propeller water-velocity estimation was set up by using a first order filter to represent the engine dynamics as

$$\dot{\omega_e} = -\omega_e + rpm_d, \tag{6.54}$$

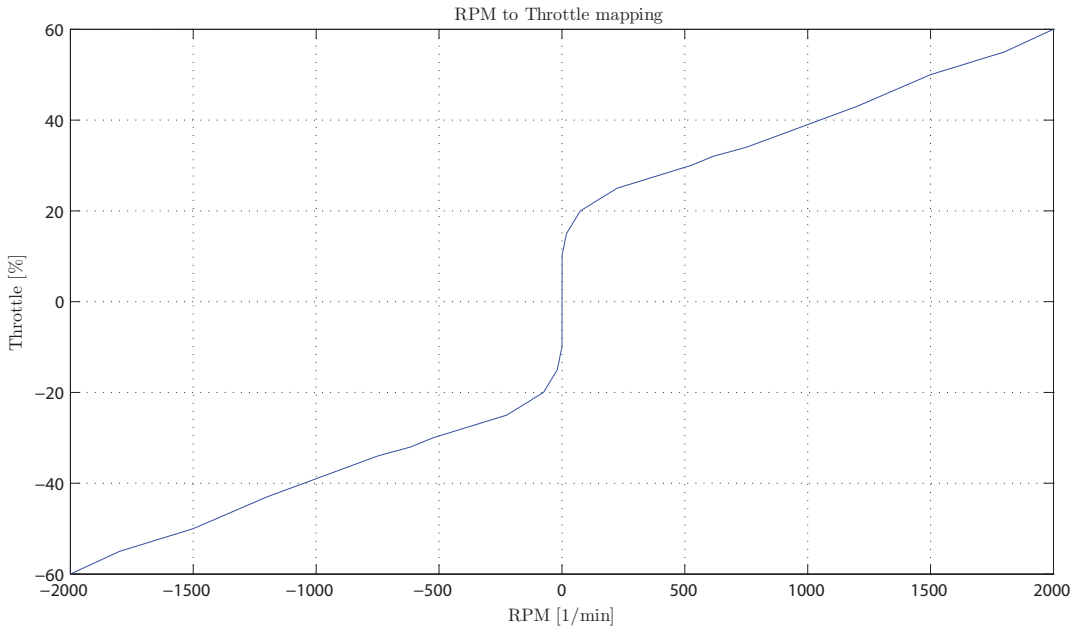

Figure 6.10: RPM to throttle mapping used in the thrust allocation.

where rpm_d is the desired rpm calculated by the surge allocation. ω_e is used as input to a propeller model along with the forward velocity using the same model tuning as described in (6.26). The calculated thrust from the propeller model was used as input to the same model as described in section 6.3.8 estimating the velocity of water through the propeller.

Surge allocation

The rudder allocation was set up as described in Section 5.2.1 and the rudder model featured in 6.3.6 was applied. The proposed simplification was used to derive ω was also used, which gives

$$\omega = \frac{X}{|X|}\sqrt{122.5\,|X|} + 6.65u_a \tag{6.55}$$

As it is not the true solution of (5.4), this approach has several problems, however the deviation is small. This could have been solved numerically, but a continuous approach was preferred due to the better real-time capabilities. The mapping between ω is displayed in Figure 6.10 and is a product of recorded data and qualified guesses based on a few trial and error iterations.

Rudder allocation

The rudder allocation was set up as described in Section 5.3.2 which gives the following

$$\delta = \frac{N}{717.3u_p^2} \tag{6.56}$$

In order to protect δ from becoming infinite u_p is set to 0.1 [m/s] if closer to zero. This is not a practical problem as the tunnel thruster will operate in the previously mentioned rudder water-speed range. To provide a signal for the rudder actuator to follow, the rudder machinery model was implemented post the angle calculation. The dynamics of this were set up to be the same as for the rudder machinery, seen in (6.17).

Tunnel thruster allocation

The tunnel thruster allocation was set up as described in Section 5.3.1 and the implementation where done by code running through a MATLAB function block. The relay zone Φ was set to have an amplitude of 5 [deg] and the breaking zone 3 [deg] which in worst case give a total gives a heading deviation of 5 [deg], Λ was set to 0.5 [deg/s] and the shortest burst interval Δt to 0.1 [s]. The tunnel thruster buffer was also implemented, but was used for blocking thruster usage only, if the thruster run-time exceeded 25 sec. Due to not implemented on the real world vessel, and as it was hard not to violate, given the vessel setup , the limitation on mean usage was not used during simulations.

6.6 Simulation results

In order to refer the weather conditions used in the simulations to the real world the Beaufort wind scale force was updated using (3.54) to include the wind-speeds 1 [m] above the surface instead of 10 [m]. Table 6.6 contains the updated wind data. In sheltered waters the wave heights are assumed to be significantly lower than stated in the Beaufort wind scale.

6.6.1 WOHC

To display the performance of the WOHC system, a series of scenarios were simulated. The first is a simple force field displaying basic functionality and performance of the surge, rudder and tunnel thruster controllers. The second is a more complex sea state with minor waves and wind. The last one is harsh conditions with heavy wind, waves and current. The simulations features the extremes of what can be expected operating range in the real world. In the scenarios outlined, three simulations are carried out to display the pendulum length

Beaufort nbr	Description	Wind speed	Wave height	Sea conditions
0	Calm	< 0.1 m/s	0 m	Calm (glassy).
1	Light air	0.1-0.6 m/s	0-0.2 m	Calm (rippled).
2	Light breeze	0.6-1.3 m/s	0.2-0.5 m	Smooth (wavelets).
3	Gentle breeze	1.3-2.1 m/s	0.5-1 m	Slight.
4	Moderate breeze	2.1-3.1 m/s	1-2 m	Slight-Moderate.
5	Fresh breeze	3.1-4.3 m/s	2-3 m	Moderate.
6	Strong breeze	4.3-5.5 m/s	3-4 m	Rough.
7	Near gale	5.5-6.8 m/s	4-5.5 m	Rough-Very rough.
8	Gale	6.8-8.2 m/s	5.5-7.5 m	Very rough-High.
9	Severe gale	8.2-9.7 m/s	7-10 m	High.
10	Storm	9.7-11.3 m/s	9-12.5 m	Very High.
11	Violent storm	11.3-13.0 m/s	11.5-16 m	Very High.
12	Hurricane	> 13.0 m/s	> 14 m	Phenomenal.

Table 6.1: The Beaufort wind force scale. Wind is measured at 1 m.

effect on the performance. The pendulum lengths considered was $r_{circle} = 8$, $r_{circle} = 30$ and $r_{circle} = 50$.

Simple force field sea state

A simple sea state is generated by only using current disturbance of 0.5 [m/s] magnitude and at 90 [deg] direction. This condition mirrors the functionality of the surge, rudder and tunnel thruster controllers and does not correspond to a state in the Beaufort scale. The only places where such conditions are found are in rivers and areas heavily affected by tides. The suspension point was set to 65 [m] at 0 [deg] ahead of the initialization of each vessel. Figure 6.11 is a visualization of the scenario where the disturbance direction can be seen as an arrow. The color bar to the right of the figure pictures the simulation time which was set to 400 [s]. The time between each vessel drawing is equal and demonstrates the relationship between convergence time and pendulum length.

The tunnel thruster effects can easily be observed in Figure 6.12 which features the heading of each vessel as discontinuous plots. The nature of the tunnel thruster makes it difficult to converge to the precise weather optimal heading, giving room for a small projected area towards the weather. With time this creates enough angular deviation for the tunnel thruster to be used. This tendency is seen in the tunnel thruster usage plot in Figure 6.14 where some bursts are used after convergence to the approximate weather optimal heading, and in Figure 6.11 through the slight misalignment of the vessels. This effect decreases with the pendulum length as the vessel must be moved a further distance for the deviation

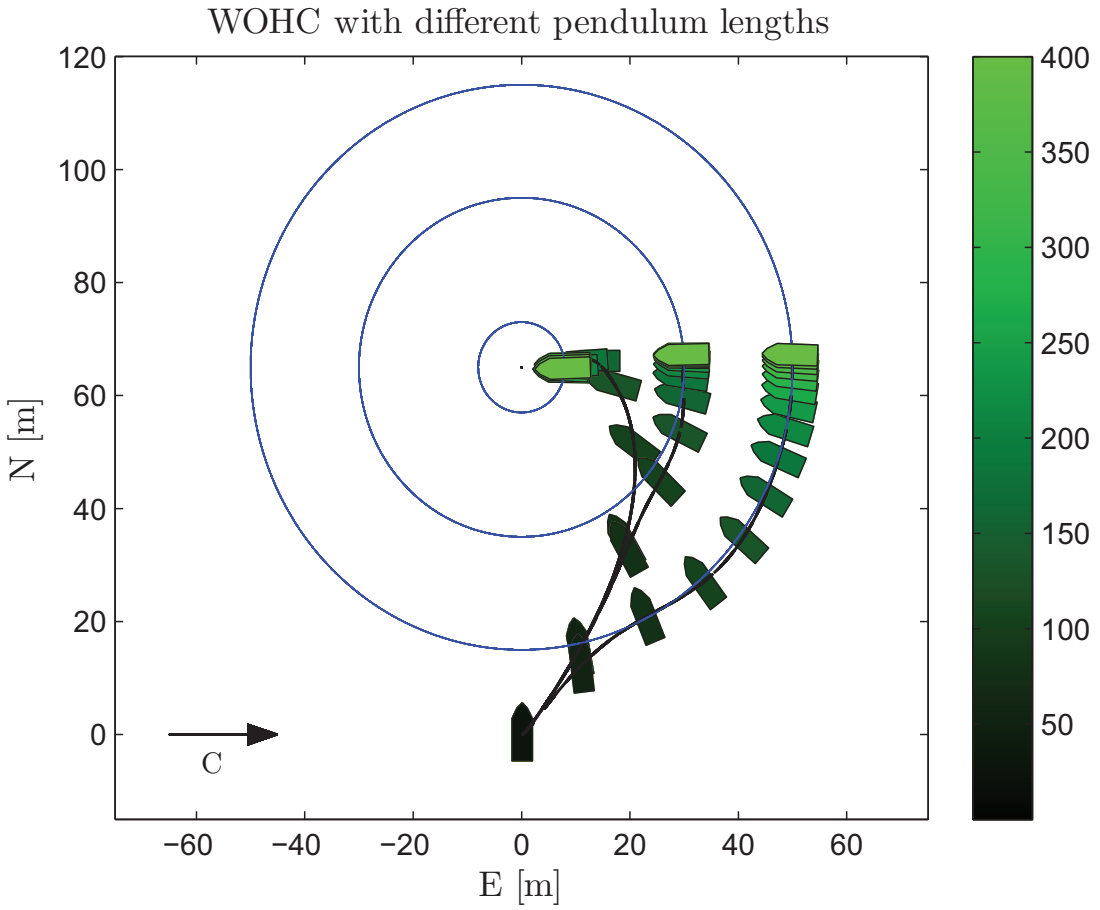

Figure 6.11: WOHC visualization in simple constant force field sea state where C marks the current force direction.

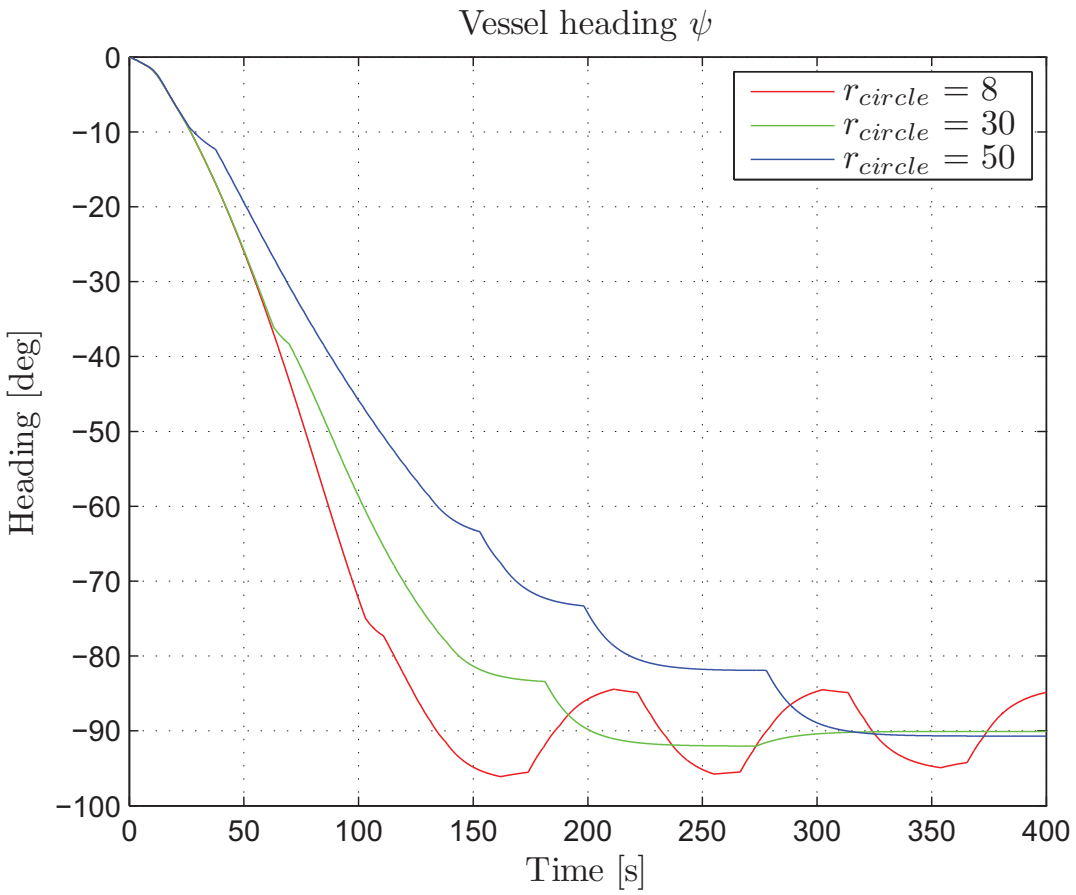

Figure 6.12: WOHC vessel heading in simple constant force field sea state.

relative the pendulum length to justify a tunnel thurster correction burst.

From Figure 6.12 it can be seen that the tunnel thruster is able to obtain a heading which in worst case is 5 [deg] from relative to the desired. Enhanced performance could possibly be achieved through by a better controller with optimal tuning. One of the major problems is the necessary enable time interval before it can be disabled, which causes a significant movement.

In Figure 6.13 the convergence to the respective circle can be seen. Convergence to the smallest circle takes the longest time, however this is natural, as the distance from the starting position is the longer one. The actuator usage of the scenario can be seen in Figure 6.14. The vessel-circle deviation is removed and the disturbance is counteracted using the main propulsion, resulting in constant throttle, proportional to the current magnitude. When traveling towards the circle, the control system uses the rudder to keep the heading towards the suspension point. Due to reduced speed and rudder efficiency on the final approach to the circle, the control system switch to tunnel thrusters heading control based

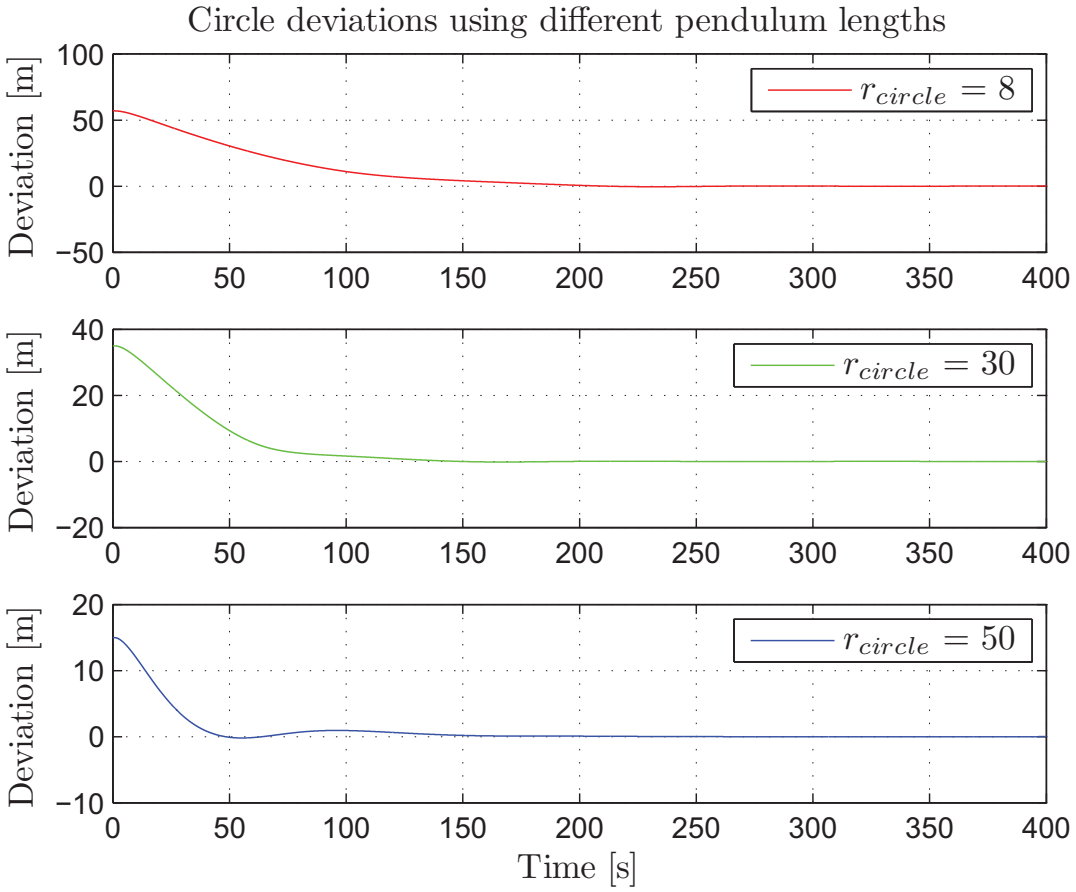

Figure 6.13: WOHC vessel deviation from circle arc in simple constant force field sea state.

on the previous mentioned switch law. This can be seen in the two lower plots of Figure 6.14 where the switch occurs after 100 [s] in case of the 8 [m] pendulum and 60 [s] for the 30 [m] pendulum. The system using the 50 [m] pendulum is sufficiently close to the arc not to gain enough water-speed past the rudder to use it.

Convergence time to the weather optimal heading is correlated to the length of the pendulum, and this is noticeable for the three selected pendulum lengths. The longest pendulum has a greater circle arc distance to travel and more time than the shorter ones. The convergence time is the same as the time to reach -90 [deg] in Figure 6.12. Under such optimal conditions, where no environmental yaw moments are affecting the vessel, an on-off tunnel thruster is sufficient, and outputs high system performance.

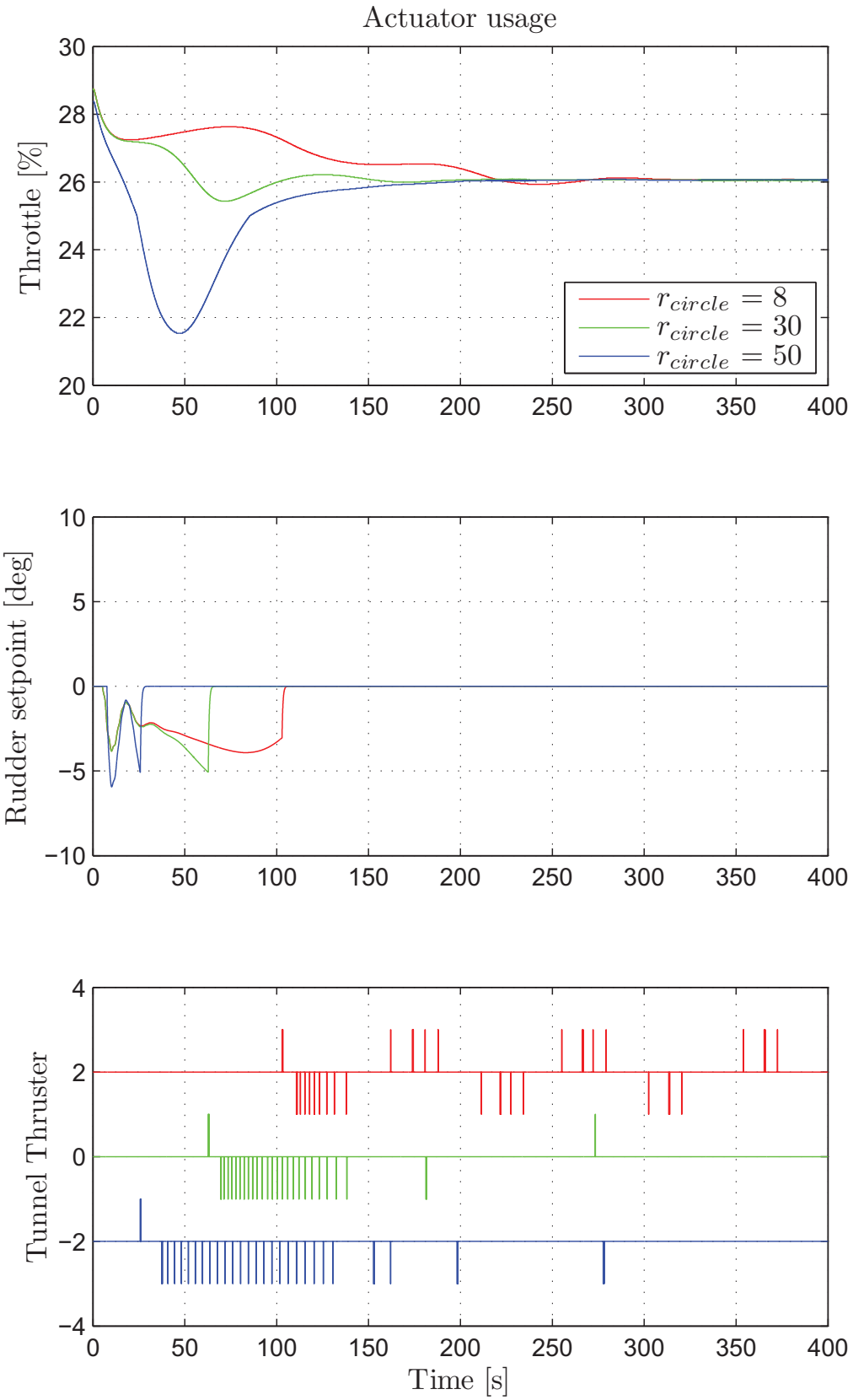

Figure 6.14: WOHC vessel actuator set-points in simple constant force field sea state. Rudder is converted from interface range to degrees for better understanding.

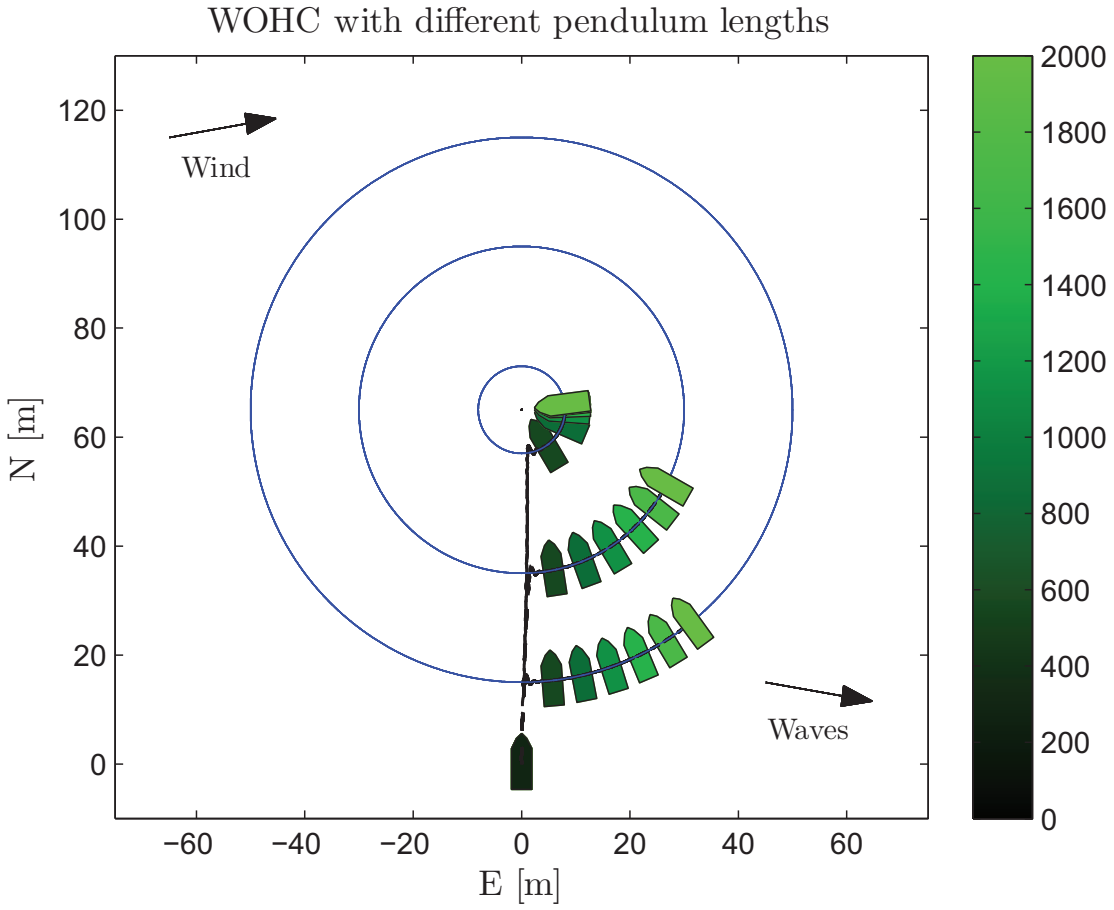

Figure 6.15: WOHC visualization in complex sea state where the arrows mark wave and wind direction.

Gentle breeze and wavelets

Sea states dominated by strong current are uncommon in the real world, despite in rivers and some areas heavily affected by tides. A more common sea state is relatively good weather where minor wind disturbances and ripples on the surface occurs. When the driving forces of the system are small, and due to little environmental force driving the system, the convergence time will be high. A scenario reflecting such conditions was set up by using 1.5 [m/s] wind-speed at 80 [deg] and wave disturbance based on the ITTC spectrum, holding 0.2 [m] significant wave height at 100 [deg] direction. This sea state corresponds to Beaufort 3 which is gentle breeze with wavelets on the surface. The simulation time was set to 2000 [s]. The suspension point was set to 65 [m] at 0 [deg] ahead of the initialization of each vessels using the same pendulum lengths as above.

Figure 6.15 features a visualization of the scenario where it can be seen that only one vessel

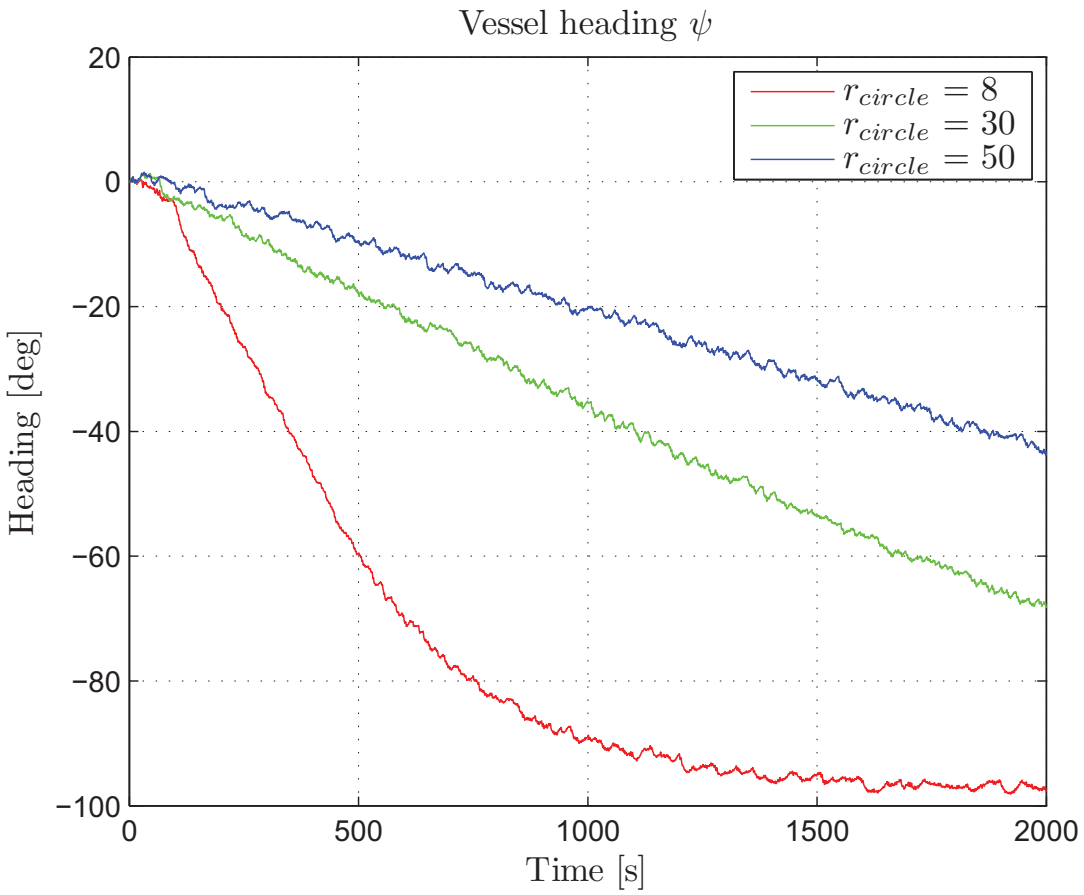

Figure 6.16: WOHC vessel heading in complex sea state.

have not converged to the optimal heading. The heading angle plot in Figure 6.16 confirms this where only one stable heading is obtained. Even though little drift forces are present the system works and the two vessels using the longer pendulums will slowly converge. The wave disturbance creates a oscillatory throttle usage, which is seen in the top plot of Figure 6.18. Due to nonlinear response and the dead-zone between ± 20 % the throttle usage seems more violent than it actually is. However, as expexted, it becomes clear that the prime mover is not capable of fully couteracting the oscillatory wave disturbance.. Some form of wave filtering could possibly enhance performance, but several difficulties are tied to this due to the small vessel inertia and first order wave imposed motions.

The circle deviation can be seen in Figure 6.17 where a minor overshoot can be observed. It is believed that this comes form the integral effect, and could possibly be avoided by other tuning. However this would most likely affect the convergence time in harsh weather. This indicates that having a sea state adaptive controller might be feasible to obtain the best performance in every scenario.

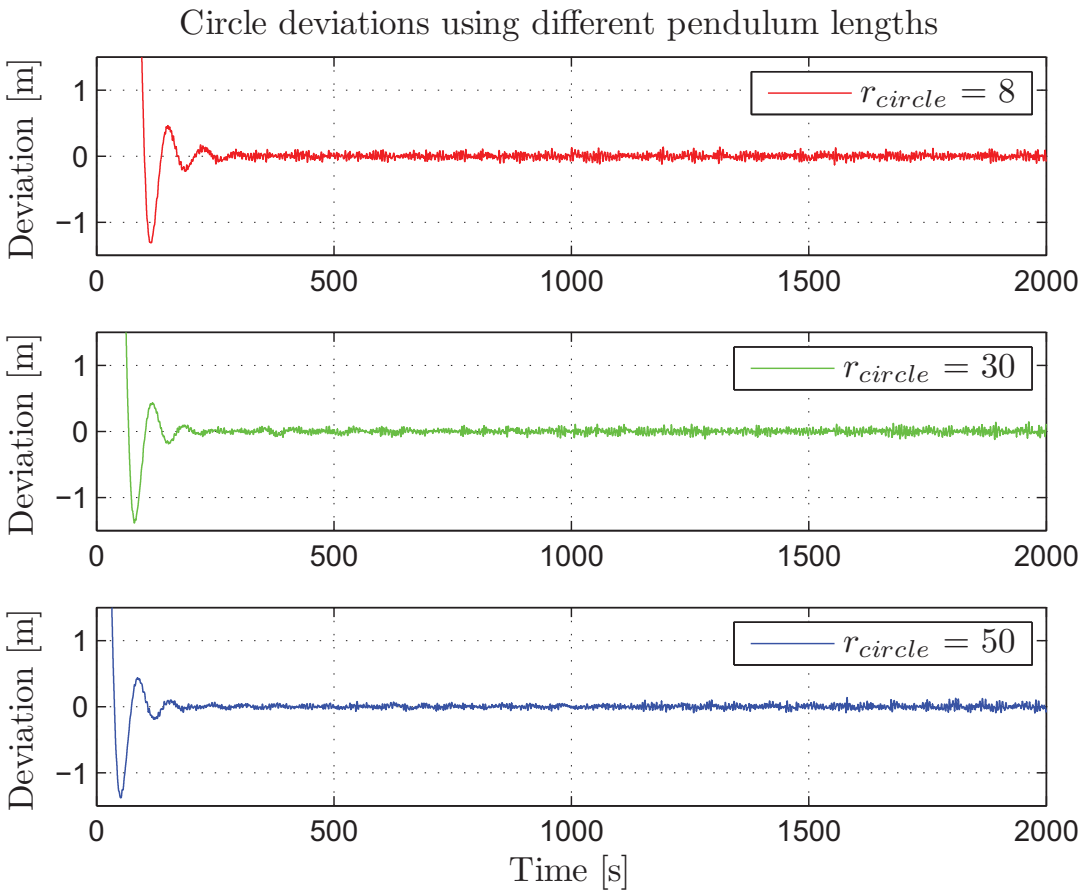

Figure 6.17: WOHC vessel deviation from circle arc in complex sea state.

The tunnel thrusters/rudder interaction is equal to the one used in the case of the simple sea state. The rudder is used when approaching the circle, and the tunnel thruster on and close to it. During convergence the tunnel thruster is used to correct the heading deviation, the result of this is seen in the two bottom plots in Figure 6.18. The usage clearly exceeds the limit 8% of total time, but the constraint was deliberately dismissed due to system performance issues. The weather optimal heading convergence time justifies having a short pendulum, even though it is assumed to use the tunnel thurster after convergence. A scheme might be to use a short pendulum, and increase the length after convergence. However this would cause extra movement, after the optimal heading is found.

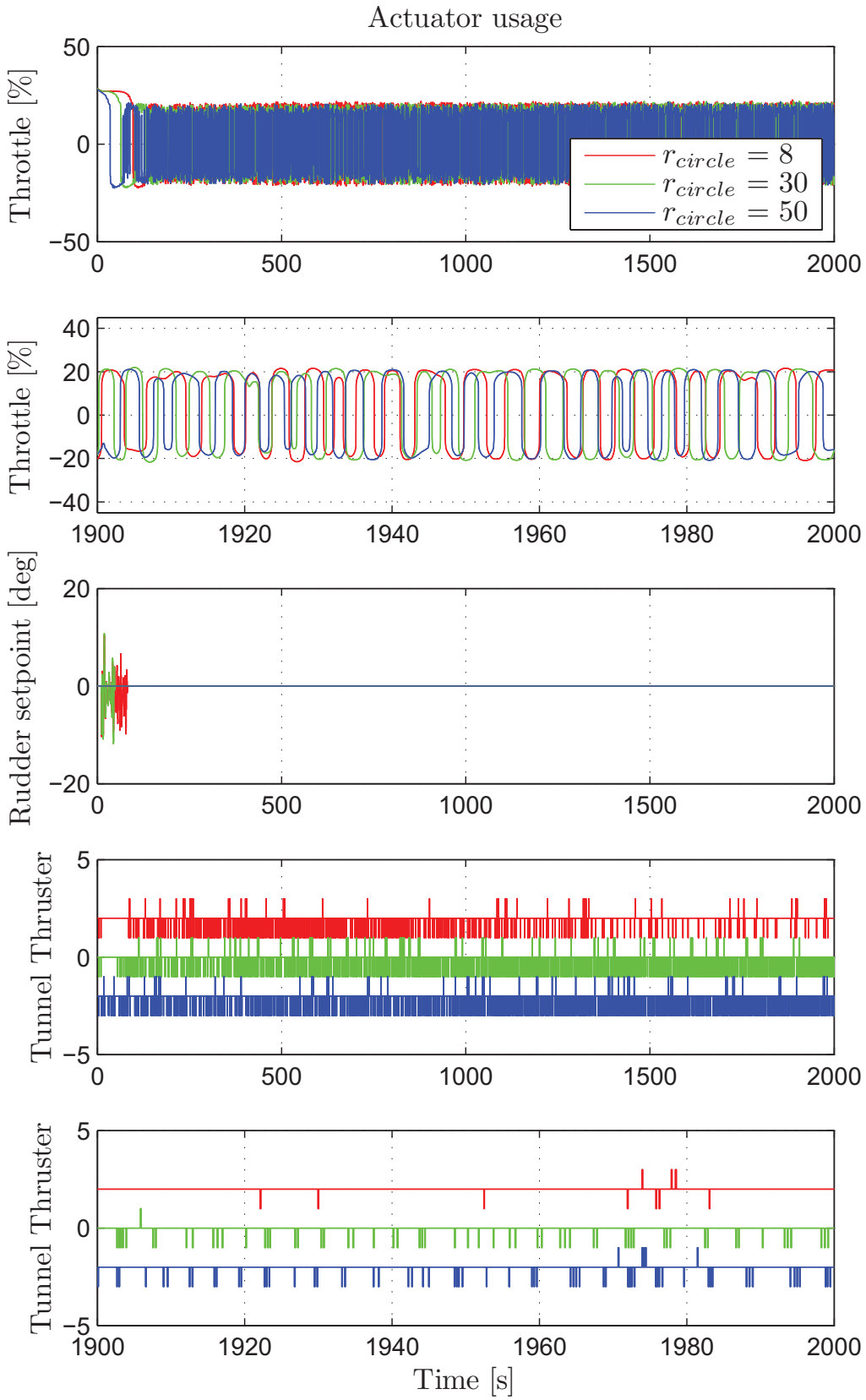

Figure 6.18: WOHC vessel actuator set-points in complex sea state. Rudder is converted from interface range to degrees for better understanding.

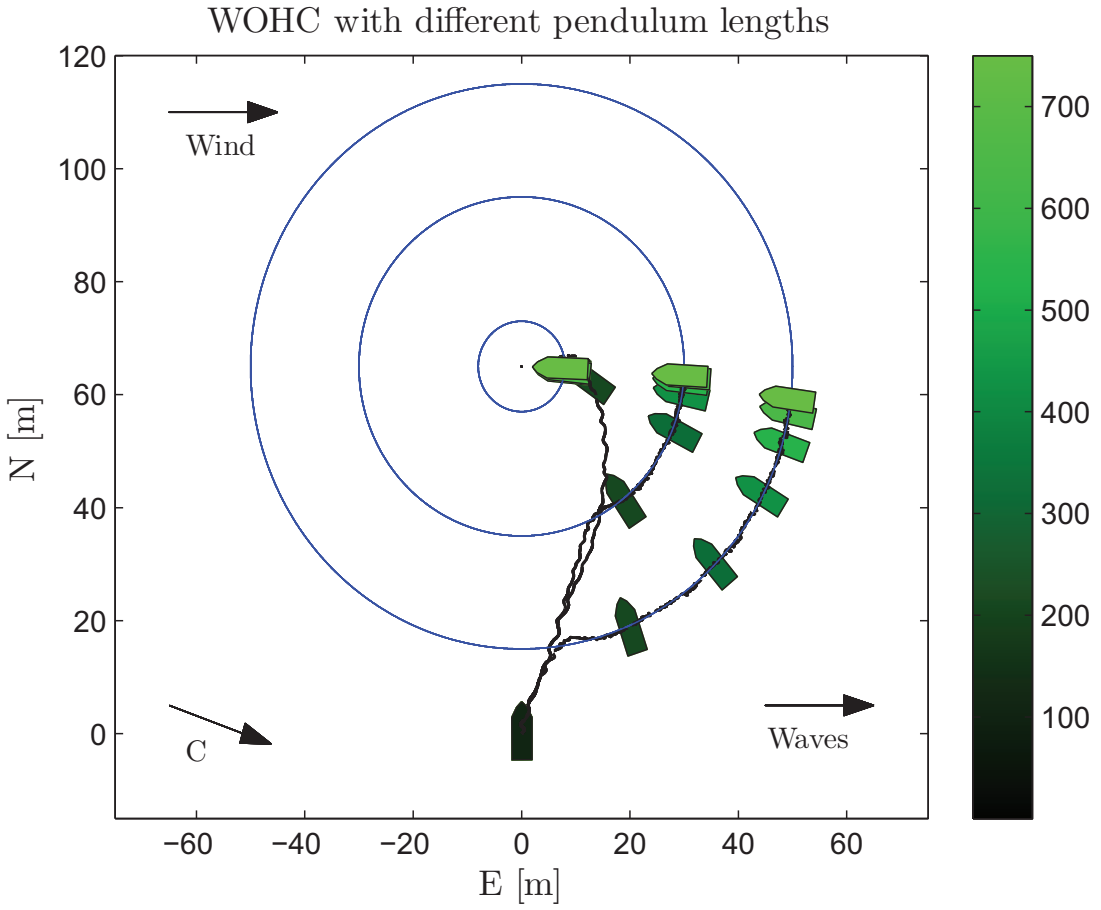

Figure 6.19: WOHC visualization in harsh sea state where the arrows mark wind, wave and current direction.

Strong breeze and slight moderate waves

In Nordic conditions the weather often gets quite harsh and to test this the simulator was set up with 4.5 [m/s] wind at 90 [deg] , 1 [m] significant wave height and 0.05 [m/s] current at 110 [deg] direction. This is a possible real world scenario where the sea state corresponds to Beaufort 6 where the wave height is somewhat downscaled, based on the assumption of smaller waves in sheltered waters. The simulations time was set to 600 [s] and the same pendulum lengths as above where used. The wind-speed limit of the vessel was found to be approximately 5 [m/s], above this the tunnel thruster was not capable of converging the heading to the desired angle.

Figure 6.19 features a visualization of the scenario, where the effect of the integral effect on the surge deviation is easily seen on the system using the 8 [m] pendulum. The vessel converges towards the circle, and when in range the integral effect builds up and coincides

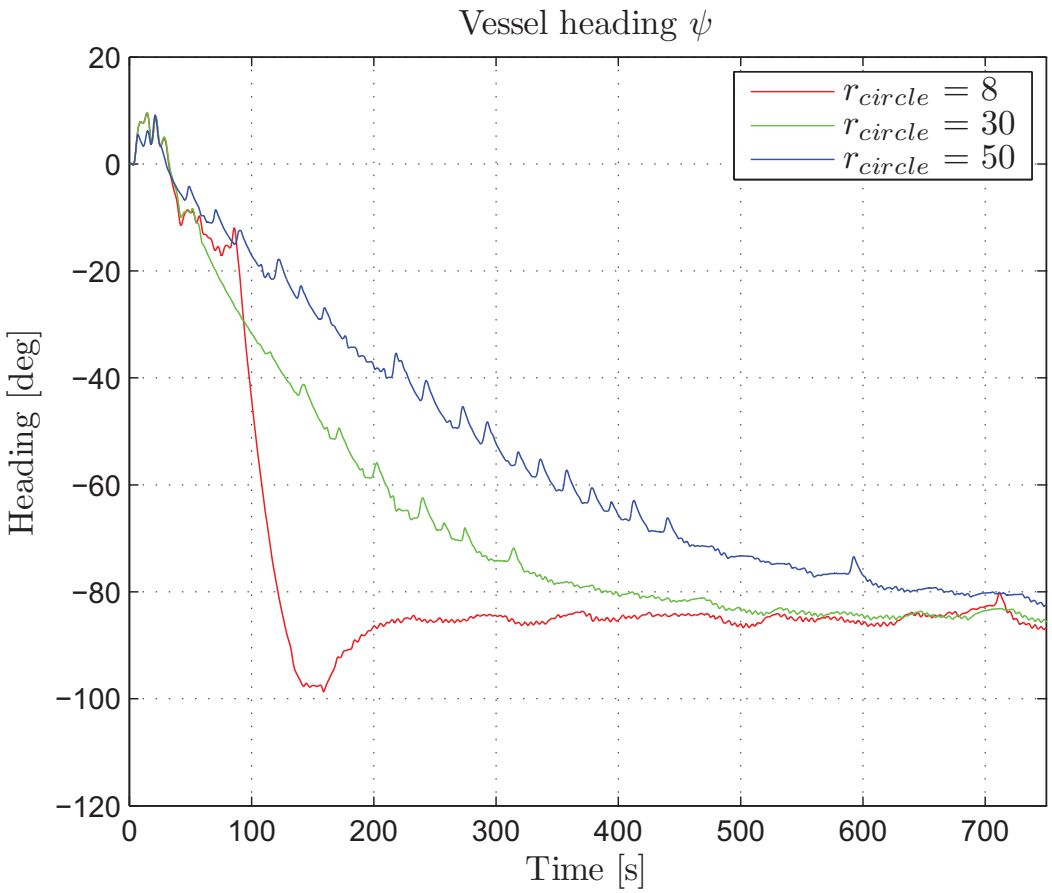

Figure 6.20: WOHC vessel heading in harsh sea state.

the vessel with the circle arc. Figure 6.20 shows the heading and indirectly the systems convergence. As in the other scenarios the shortest pendulum has the fastest convergence. Even though the vessels are affected by heavy waves and wind they maintain position within $\pm$ 1 [m] of the circle arc, as seen in Figure 6.21.

From Figure 6.22 it can be seen that the actuator usage is high. The main propulsion often changes thrust direction to compensate for wave induced surge movements. This is undesirable, both due to gearing dynamics and wear-and-tear. It should not be necessary to change thrust direction post convergence. The reason for the frequent changes in thrust direction could be poor surge controller tuning. It might be appropriate to develop a wave management scheme handling and filtering the wave motions to achieve reduced energy consumption. Much of the tunnel thruster usage is also believed to emerge from the waves. and wind forces, creating yaw moments, due to the weather optimal heading instability. In any case this has to be compensated, a more intelligent scheme could possibly decrease the energy consumption and thruster wear-and-tear.

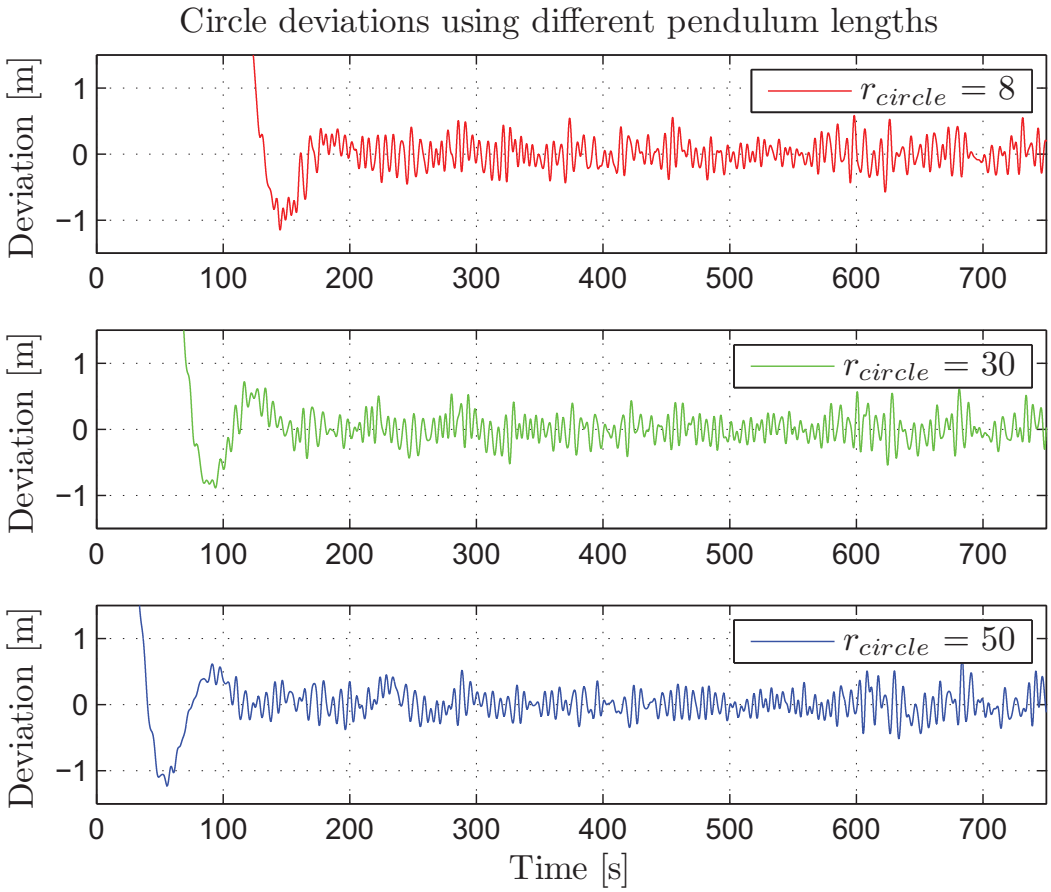

Figure 6.21: WOHC vessel deviation from circle arc in harsh sea state.

In total the WOHC system works satisfactory enabling the vessel to obtain an approximate weather optimal heading. The actuator usage could be decreased by implementing a wave management scheme incorporating some form of wave filter. Especially the main propulsion would benefit from this, as the unnecessary post convergence reversals to compensate wave induced movement could be reduced. The tunnel thruster utilization could also benefit from such a scheme, but optimal tuning and/or possibly sea state based adaptive tuning could significantly improve system performance also.

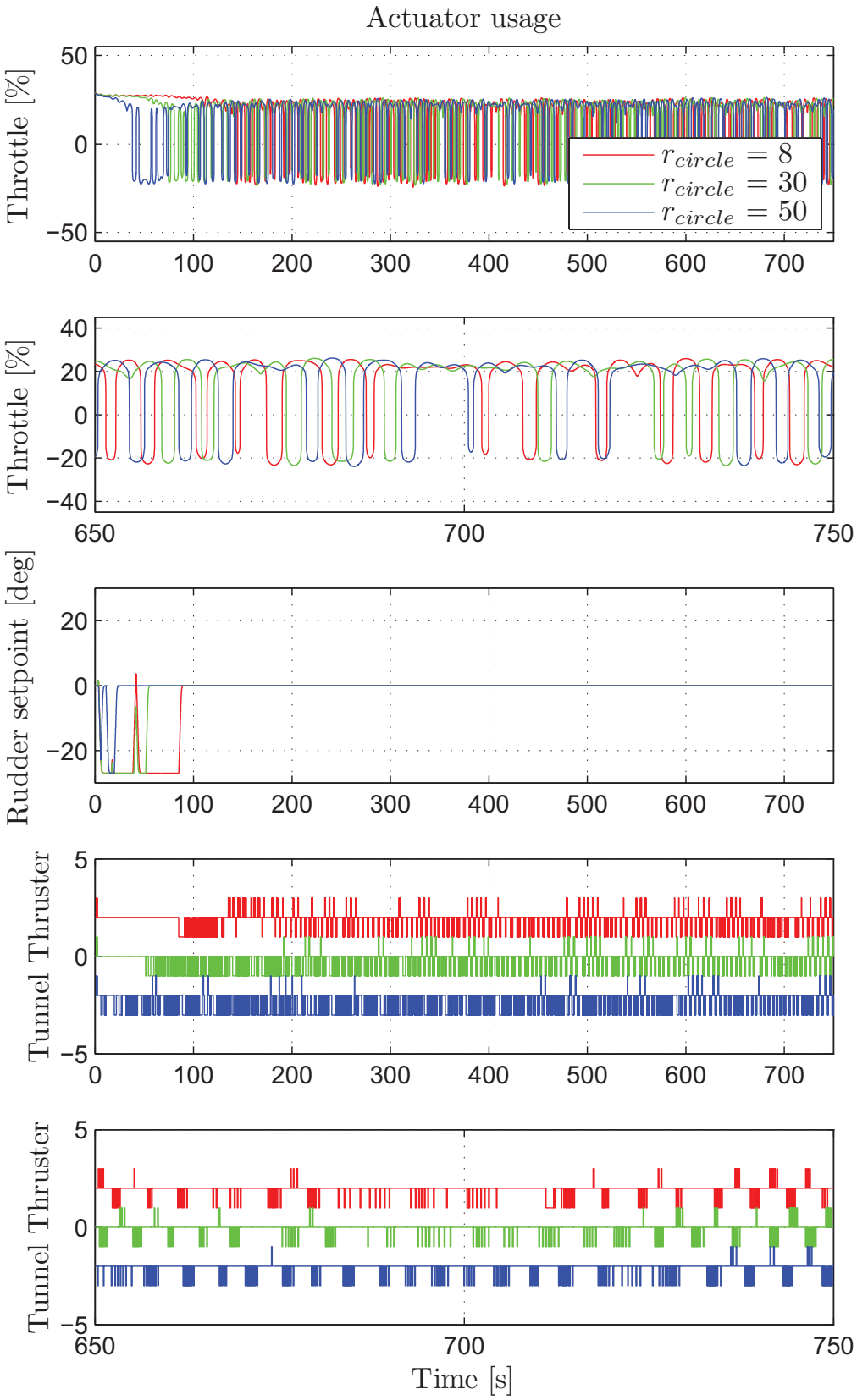

Figure 6.22: WOHC vessel actuator set-points in harsh sea state. Rudder is converted from interface range to degrees for better understanding.

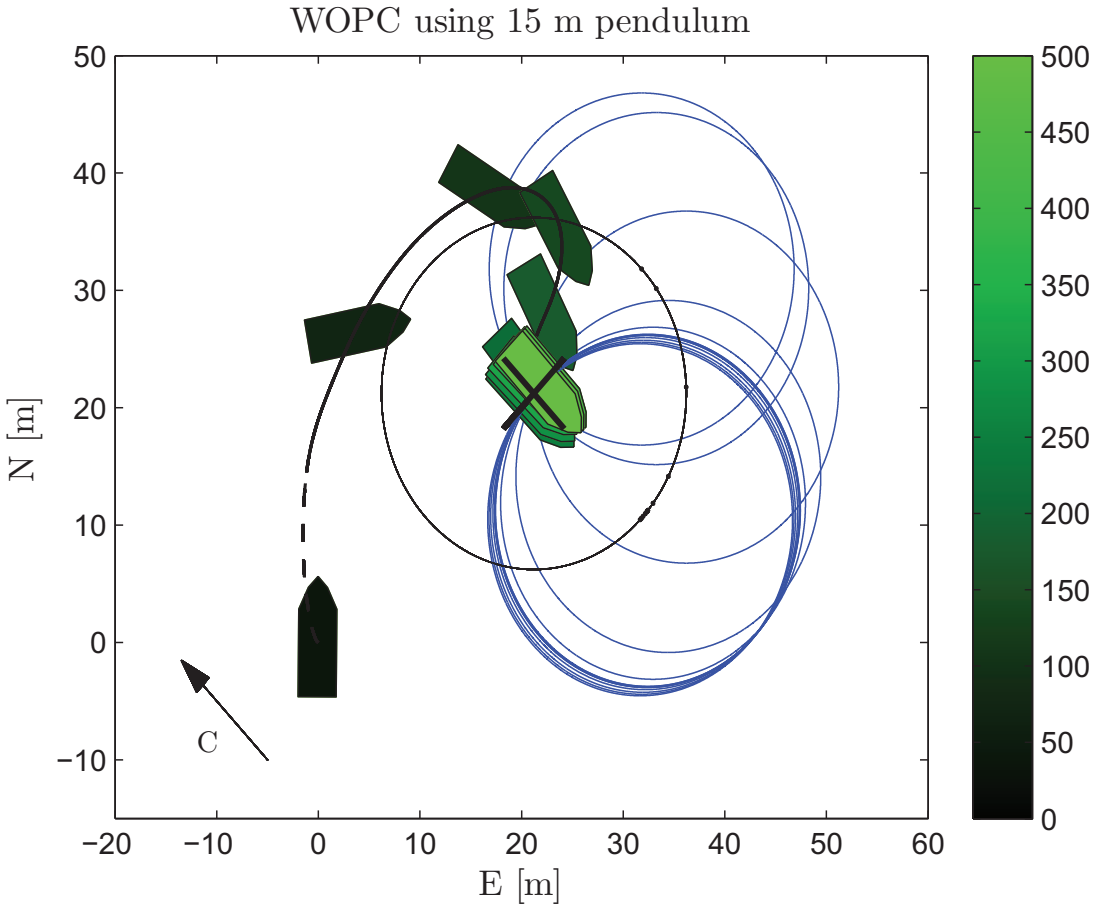

Figure 6.23: WOPC visualization in simple constant force field sea state where C marks the current force direction.

6.6.2 WOPC

To display the WOPC performance several simulations where performed. The basic functionality is shown in the first scenario featuring a simple sea state. The pendulum length affects the performance and the second scenario explores this. In the real world the environmental disturbances vary in magnitude and direction with time and this is simulated in the third scenario. In the fourth scenario harsh conditions are considered. At last a weather heading stable vessel was assumed and the scenario displays the benefits of this feature. In all scenarios the vessel was initialized in [0,0] with no velocity and 0 [deg] heading.

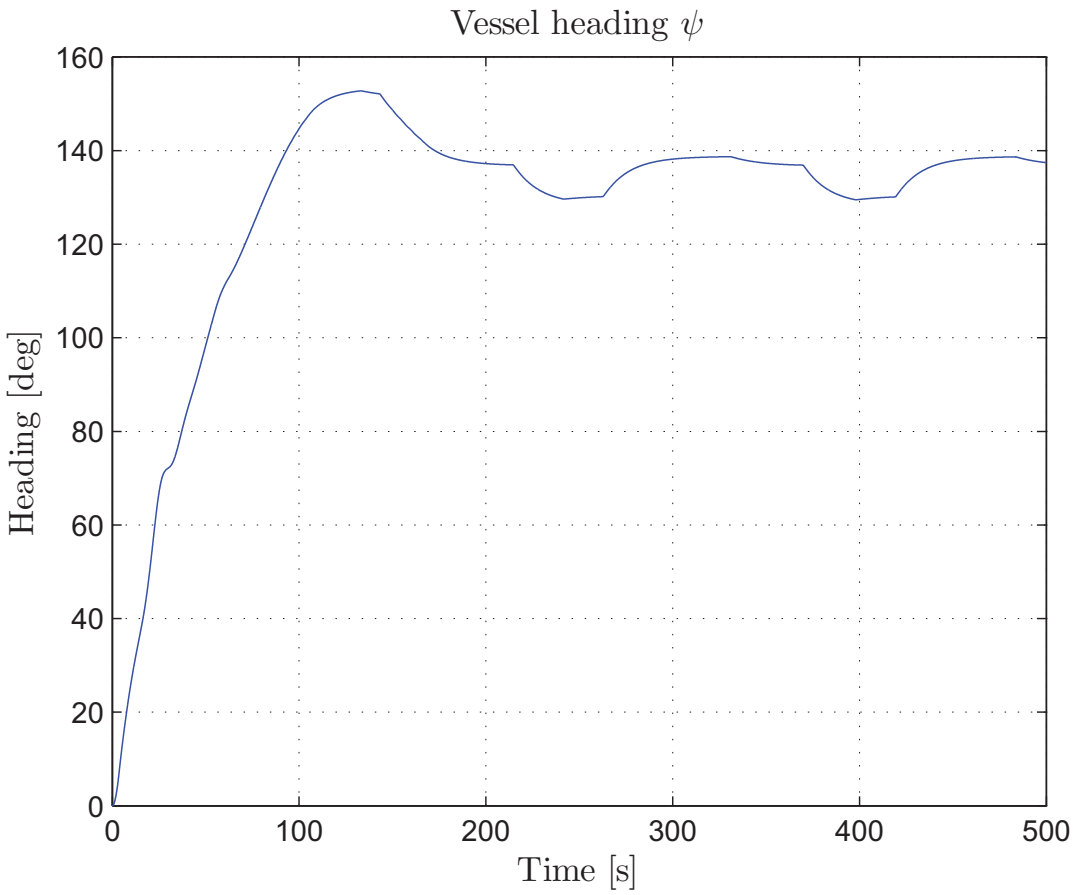

Figure 6.24: WOPC vessel heading in simple constant force field sea state.

Simple sea state

Using a static force field without wind and waves features the basic functionality of the WOPC system. The simulation time was set to 500 [s] and the current magnitude was set to 0.5 [m/s] with -45 [deg] direction. The desired position was set to be 45 [deg] and 30 [m] away from the initial condition. This corresponds to approximately [-21.2, -21.2] in the NED frame. The rationale behind the chosen vessel relative desired position, is simplified full scale testing, due to a more intuitive positioning placement concept.

Figure 6.24 is a visualization of the scenario where the current force field direction is shown as an arrow. From Figure 6.24 it can be seen that the convergence time is approximately 250 [s]. The heading overshoot heading is due to the approach of the vessel pursuing the moving suspension point along with the usage of the rudder and tunnel thruster. If only the tunnel thruster would have been used a better convergence path could possibly be achieved. The suspension point movement also creates a contribution to the assumed weather optimal heading and causes the minor position oscillations seen close to the desired position, both

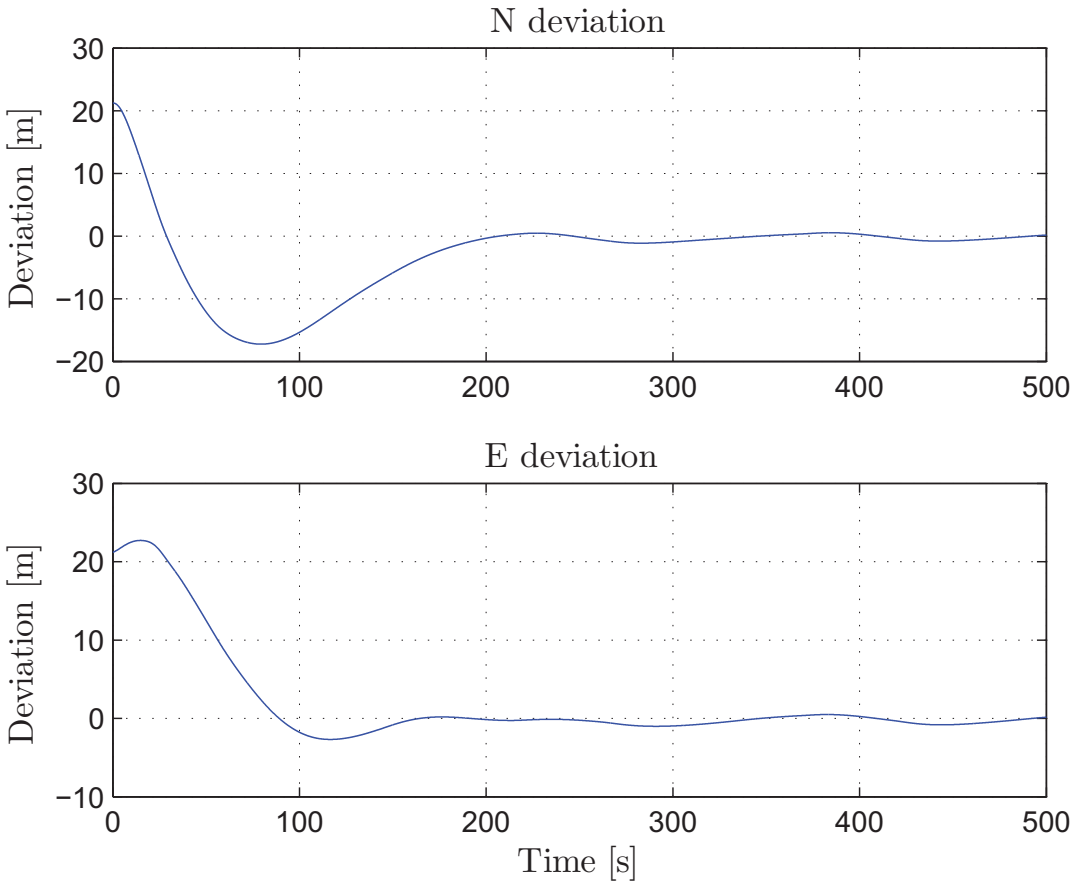

Figure 6.25: WOPC vessel deviation from circle arc in simple constant force field sea state.

Figure 6.24 and 6.25 features this. It might be possible to suppress this component by estimating and subtracting it in the suspension point controller.

After convergence the main propulsion usage is the same as in the case of the WOHC in a static force field. The level counteracting the current is found and maintained such that the vessel does not drift away. Figure 6.26 shows that the rudder is used when approaching the circle and the tunnel thruster when the speed is lower. The tunnel thruster is used to correct the heading during convergence. However the nature of the tunnel thruster makes it difficult to obtain the correct angle, without an increasing minor deviation in turn causing some correcting usage. As the static force field does not affect heading, the vessels natural desire to turn is unaffected, and this gives relatively less tunnel thruster usage.

The system has high performance in such a sea state and obtains a close to optimal heading enabling it to counteract the current using only the main propulsor.

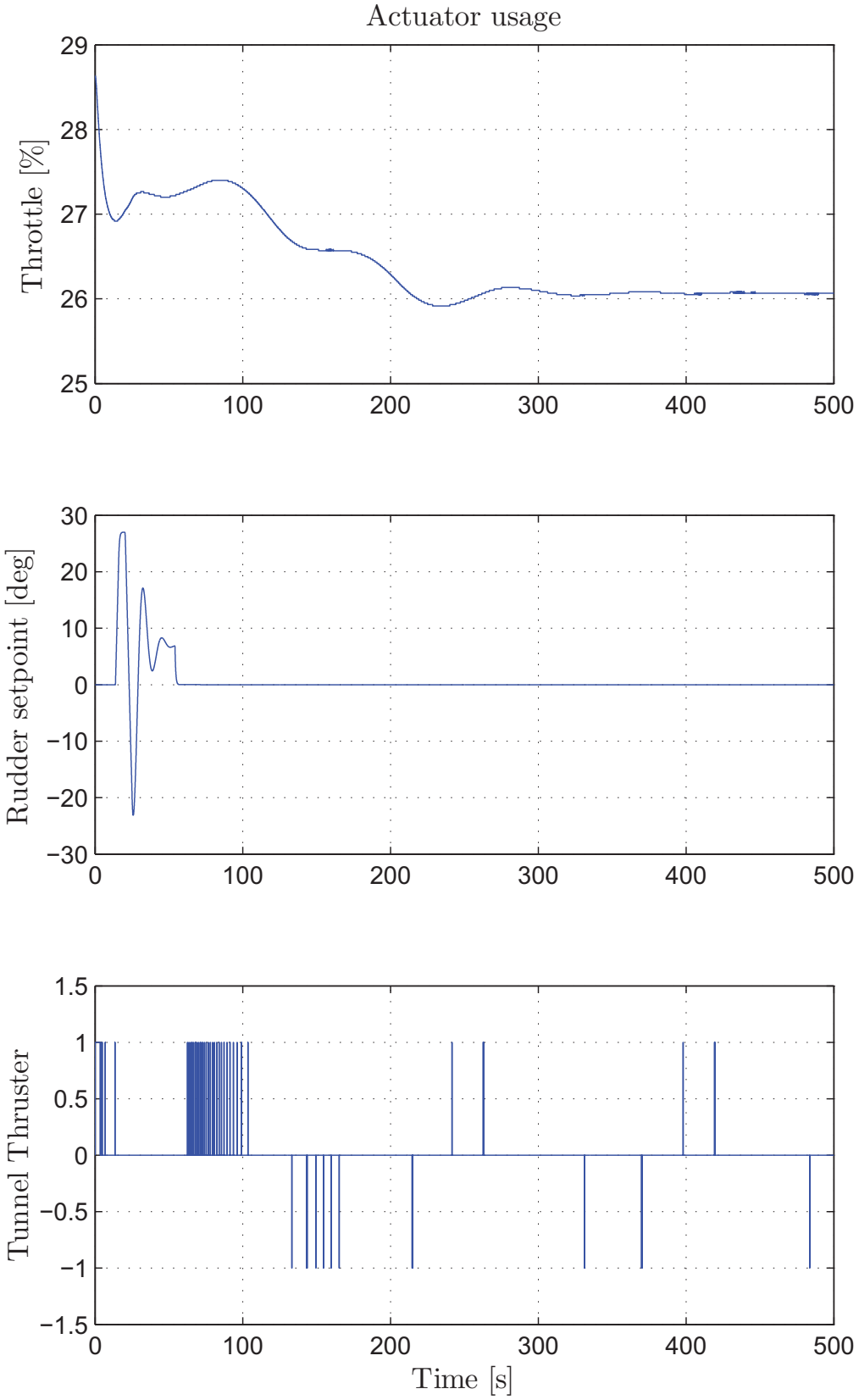

Figure 6.26: WOPC vessel actuator set-points in simple constant force field sea state. Rudder is converted from interface range to degrees for better understanding.

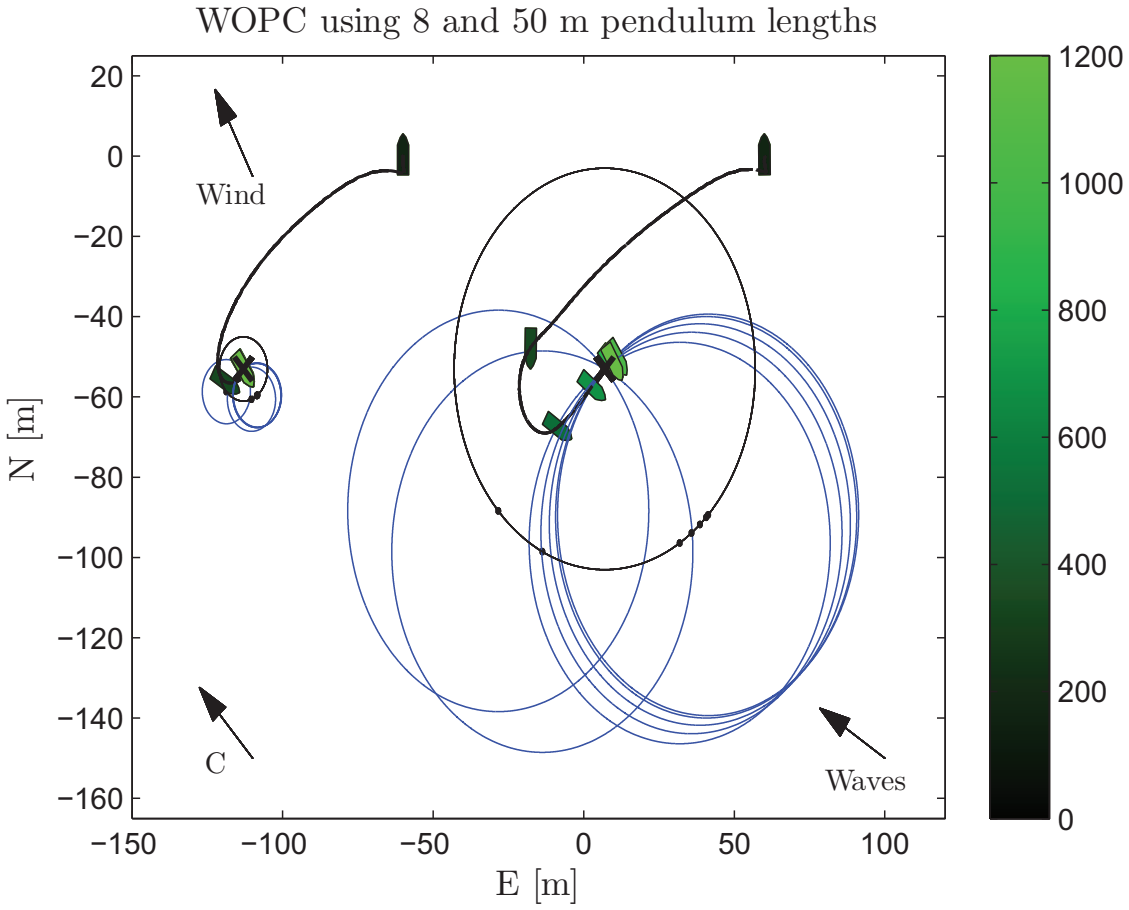

Figure 6.27: WOPC pendulum length effects visualization.

Pendulum length effects

The pendulum is an important part of the system and the length of this creates several important effects. To display this, two simulations where set up, using one short and one long pendulum. Both scenarios have the same environmental disturbances consisting of 0.1 [m/s] current at 315 [deg], 4 [m/s] wind at 330 [deg] and waves with 0.2 [m] significant wave height at 300 [deg]. This corresponds to Beaufort force 5, where the waves are significantly downscaled, based on the same arguments as above. The vessels were initialized 120 [m] apart at [0,-60] and [0, 60] both having 0 [deg] heading and both pursuing a desired position 75 [m] away at 300 [deg] relative to the respective initial position.

Figure 6.28 visualizes the scenarios where it can be seen that the vessel using the 50 [m] pendulum has a longer travelled path towards the desired position compared to the one using 8 [m] pendulum. From Figure 6.28 it can be seen that the vessel using the shortest pendulum converges to a stable heading much faster than the other. This is due

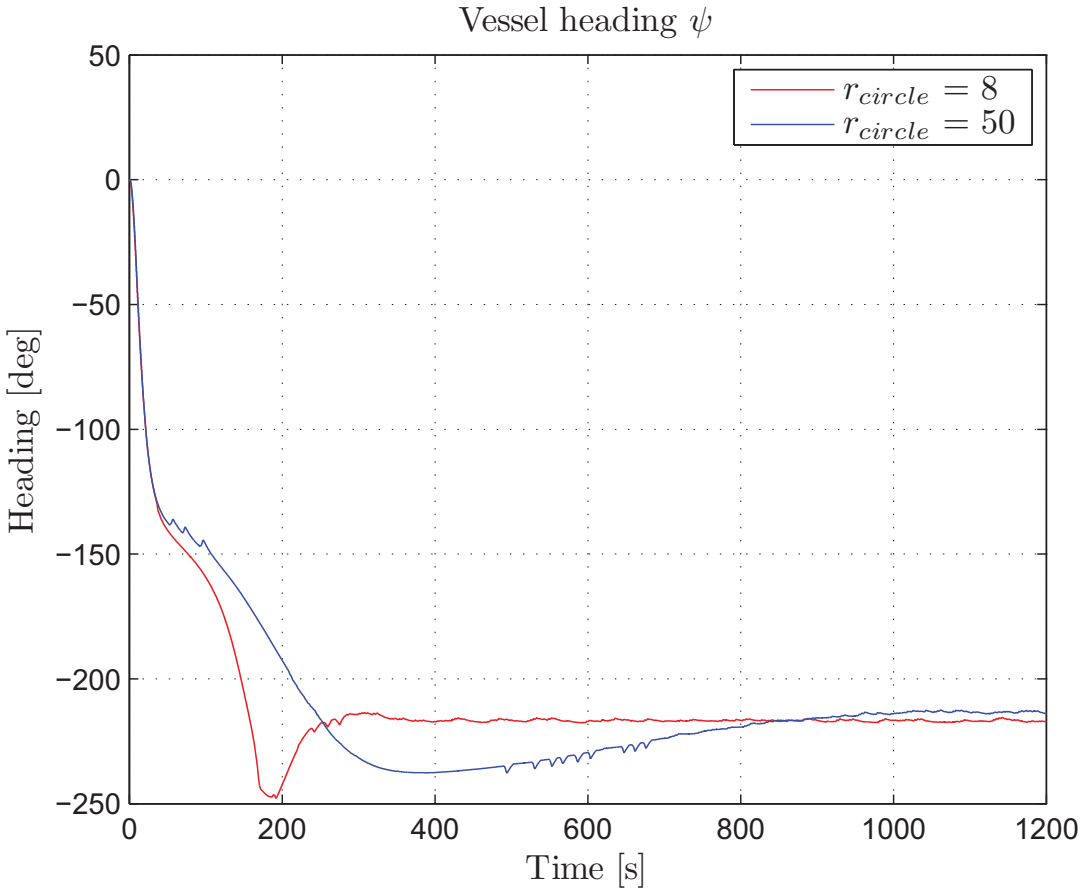

Figure 6.28: WOPC pendulum length effects on heading.

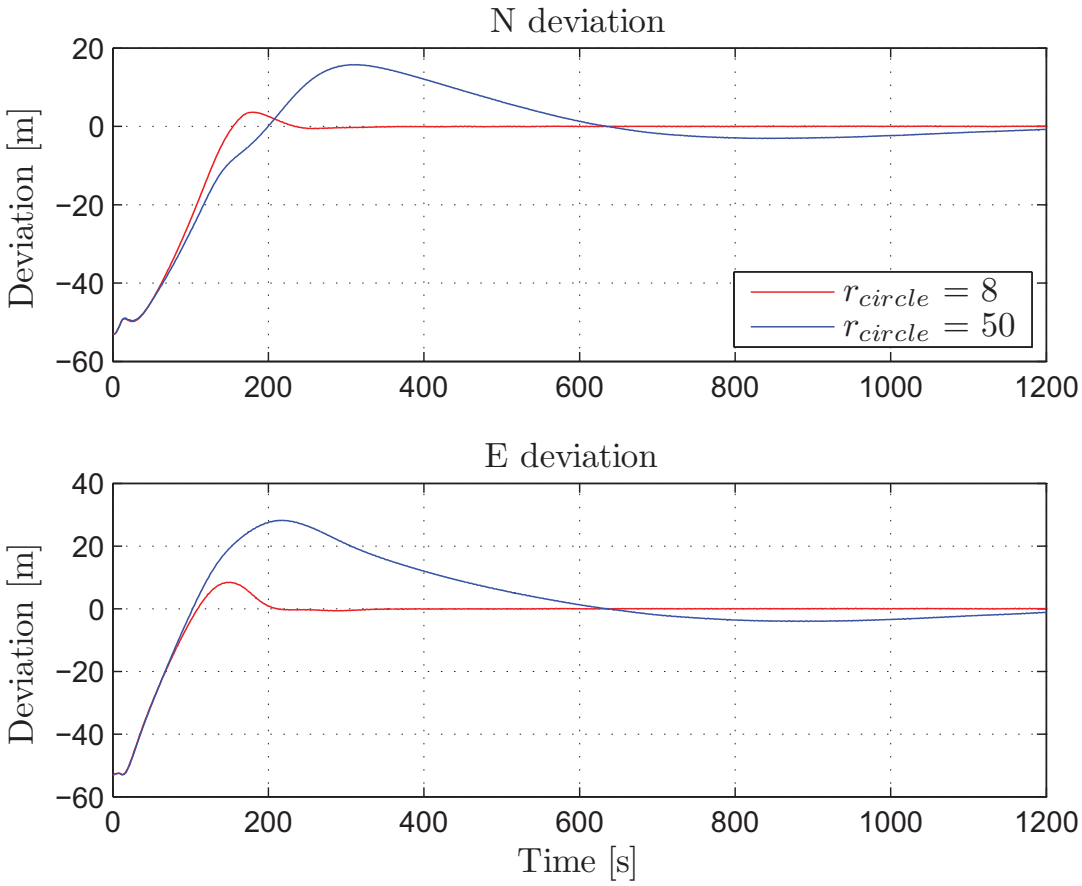

Figure 6.29: WOPC pendulum length effects on deviation from desired position.

to the longer circle arc distance which needs to be traveled by the vessel using 50 [m] pendulum. During convergence, as seen in Figure 6.29 the short pendulum vessel also has less oscillations around the desired position.

Both vessels converge to the desired position achieving weather optimal heading using the same amount of throttle to compensate the environmental disturbances. The difference in actuator usage can be seen in the tunnel thruster usage. The vessel using the long pendulum seems to use the thruster slightly less, which is logical due to the fact that for a given sway deviation, the suspension point angle grows as the pendulum length is shortened. This effect can be seen in the two bottom plots of Figure 6.30.

The benefits of using short pendulums are faster convergence and less deviations during the desired position approach. The disadvantages are more tunnel thruster usage leading to higher fuel consumption and more thruster wear-and-tear. In turn, this gives faster dynamics. In this way, the time away from the desired position if occuring, is shorter than for long pendulums, which benefits from slow dynamics and less tunnel thruster usage.

The pendulum length could be regarded as a means of system gain where short pendulums can be treated as high gain, and the opposite long pendulums as low gain. An alternative approach could be to have varying pendulum length based on certain criteria, such as distance from desired position and pendulum deviation. By using the short pendulum for the convergence phase a faster and more precise position homing is obtained. Then, and when close to the weather optimal heading, the pendulum length could be increased to provide stable low dynamics positioning schemes optimized fuel economy and long operations.

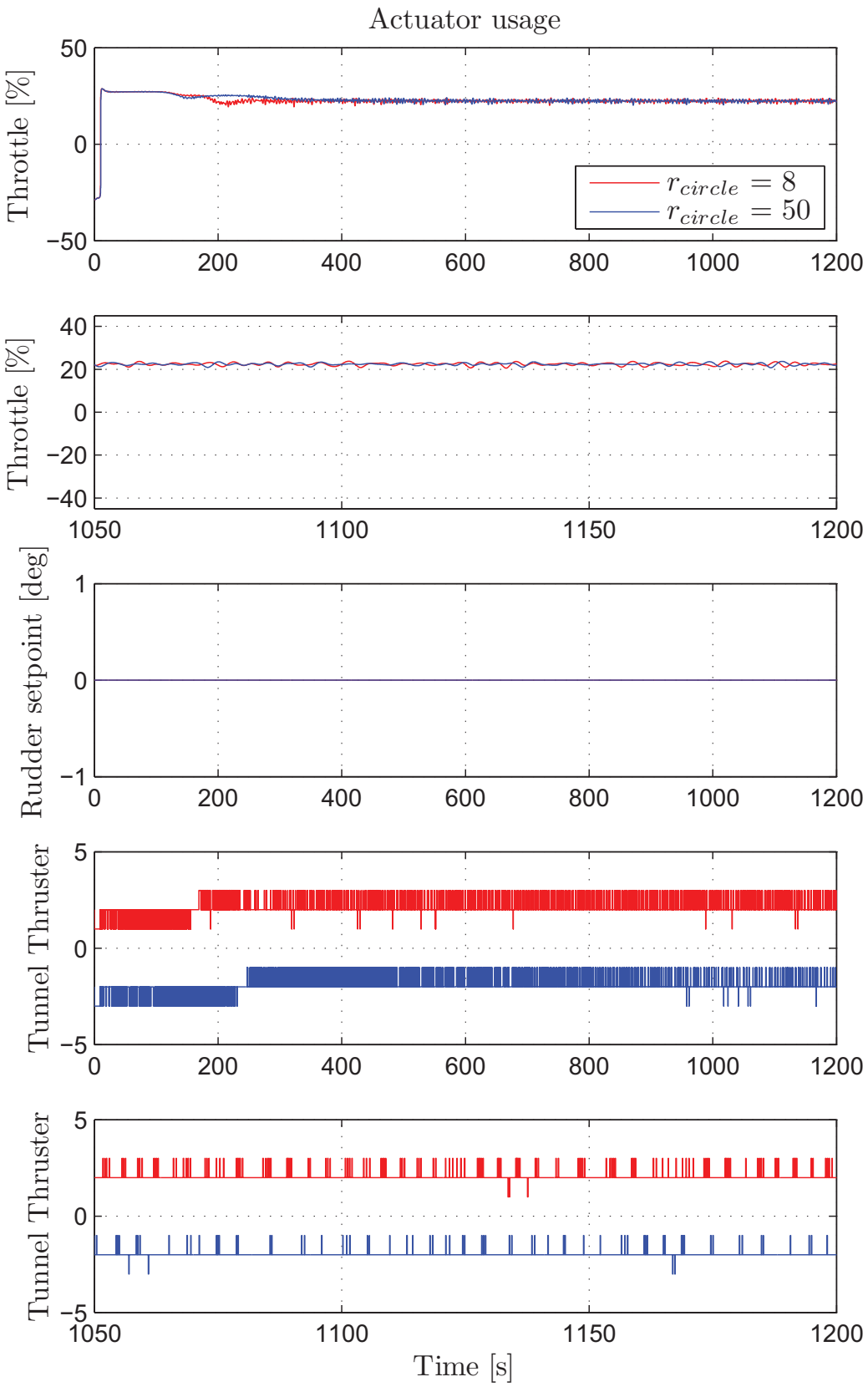

Figure 6.30: Actuator effects of using different pendulum lengths in WOPC.

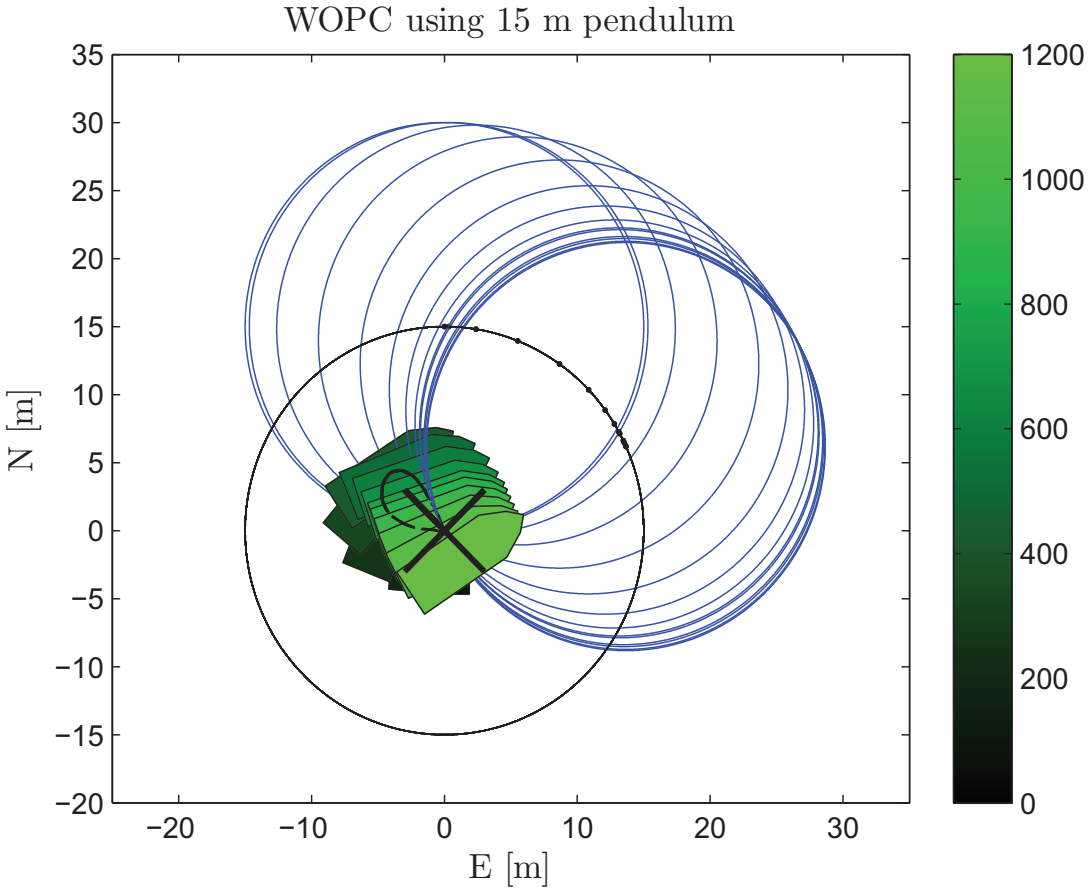

Figure 6.31: Visualization WOPC influenced by turning winds.

Varying environmental direction

In the real world the wind is not a simple constant disturbance as it fluctuates in both magnitude and direction. To test the WOPC system against this the wind model was augmented with fluctuating components described by (6.39) and (6.40). The wind model was set up to start at 180 [deg] direction and turn 45 [deg] as a first order process with a 50 [s] time constant. The mean wind was set to 3 [m/s] and the vessel was initialized in [0,0] which also was set as the desired position. The initial angle of the suspension point was set to 0 [deg]. The simulation time was set to 1200 [s].

Figure 6.31 visualizes the scenario where the suspension point is moved to counteract the turning wind, displayed in Figure 6.32. Figures 6.33 and 6.34 features the vessel heading and desired position deviation. These illustrations show that the wind creates a deviation, and how the system minimizes this.

The fluctuating magnitude of the wind does not seem to affect the surge deviation much as

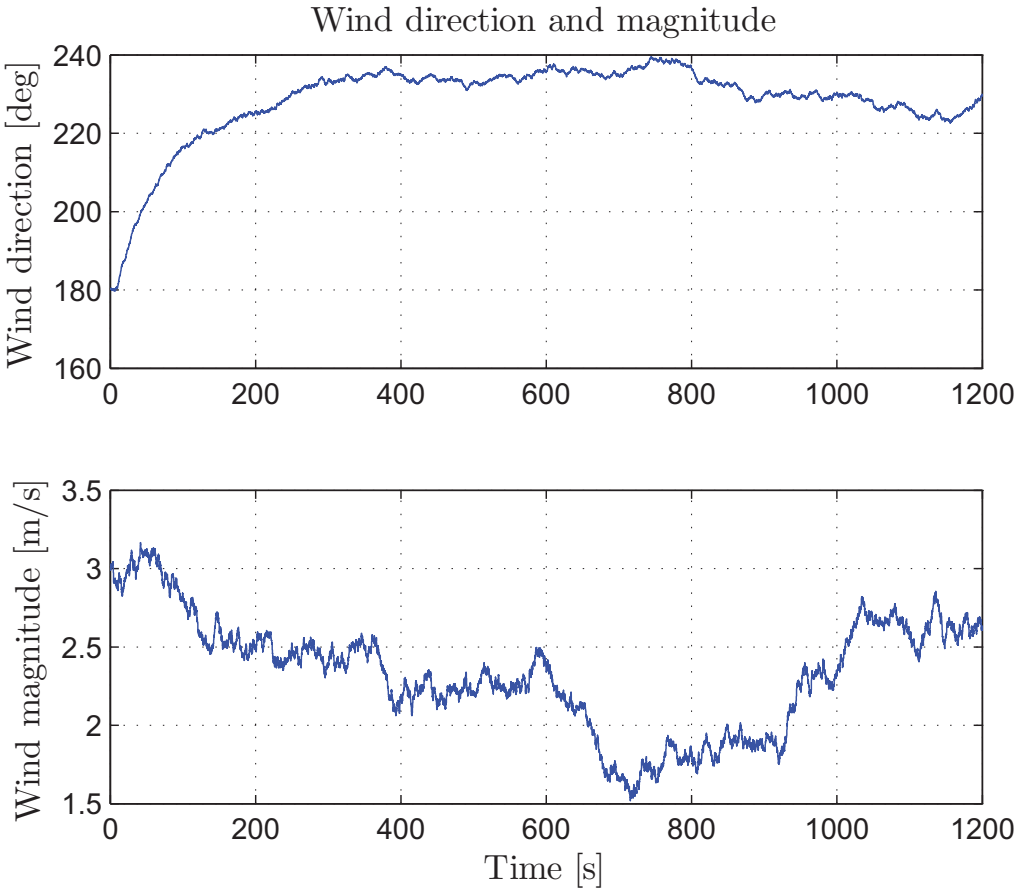

Figure 6.32: Wind magnitude and direction.

a almost constant throttle was found and maintained through the whole scenario. Figure 6.35 also shows that the rudder was unused as the propeller does not give enough thrust for it to be effective. The tunnel thruster usage was high due to following the turning wind. The turning wind reveals that the tunnel thruster usage is highly correlated to the deviation from the weather optimal heading. The tunnel thruster relay zone can easily be seen in the second plot of Figure 6.33 where it also can be seen that the wind pushes the heading out through the relay zone again as soon as it enters the breaking zone and the deviation from the weather optimal heading is kept within $\pm$ 5 [deg]. The two last plots of the figure feature the desired heading and the angular deviation between the vector from vessel to suspension point and desired position and suspension point.

The actuator usage is as expected where the tunnel thruster is heavily loaded to follow the heading towards the suspension point. As there are only one direction shift means that the heading stays withing 5 [deg] on one side of the desired heading and does not oscillate around it.

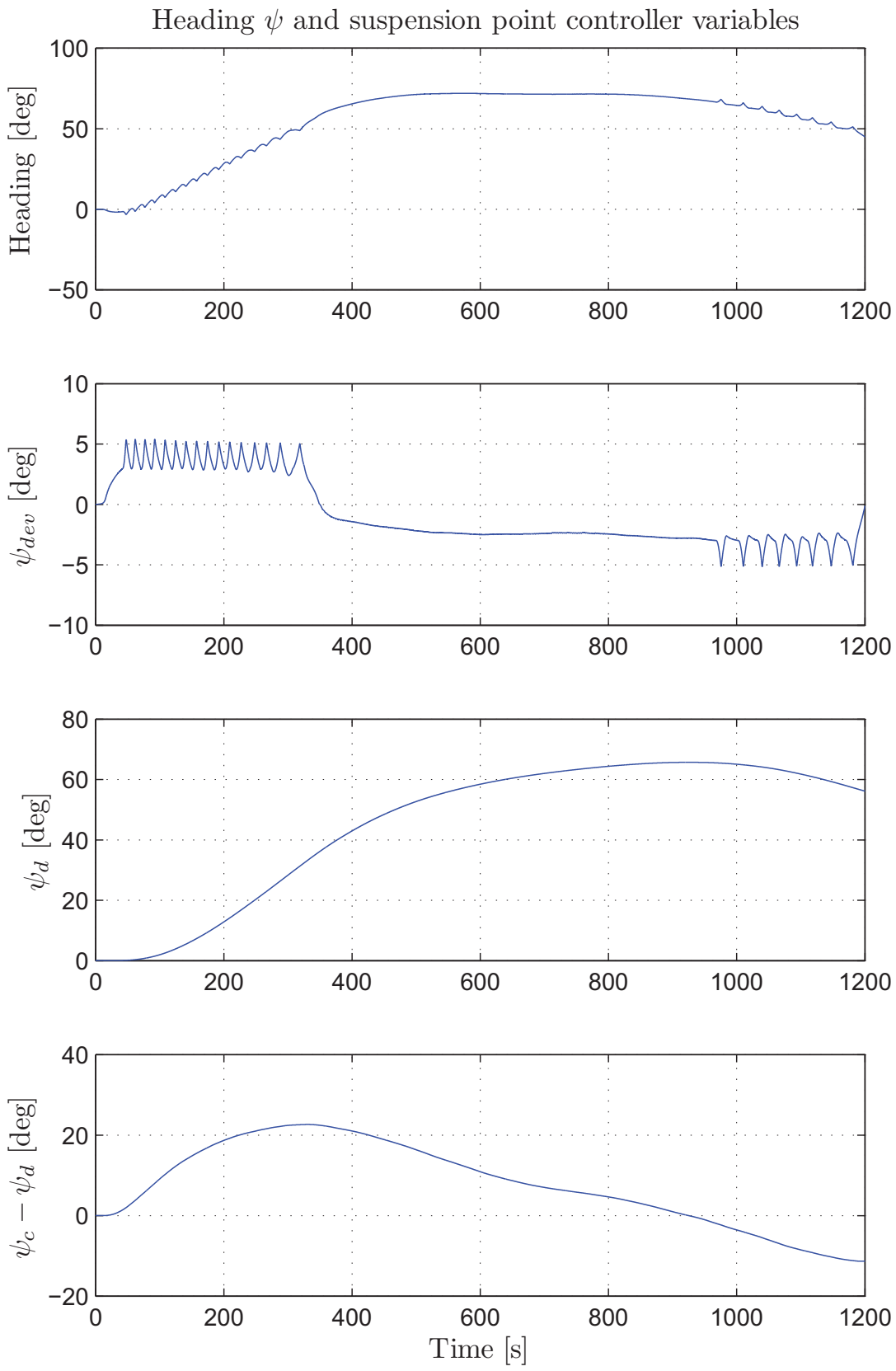

Figure 6.33: Important heading and suspension point variables as effects of turning winds.

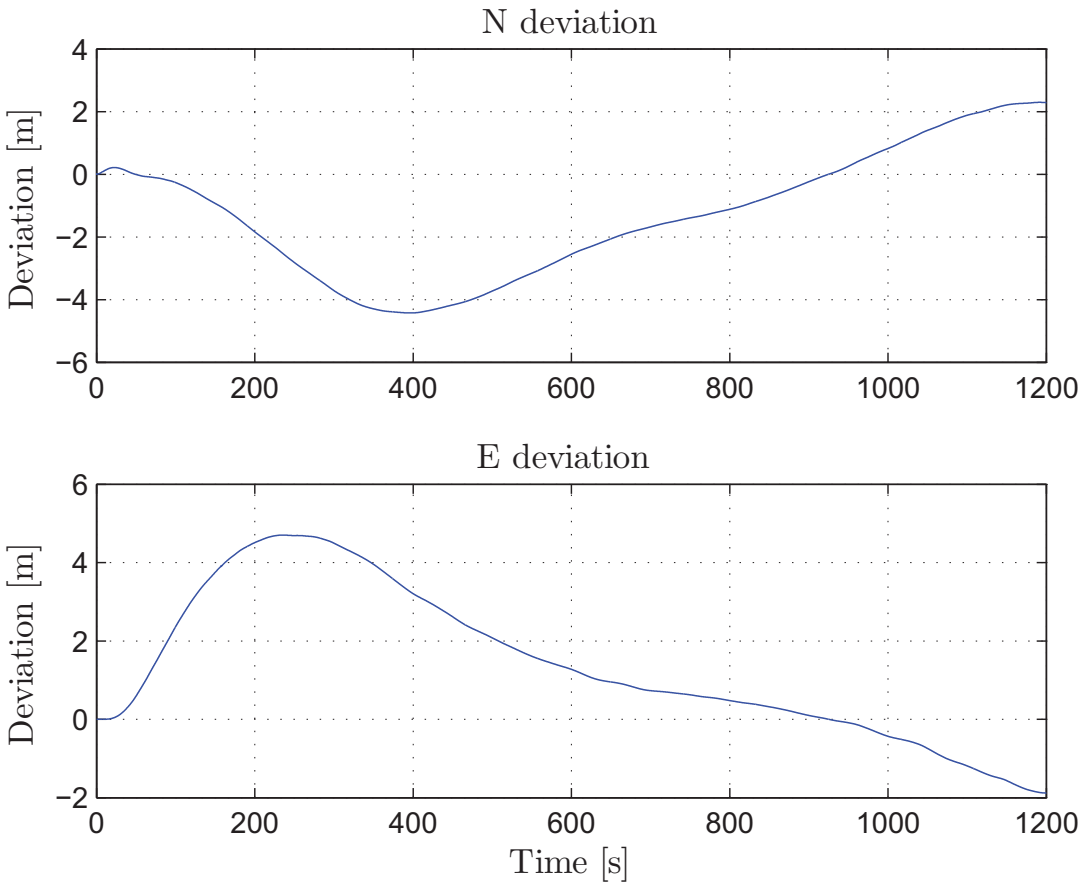

Figure 6.34: WOPC desired position deviations as a result of turning winds.

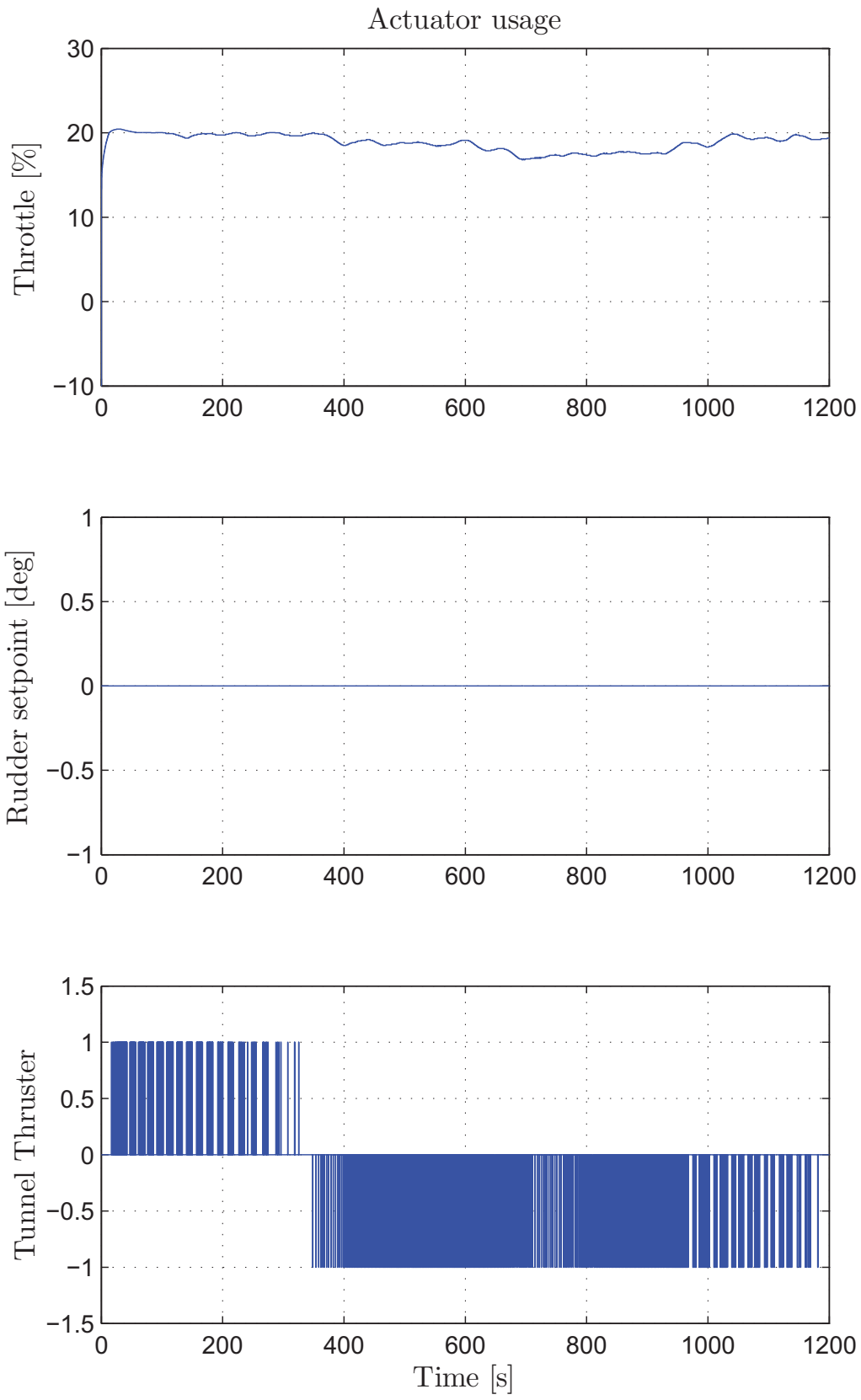

Figure 6.35: Actuator usage as a result of turning winds.

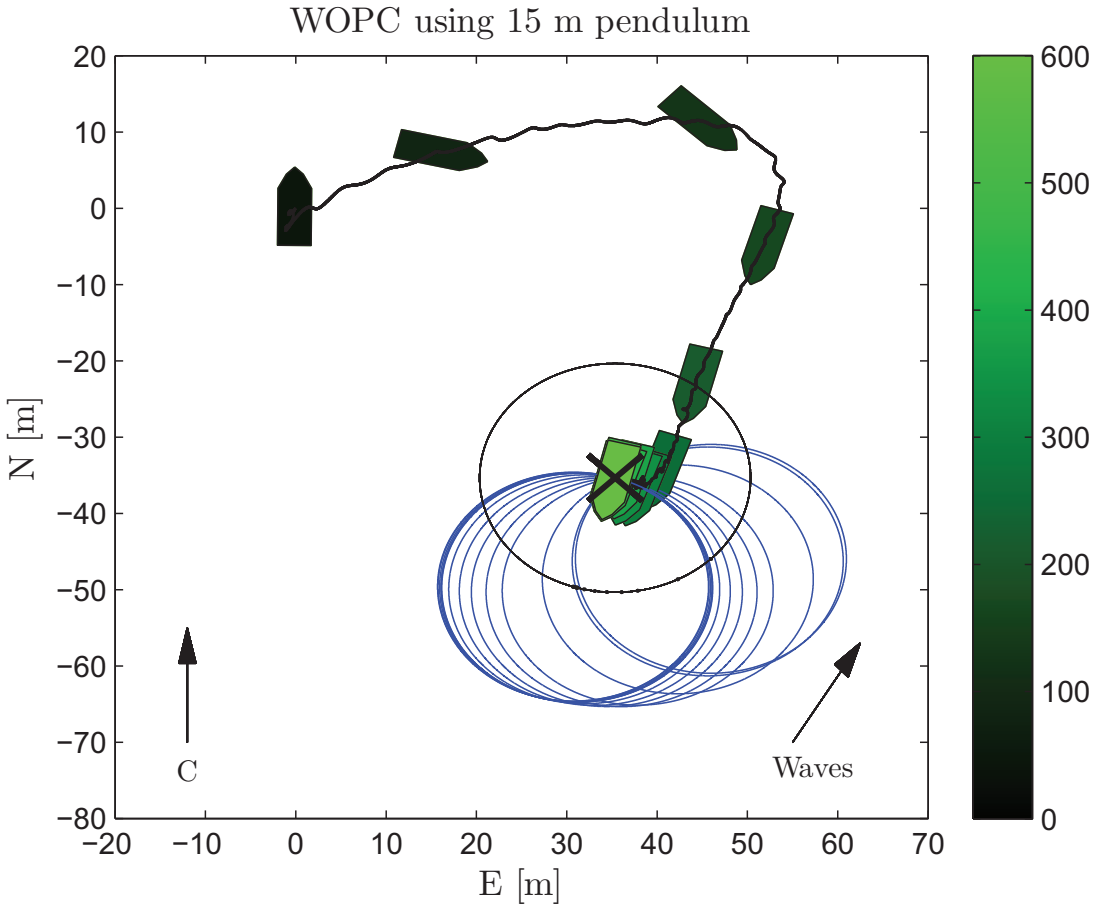

Figure 6.36: WOPC visualization in harsh weather.

Harsh weather

To test the WOPC system in harsh conditions the simulator was set up to have 0.25 [m/s] current at 0 [deg] and 1.5 [m] significant wave height at 30 [deg]. The wind was set up to turn 45 [deg] starting at 0 [deg] and is featured in Figure 6.37. The desired position was set to 50 [m] at 135 [deg] from the initial position.

From figures 6.36, 6.38 and 6.39 it can be seen that although strong environmental forces act on the vessel it converges to the desired position and obtains an approximate weather optimal heading. The actuator usage is as expected where the rudder is used during the homing phase and the tunnel thruster afterward.

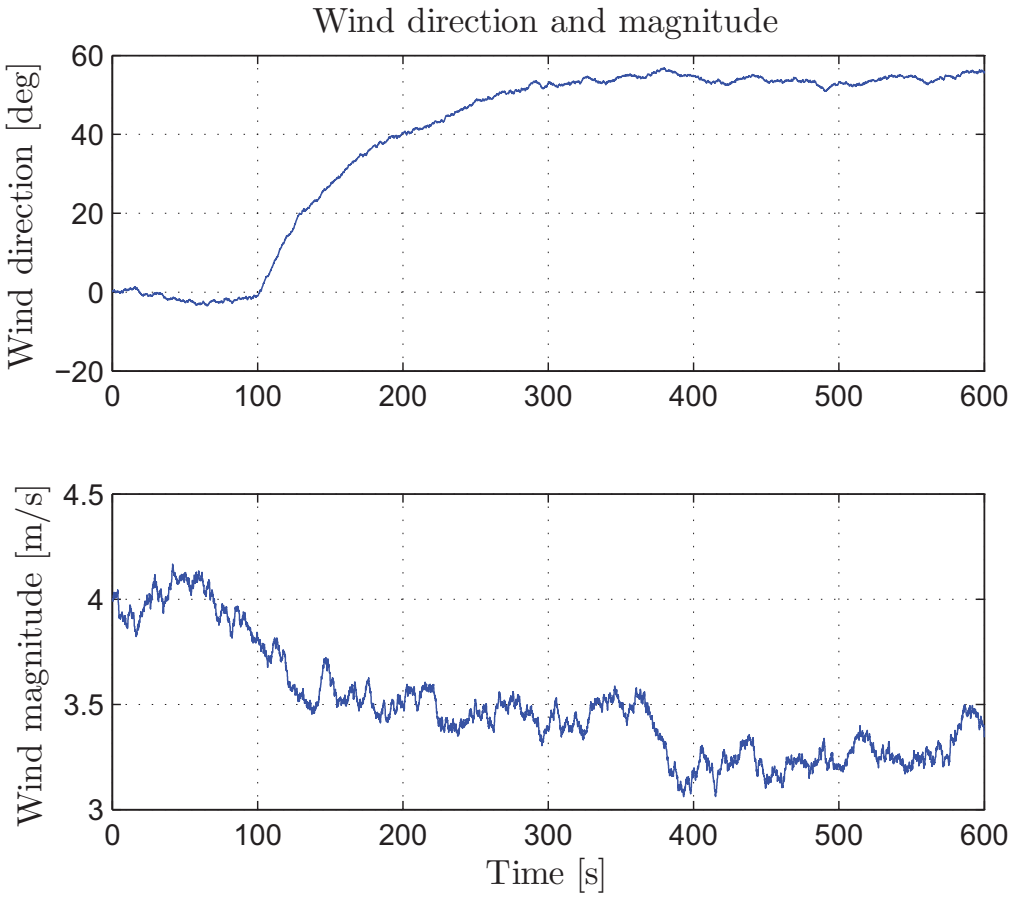

Figure 6.37: Wind magnitude and direction used in harsh weather WOPC simulation.

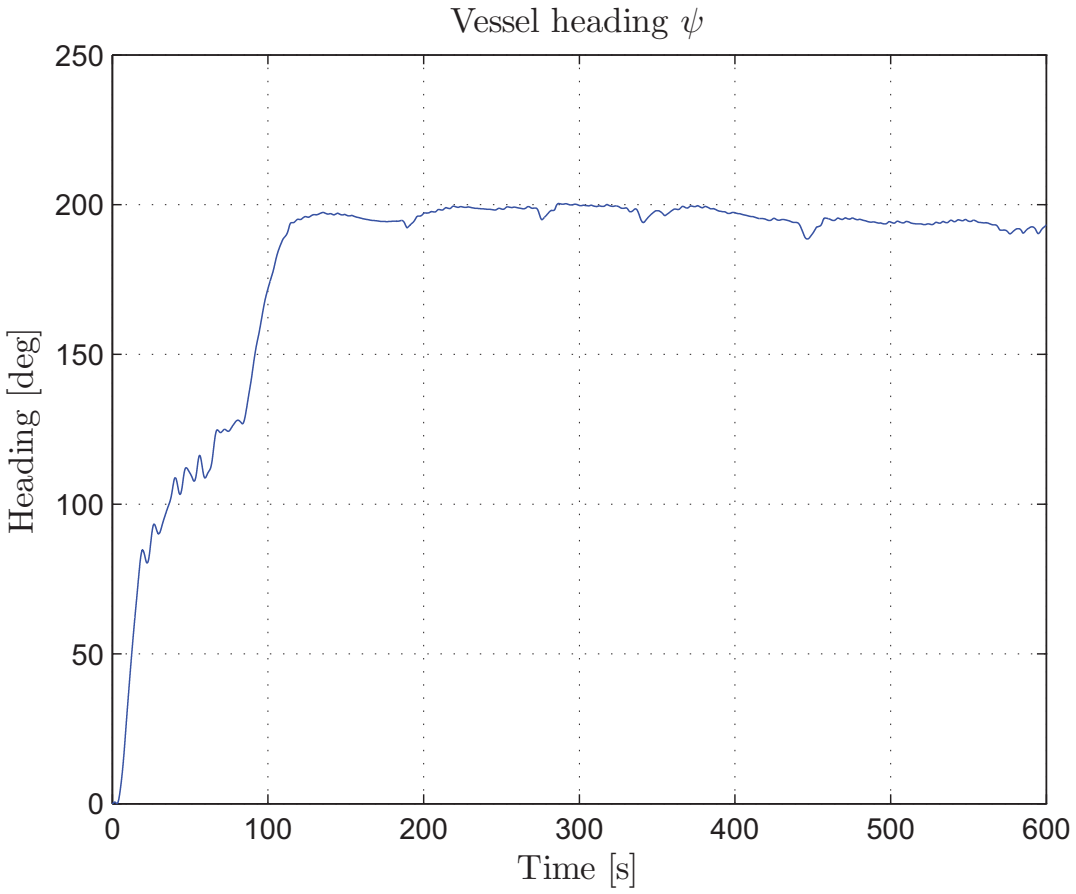

Figure 6.38: WOPC heading in harsh weather.

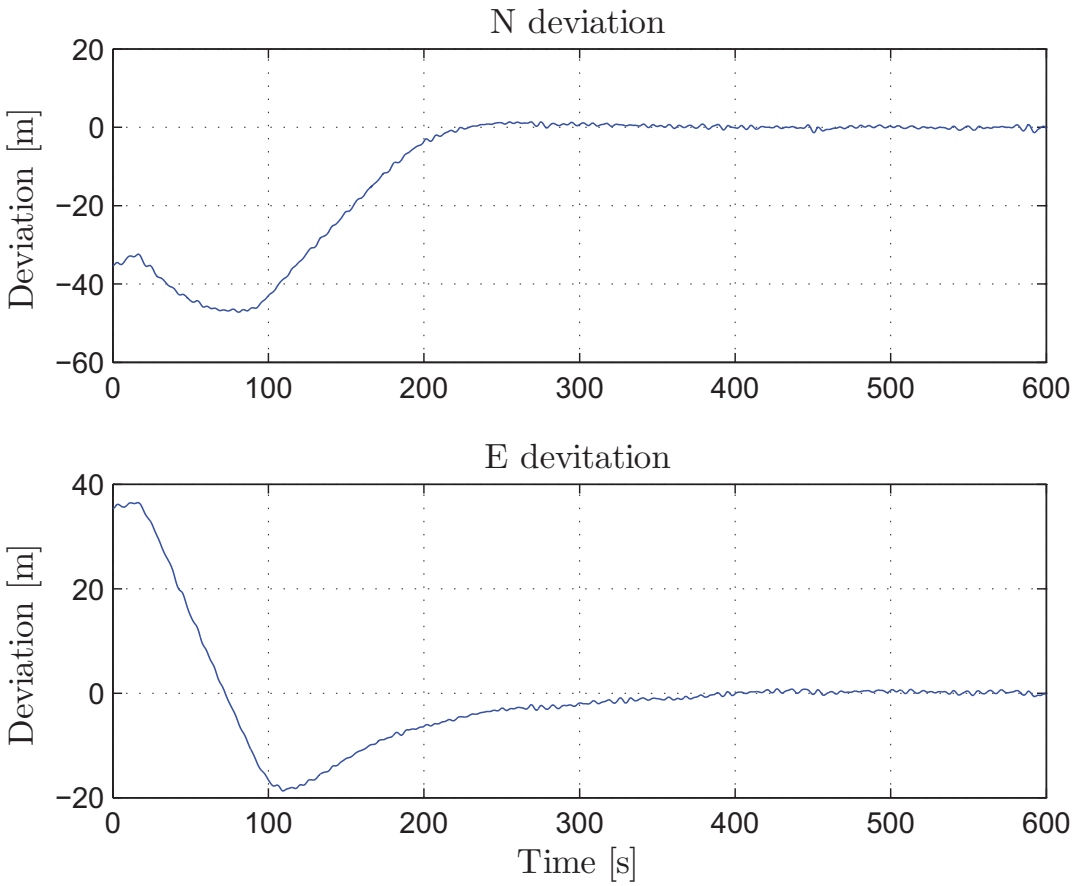

Figure 6.39: WOPC deviations in harsh weather.

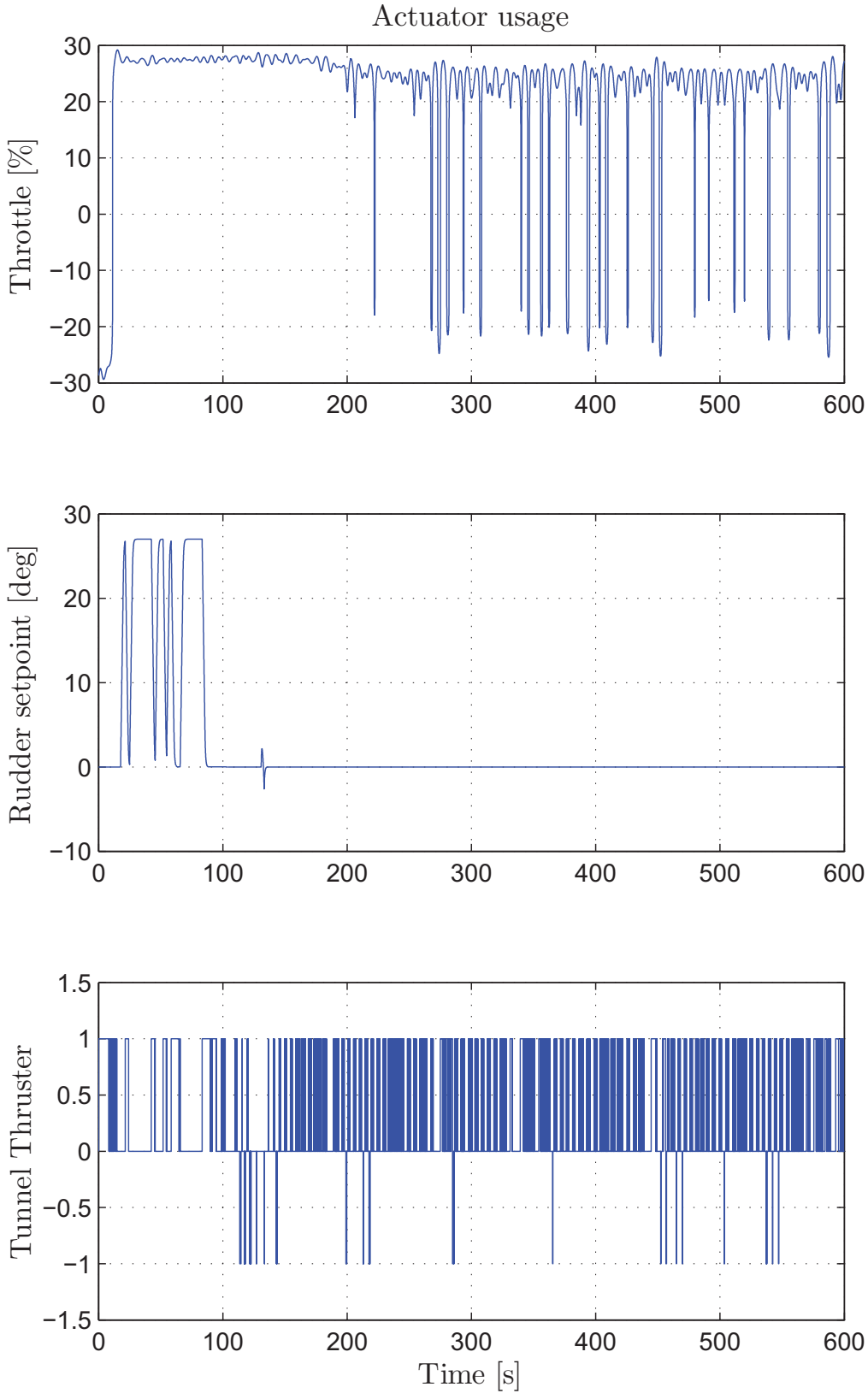

Figure 6.40: WOPC actuator usage in harsh weather.

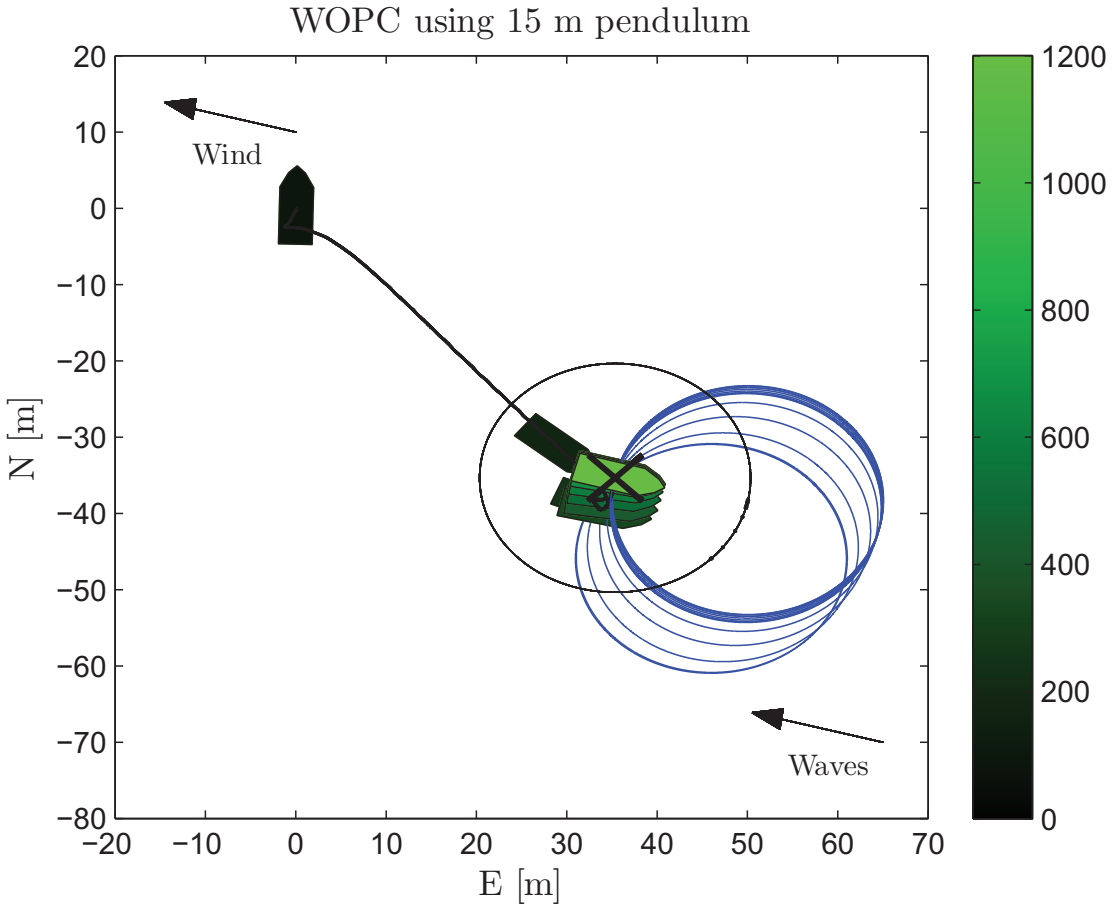

Figure 6.41: WOPC visualization using a weather optimal heading stable vessel.

Weather stable vessel

To document the importance of a vessel which is stable when heading up against the weather, the wind model was changed. The assumed vessel type was changed to number 2 [Blendermann, 1994] which is a cargo vessel with the wheelhouse superstructure astern. In addition to this the centroid of the longitudinal projected area was moved behind the center-line of the projection. This gives a vessel which when influenced by wind, is passively turned up against the wind.

The simulator was set up with 5 [m/s] wind and waves with 0.2 significant wave height at 285 [deg]. The simulation time was set to 1200 [s] and the desired position was set to 50 [m] at 135 [deg] relative to the initial position and heading.

Figures 6.41, 6.42 and 6.43 shows normal convergence which deviates little from the above scenarios. The major difference is the tunnel thruster usage, seen in the bottom plot of

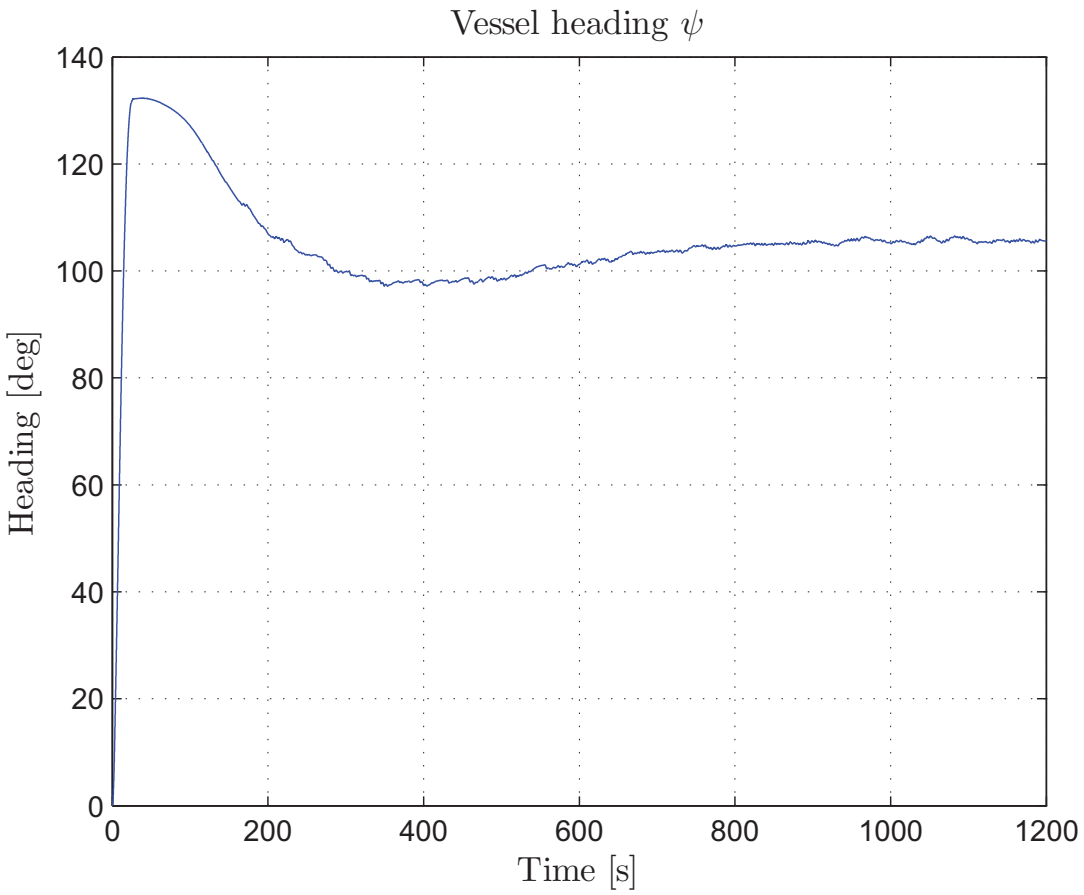

Figure 6.42: WOPC heading using a weather optimal heading stable vessel.

Figure 6.44. As the wind keeps the vessel at its heading, after the vessel is turned up against the wind, the tunnel thruster does not need to be used. In contrast to the unstable case, the vessel obtains the optimal heading. By actively using the wind the stability contributes to less tunnel thruster usage. Using such a vessel an electrical on-off tunnel thruster is sufficient.

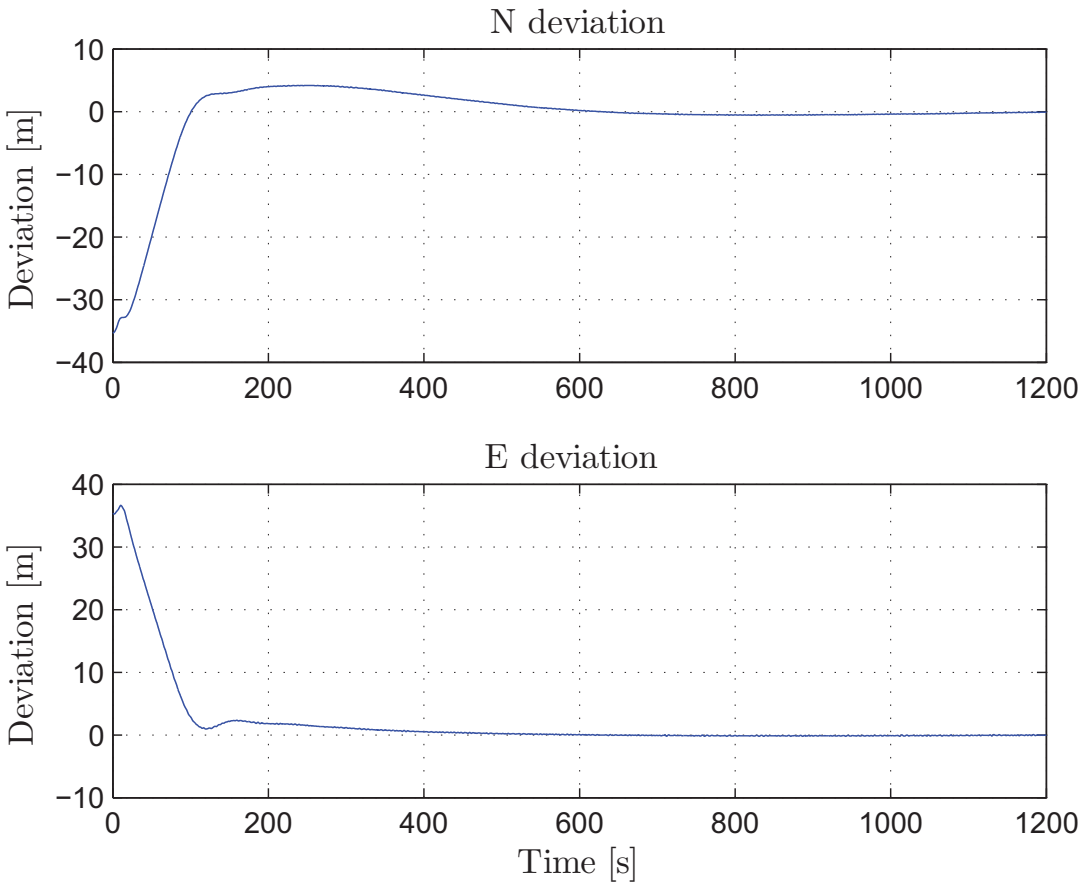

Figure 6.43: WOPC deviations using a weather optimal heading stable vessel.

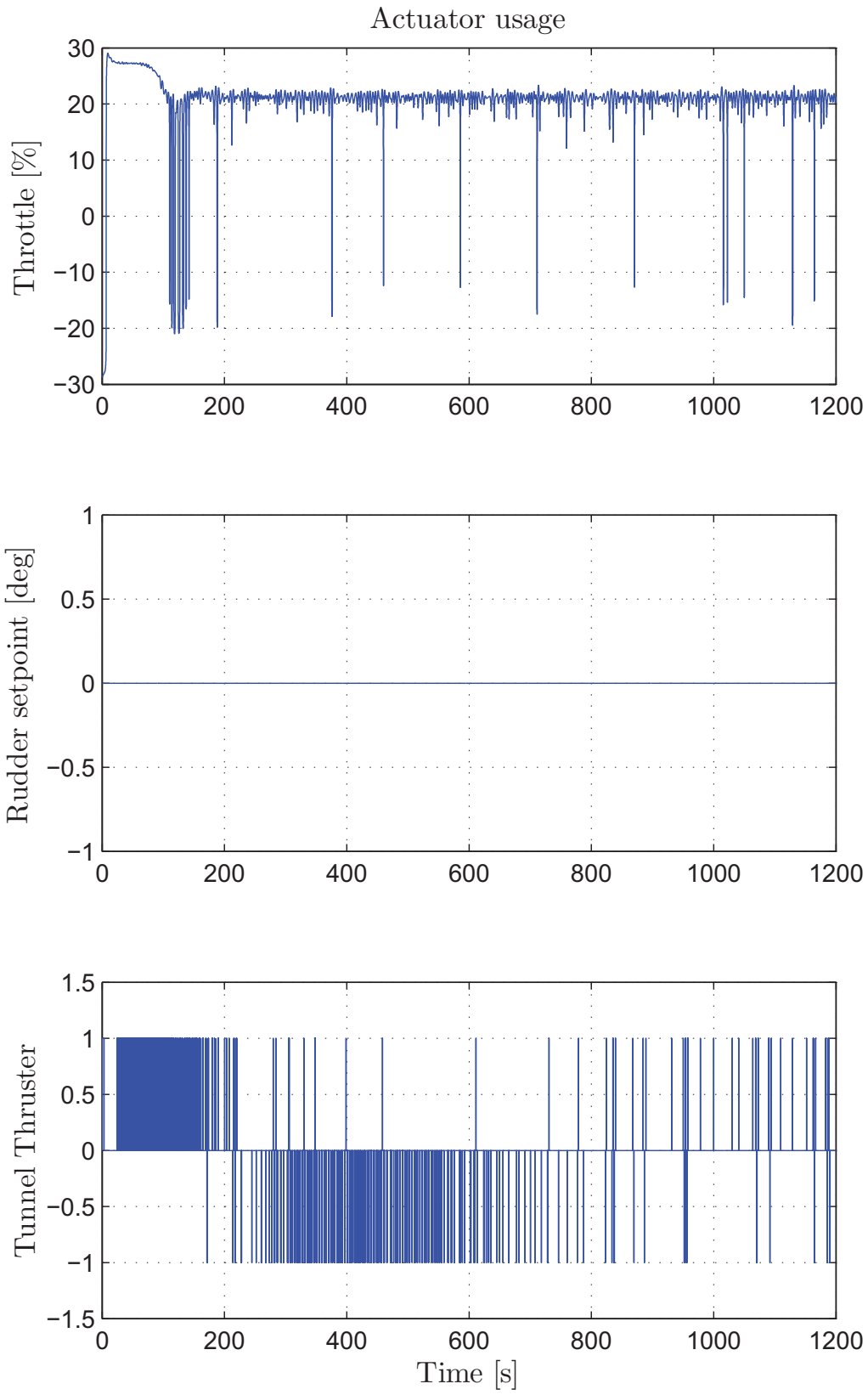

Figure 6.44: WOPC actuator usage using a weather optimal heading stable vessel.

6.6.3 System and simulator performance discussion

The simulator appears to work satisfactory even though simplified models and deviating parameters are applied. The simplified models encompass the most important dynamics of the operating range used by the control system. Most of the vessel parameters apart from the non-linear surge damping was found by trial and error, although all could possibly be improved by performing full scale vessel experiments.

One of the most significant parameters of the vessel model is the mass which was calculated by the hydrodynamics software to be approximately 40 % larger than the data supplied by the manufacturer. These parameters are found by using the vessels line drawings, on the other hand the accuracy of the hydrodynamics software when calculating parameters of small vessels is left not verified. The draught of the vessel was calculated to be 0.76 [m] when it is stated to be 0.59 [m]. Why this difference has occurred is unknown. A larger mass and draught seems to have affected the other parameters, calculated by the hydrodynamics software. However, similar performance as the recorded vessel data was achieved in the simulator. A reason for this could be that some of the effects of the divergent parameters were reduced by the tuning of the actuator models. To further correct the vessel model parameters, experiments could be performed, in addition to be time consuming this would require expensive high precision instruments out of reach for this thesis. Another alternative could be to recalculate the parameters using other settings.

The wind model in particular might deviate significantly from the real world due to the vessel type assumption and aerodynamic properties of the vessel. This could be corrected through experiments and calculations of the wind coefficients. However the most important aspect of the wind model is that it delivers a yaw moment which correlates to the structural design of the vessel. It is critical to counteract this disturbance effectively for good system performance.

The weather models are unconnected, meaning that the setup of one model, does not affect the others. An example of this is that wind does not affect the waves in either magnitude or direction. To obtain realistic scenarios, the environmental models was set up manually. The Beaufort wind scale was used to find the appropriate wave height at given wind speeds. However, in sheltered waters where small vessels mostly operate, this does not comply precisely. Obstacles and shallow water depths both affect the wave speed and height in addition to wind direction. The wave heights in sheltered waters are assumed to be lower than ocean waves, which can be fully developed over vast distances.

In general, the control system has good performance as the system converges to the desired position within reasonable time. The weather optimal heading is found without the need of estimation through controlling the heading towards a given point. The tuning of the system is assumed to be sub-optimal and increased performance could possibly be achieved through optimal parameters. High frequency disturbances influence the controllers, and occasionally create unwanted behaviour, such as using reverse to correct the pendulum length

when heading up against the weather. This could be a tuning issue, but an effective wave filtering scheme could possibly help lower the total actuator usage and reduce mechanical wear-and-tear. A passive wave filter as described in [Fossen, 2002]was implemented but the performance enhancement was unnoticeable. This could possibly also, be a product of poor tuning, but as the vessel dynamics are highly influenced by the waves, this is a matter which cannot be filtered as noise, and due to the potential loss of dynamics this tuning must be highly accurate to discriminate unwanted effects and preserve the essentials. More research must be undertaken to investigate how to obtain the best possible signals.

The surge controller can be improved in several ways. Due to the implementation of the area restricted integral effect, possibilities for ending up outside of this, in a stationary deviation, are always present. This offset from desired area can be detected and trigger a widening of the integral zone. As both deviation from the suspension point and integral zone is stated in meters, a direct update of the integral zone can be immediately achieved. Another issue when facing into the environmental force is the use of reversed propulsion power. This should be unnecessary as the environmental force will push the vessel backwards, if the throttle is reduced to be less than the force equilibrium between wind influence and propulsion thrust. This is a tuning issue, and an adaptive gain, which is related to the environmental force magnitude, could most probably yield good results. In good weather a slow controller is desirable and in harsh it needs to be more aggressive.

The switching between the yaw controllers always chooses one of the actuators to create the necessary yaw moment. This is not always the best solution, as an active rudder could be used to correct the minor deviations. However at low throttle, due to low water speed over the rudder surface, the rudder has low efficiency, in many cases unable to create noticeable rate of turn. At very harsh conditions, active rudder could be a feasible approach to ease the tunnel thruster load.

The tunnel thruster controller performance is one of the major drawbacks of this implementation. It exceeds the limitation of 8 % of time by far and is pulsed on and of rapidly to correct the angular deviation. Better tuning could possibly help some, but the main reason for the high usage, is the physical naturally weather unstable vessel design. This means, if the vessel heads into the weather, it will be turned away when produced yaw moment is zero. This is somewhat analogue to an inverted pendulum in a gravity field. The difference is that the force acting on the vessel is proportional to the longitudinal projected area against the wind and waves. At weather optimal heading the vessel is not affected by a turning moment from the wind and waves, but a stable weather optimal heading is almost impossible to using the on-off tunnel thruster. In harsh conditions the yaw deviation is approximately the same as the size of the relay zone around the weather optimal heading.. To obtain a stable weather optimal heading two approaches could be taken. In the first scheme, a proportional thruster could replace the present on-off type. This would cater for minimized wind and wave moments which in turn most certainly would result in significant in energy consumption drop, and yield a more efficient and environmental friendly positioning system. The other approach is to alter the vessel geometry making it

stable. On the Vikens 830, this could easily be achieved by mounting a spanker sail and or a canopy covering the area behind the wheelhouse. However, the latter suggestion would not affect the wave influence on the yaw dynamics. As long as the wind induced moment is larger than the wave moment, the vessel would be weather optimal heading stable. This opens for the continued use of the presently installed electrical on-off tunnel thruster which could be incorporated in a more sophisticated control scheme, utilizing the wind to turn the vessel.

The suspension point controller makes the vessel coincide with the desired position, and the angular rate of the suspension point is limited of the vessel yaw rate, and pendulum dynamics. If the suspension point is moved too fast, oscillations will incur, in the worst case convergence is not obtained. The suspension point change rate for a given scenario is dependent on the magnitude of the environmental resultant force. As this is difficult to gauge during convergence, the angular speed rate of the vector between the vessel and suspension point was used. Somewhat better convergence time could possibly be obtained by better tuning and more sophisticated gain update or movement update laws, which also considers the angular deviation between heading and suspension point.

By utilizing the different effects of the length of the pendulum, the performance could be improved. To minimize convergence time a short pendulum could be used as the system converges and when close to the desired position and optimal heading, a longer pendulum could be applied. Determination of the two extreme lengths could be done by applying statistical tools to the deviations, and through this updating the pendulum lengths, to meet preset requirements on maximum deviations and thruster usage after convergence. In any case it would be beneficial to use a small pendulum during convergence as this minimizes the convergence time and deviation. A short pendulum system can be regarded as a high gain system, as it will be more aggressive than one using a long pendulum, which has low gain characteristics. From the simulation study, it seems like a pendulum length of twice the vessel length yields desirable convergence performance and stability.

The motivation for the making of control and allocation system as presented was to create something that could easily be exported to the real world vessel holding capacities to suffice a wide range of applications. In addition to the proposed suggestions there are several others which also could increase the system performance. To help create more precise controllers and thrust allocation, feedback from the actuators could be mounted. An inertial navigation system could be created by installing accelerometers and gyros, which signal is integrated into a Kalman filter, along with GPS data. Hybrid diesel electric propulsion could be installed. This would require extensive mechanical work, on the other hand a high bandwidth, high precision propulsion solution, independent of trolling gear, would be achieved. It would also cater for better weight distribution and the utilisation of green energy to charge the battery pack. Adding solar panels and wave regeneration devices, would extend operation time, introduce a green profile and be more environmental friendly. A wave regeneration device could possibly be realized by suspending a mass in springs, and use the inertia to drive an electric motor. The same principle could also

possibly be used with magnets.

Chapter 7

Experimental implementation and results

Simulations are excellent tools for system development, experiment design and performance testing. It is like mapping and printing charts, correct scaled mirror landscape images, depend heavily on correct real world measurements.

Bearing in mind the fact that simulations are synthesized reality implicate simplifications and inaccuracies. Simulated scenarios performance has to be verified through real world experiments, preferably as iterations. If the dualistic interrelation is neglected it might jeopardize both problem understanding and solutions. In case of this thesis this means developing and implementing the WOPC system into the Viknes 830 USV, owned by Maritime Robotics, heavily depends on successful full scale testing.

If the system works during simulations it is a fair chance that it will be working in real life also. Full scale experiments are important to disclose and surface system integration problems and onwards verify the actual system performance, as this operates under non-optimal conditions.

7.1 Setup and implementation

The control hierarchy of the Viknes 830 USV is displayed in Figure 7.1. This solution, implemented by Maritime Robotics, applies standard MATLAB / Simulink software on the laptop to calculate the appropriate actuator set-points, and send the results to the OBC which communicates with each of the electromechanical actuator interfaces. This implementation scheme has proved to function in other experiments although of other applications.

The communication between the laptop and OBC is through a twisted-pair cable where

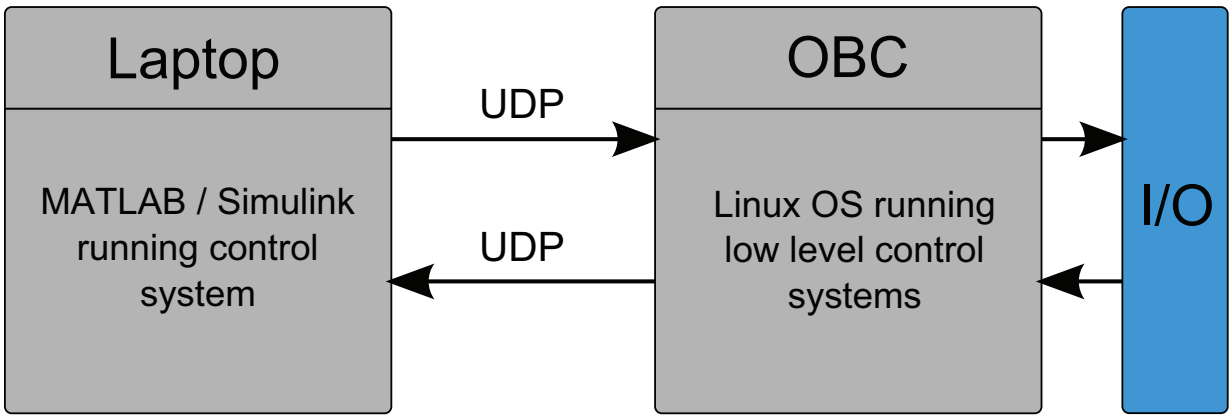

Figure 7.1: The control hierarchy of the Viknes 830 USV.

UDP packages are sent. The OBC feeds position and velocity data through this interface and obtains calculated actuator set-points. In all of the experiments a HP dv2000 laptop running Windows XP was used to run MATLAB version R2008b. To apply this to the Simulink interface offered by Maritime Robotics, no alterations to the control system used in the simulation had to be introduced.

7.2 Experiments

Four separate sea trials were conducted. The purpose of the first sea trial was to obtain a feel for, and outline a strategy of what needed to be done, in order to create a working WOPC system and record data. Furthermore, actions to enhance the 6 DOF Viknes 830 model, and actuator models, and help create a thrust allocation scheme were considered. The investigated aspects were; the throttle to engine rpm dynamics; the trolling gear dynamics; and the low speed rudder- and tunnel thruster dynamics. In this operation an attempt to keep the vessel in position (DP) by manual control was made. These tests discovered several important aspects upon deciding system design. The existing implementation of the controller switching, was based on measured rudder efficiency which was found to be low at assumed operating velocities, whereby the tunnel thruster was found superior. Based on this, given the current thruster configuration, and as the tunnel thruster control interface was scheduled to be implemented within short time, creation of a WOPC system was concluded to be possible. At the time of the test, the tunnel thruster was operated by manual control.

The second sea trial was intended to be an initial systems test, collect data and point out problems to be corrected. After some initial difficulties the system worked sufficiently to record data, appropriately displaying the functionality. As it barely managed to keep the vessel within 25 [deg] of the intended heading, the implemented tunnel thruster controller was found to be insufficient.

The third and fourth tests were intended to be a tunnel thruster controller and systems test respectively, but a series of unforeseeable problems occurred, and to some extent prevented this. The third test was shortened, due to problems with the vessel on-board systems, in addition to severe tunnel thruster controller encountered oscillations during testing. These were believed to be result of bad tuning and buggy implementation. The system was examined and slightly adjusted before the last sea trial. The problem continued and neither the WOHC, nor WOPC system, could be tested due to heading control malfunctioning.

7.3 Problems analysis

After the fourth sea trial the recorded data of the faulty behavior was analyzed to point out the source of error. Seemingly there is a significant delay in the heading measurement and yaw-rate signal, sending the controller into constant oscillations, trying to compensate the deviating heading and yaw rate. Figure 7.2 features the problem where it can be seen how the tunnel thruster is held high, to create the desired yaw rate towards the desired heading. It is kept high until the desired yaw rate is measured. Due to the fact that these should be aligned, the delay time can be measured between the falling edge of the tunnel thruster and the top of the measured yaw rate. When no tunnel thruster moment is applied the yaw rate curve turns as a result of damping. It could be questioned, however, whether the tunnel thruster actually was on during the whole high signal interval but the tunnel thruster spin-up time to full thrust is short and no significant delay on the output of set-points to the actuators was experienced. The yaw-rate magnitude indicates that the thruster must have been on for some time to gain the observed angular velocity. The tunnel thruster controller used when gathering these data is simplified due to the experienced problems and it only tries to correct the heading within a band of $\pm$ 1 [deg/s] of the desired trajectory. This was done in an attempt to see if this rather simple measure of performance could be achieved.

Figure 7.3 shows the heading measurement of the test which yaw rate is displayed in Figure 7.2. The heading can be observed as it converges slowly to the desired course, despite severe oscillations. Whether other variables in $\boldsymbol{\eta}$ and $\boldsymbol{\nu}$ has the same delay is not verified. This could be achieved by applying thrust to the propeller and observe if the velocity and position variables and are correctly updated.

Several possible explanations for the delay are available, of which the most probable is interaction issues between the laptop running the control system and the OBC. As mentioned the link between the two consist of UDP packages, and somehow the data stream is delayed, either at the laptop end, at the OBC, or in the Furuno GPS system. It could be that the Furuno GPS system takes some time to obtain the correct variable values, based on the low frequency GPS signal, and this in conjunction with the signal filtering creates a significant delay. An alternative hypothesis is that the OBC prioritizes the data transmission badly or is overloaded. However, this is unlikely as the output is a continuous

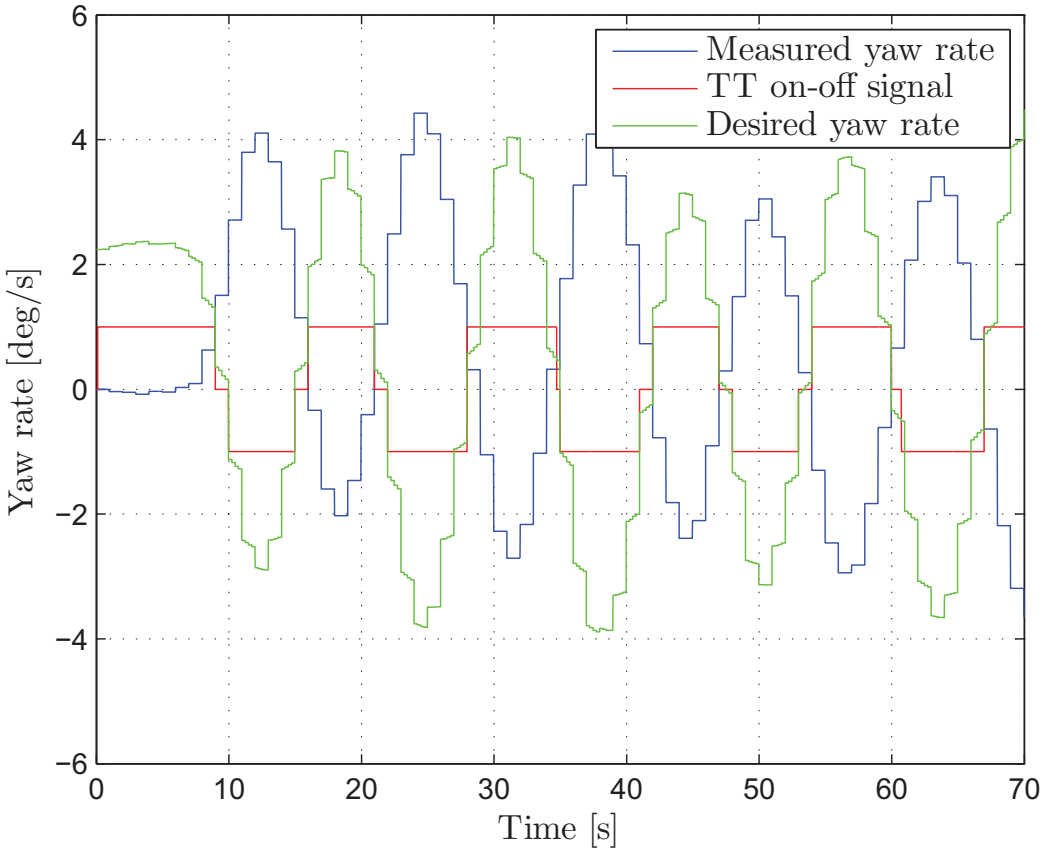

Figure 7.2: Yaw rate delay problem during experimental tests.

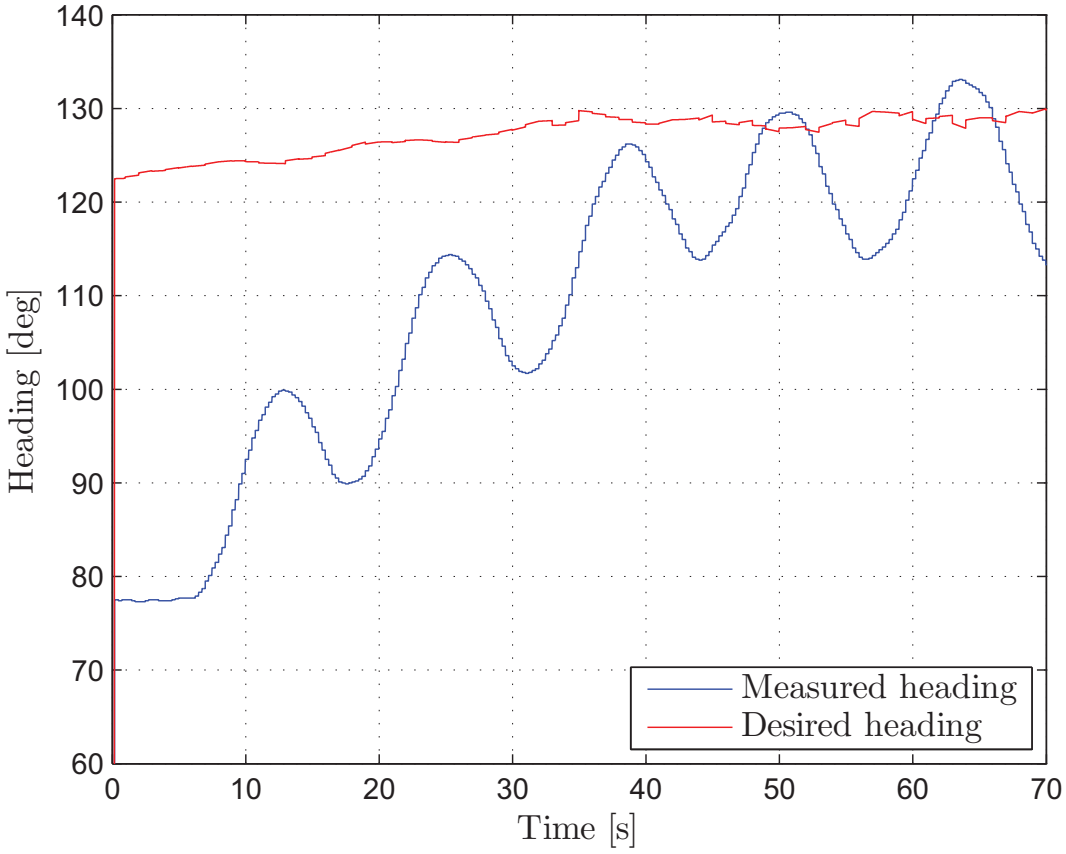

Figure 7.3: Heading delay problem during experimental tests.

data stream with an almost constant delay. Another possibility is control system laptop overload, malicious software, or hardware creating the problem. On the other hand as similar problems were seen using another laptop in a different experiment, this is unlikely. The suggestions above are merely speculations and the actual reasons to the problem remain unrevealed. Further investigation must be conducted to find and solve the problem.

During the second sea trial, the system performance was much better. Figure 7.4 features a yaw rate plot from the data gathered during the successful tests. It can be seen that the yaw rate delay is not as significant as encountered in the final sea trials. However, the problem is present, and can be seen as the top of the yaw rate does not culminate when the tunnel thruster is shut off. It should be noted that the Simulink time for unknown reasons was slower than real time, how this affected the yaw rate measurements has not been investigated as it was discovered in a late stage of the experimental tests. However the total performance of the system was significantly higher during the second sea trial. It should be noted that the exact same setup as used in the second sea trial was tested during the last experiments without gaining close to the same performance. As with the updated system used in the simulations and during the last sea trial it was not able to achieve high enough performance to do anything useful.

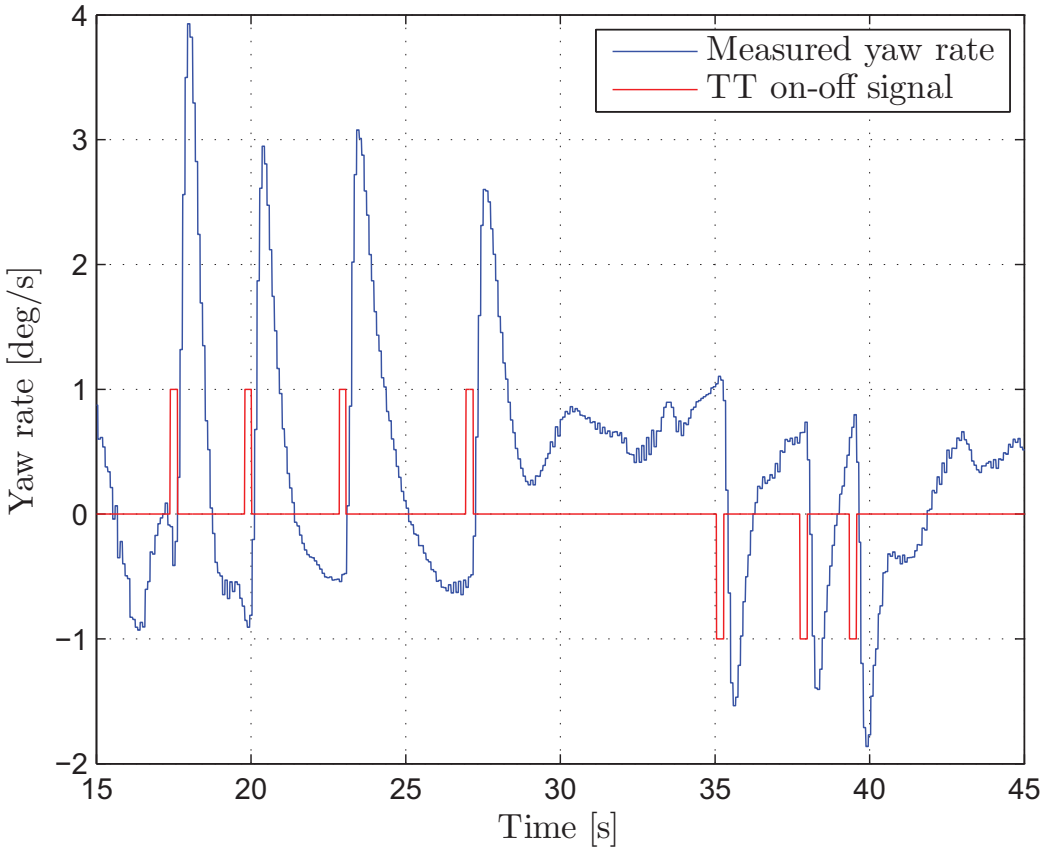

Figure 7.4: Reduced yaw rate delay problem during experimental tests.

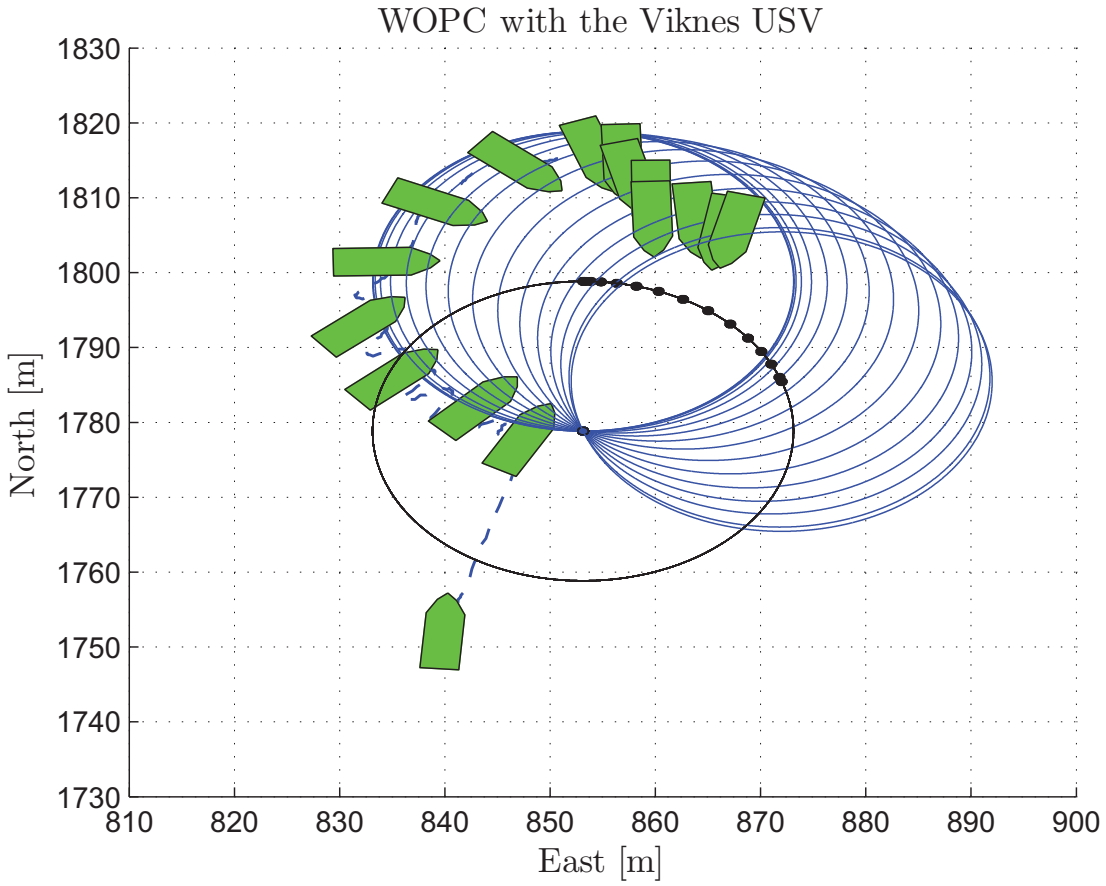

Figure 7.5: Visualization of WOPC sea trial experiment.

7.4 Experimental results

As mentioned the second sea trial provided test results where the system functioned as supposed. Figure 7.5 features a visualization of the recorded data where a 20 [m] pendulum was used. The vessel can be observed as it manages to converge to the suspension point circle, and follow this as it is moved towards the position where the vessel and desired position coincides. The conditions on that day were clearly a Beaufort 0. As the weather was fine and no wind was present the experiment was conducted outside the river mouth of Nidelva in the Trondheimsfjord. The conditions are assumed to be approximately the same as in the described simple sea state simulations in Chapter 6. The system was initialized with the stern facing the river current, and it can be seen that the vessel turns to face the disturbance. There was also a problem during this experiment, the Simulink time was not correct and appeared to be 2-4 times slower than real time. What caused this has not been possible to investigate thoroughly, it is, however, assumed to be a computer or program overload problem. Simulink as it was used during these experiments is not designed to

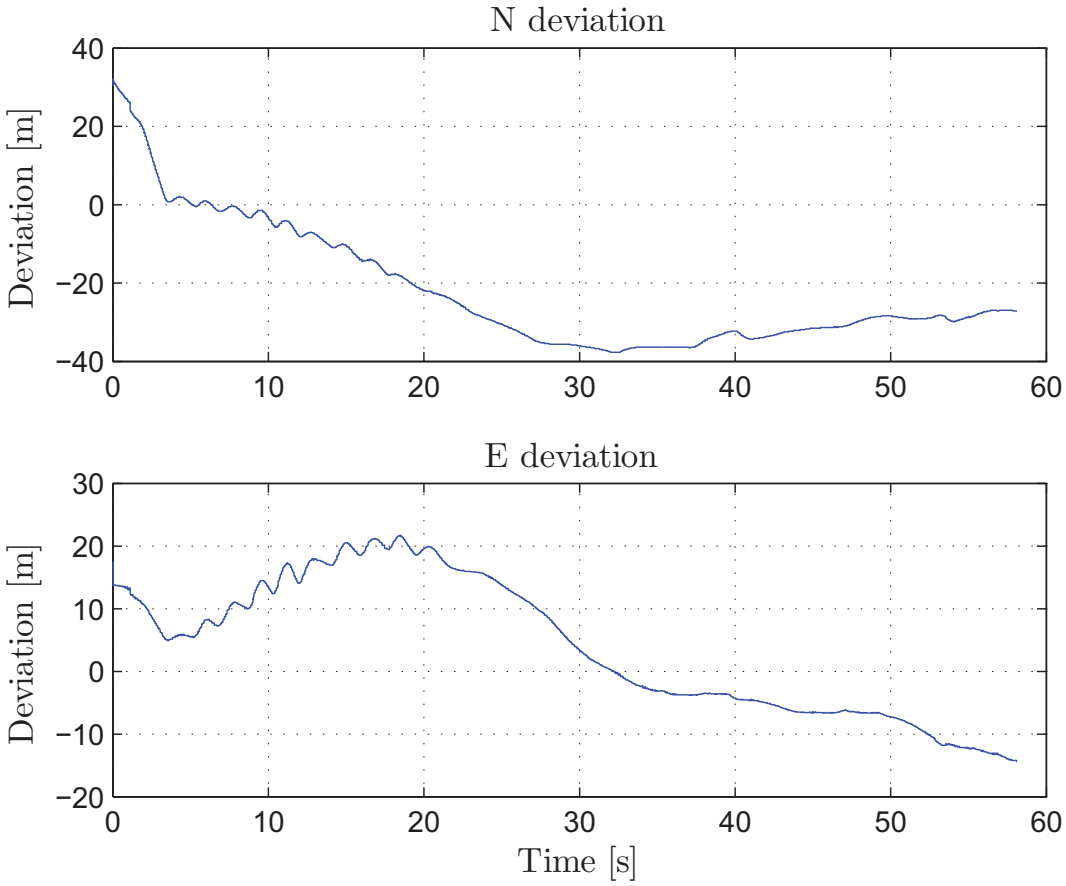

Figure 7.6: WOPC sea trial deviations from desired position.

operate as a real time control system and logging tool.

Due to the misconception that it was converged, time limitations, and the fact that this was only meant as a systems test to see if it worked, the experiment was unfortunately terminated before full convergence was obtained. The initial plan was to use this data to gain higher performance and record other datasets on a later stage in the development which could be used in this thesis, however due to the signal problems, this could not be done.

Figure 7.6 features the deviation from the desired position as the vessel converges. It can clearly be seen that the north deviation is on its way towards 0. For the east deviation, as the system converges it would have increased until approximately -20 [m], as the suspension point obtains 90 [deg] angle from the desired position, and then it would have decreased to 0 as the suspension point is moved to coincide vessel and desired position.

Figure 7.7 feature the desired and actual angle from desired position to suspension point which is moved by the suspension point controller to make the vessel coincide with the

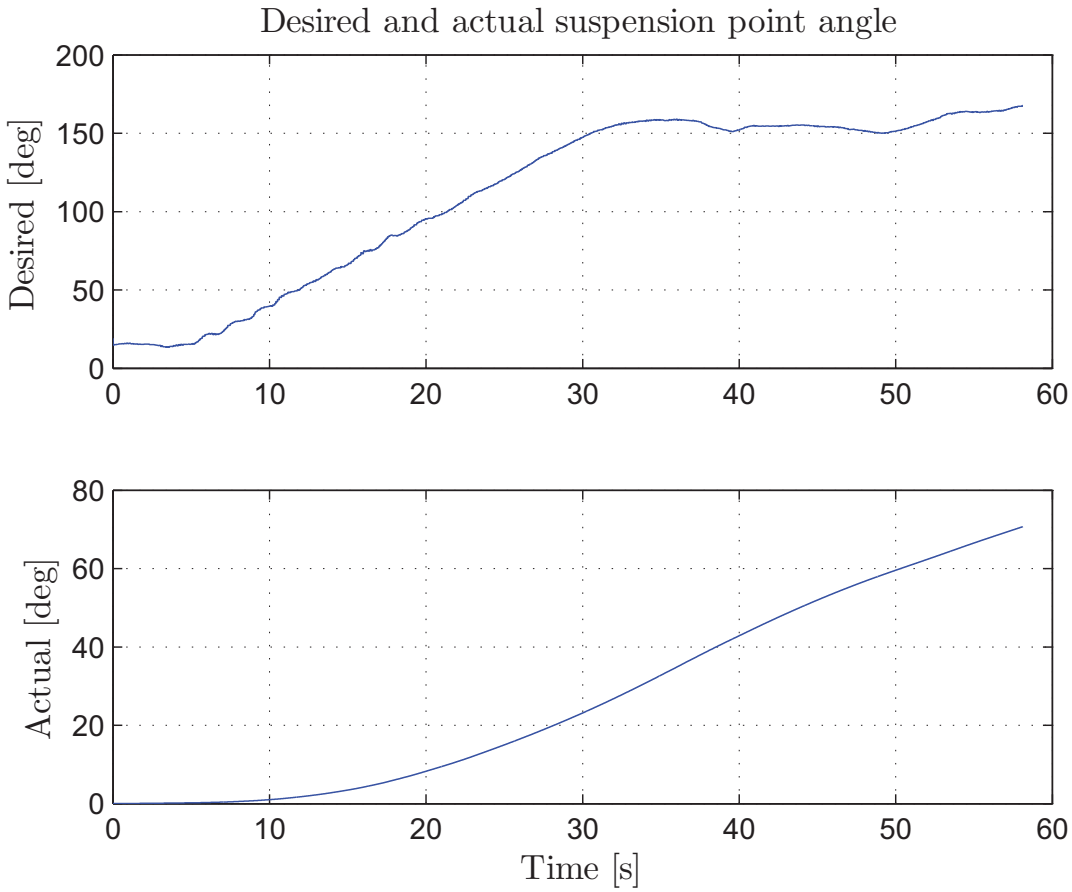

Figure 7.7: WOPC sea trial desired and actual suspension point angles.

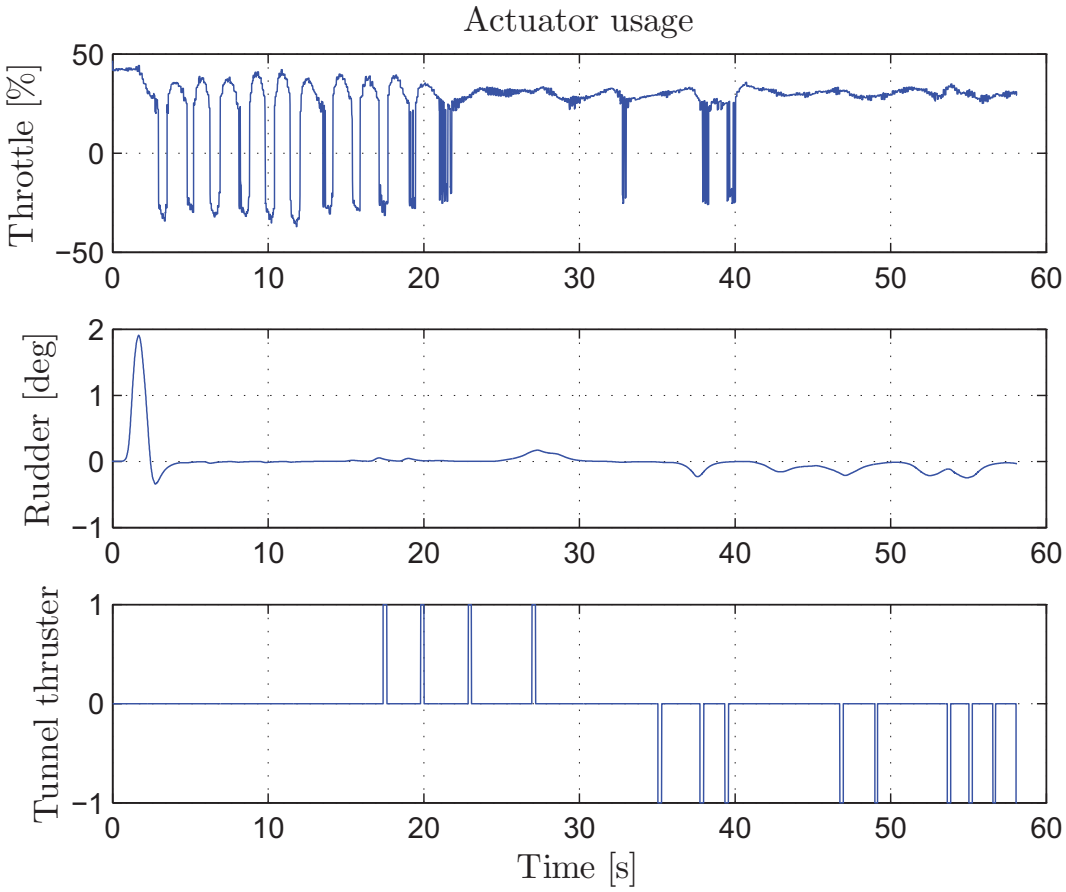

Figure 7.8: WOPC sea trial suspension actuator usage.

desired position. This test was done before the initialization scheme was implemented and the starting angle of the suspension point was set to 0 [deg]. From the desired angle plot it can be seen that with time the actual and desired angle will coincide at approximately 170 [deg]. Due to the poor tunnel thruster controller implementation used during this experiment, it is assumed that the movement of the suspension point would not converge to a stable angle, but remain at some slowly oscillating level. Based on the slow Simulink clock the dynamics of the suspension point movement became much slower than intended, which also caused the system to have slow convergence. Actually for how long the experiment lasted is but it is assumed to be at least 2-4 times the time of the Simulink clock.

Figure 7.8 features the actuator usage during the experiment. It can be seen that the rudder is used during the whole sequence, this is due to an experimental system, which allocated yaw moment to both thruster and rudder. This solution was dismissed as a new tunnel thruster controller was developed. The tunnel thruster controller used during the experiment was very simple and only pushed the heading towards the desired course if the deviation exceeded $\pm$ 25 [deg]. This can be verified by looking at the bottom plot

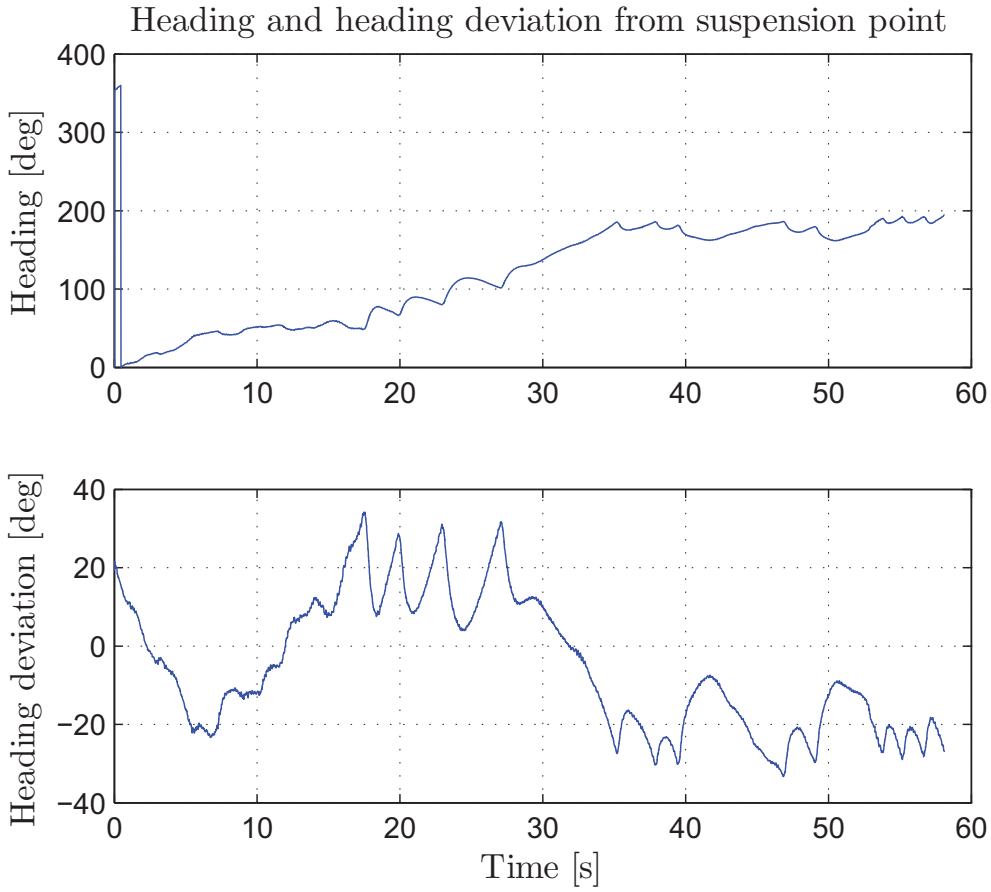

Figure 7.9: WOPC sea trial heading and heading deviation from suspension point.

of Figure 7.9, which features the heading deviation from pointing towards the suspension point. The top plot of the figure displays the vessel heading, where the effects of the tunnel thruster and the approximate weather optimal heading can be seen. The vessel stabilizes its heading at approximately 170-180 [deg] which is intuitively correct, as the vessel had approximately 0 [deg] heading when the stern was facing the river mouth.

Figure 7.10 features the second successful systems test of the second sea trial. This was placed 300 [m] 90 [deg] off the initial position of the vessel. As for the first test, it was terminated to early, due to Simulink clock problems; the uncertainty of convergence along with only being an initial systems test not assumed to be used in this thesis. This test was terminated even earlier, in the convergence, than the one presented above. The test revealed a badly tuned rudder controller which was corrected after the tests was finished. The rest of the data plots from this test can be seen in Appendix B.

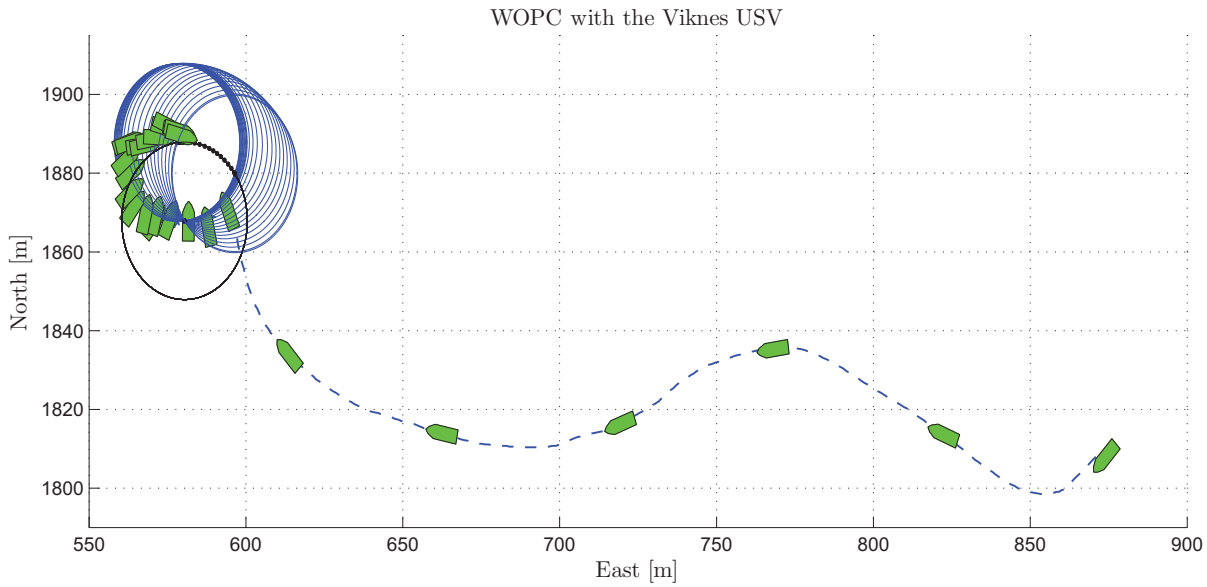

Figure 7.10: Visualization of WOPC sea trial experiment with travel distance.

7.5 Discussion and proposals

Several equipment problems and test facility access prevented experiments demonstrating the system satisfactory performance fulfilment. Despite this, enough data was gathered to conclude that the system presented in this thesis is highly capable to work as intended if the signal feed from the vessel and real-time capabilities of the platform running the control system is decent. The system presented above has shown the intended operational properties. Most of the problems encountered during experiments can be ascribed to the vessel and existing installed equipment.

To create a better test platform, several measures could be taken. For instance the model of running the control system on a separate laptop should be avoided and a proposal to an alternative control hierarchy can be seen in Figure 7.11. The benefit of this system is that the data sent between the laptop and OBC does not have the high real time demands as in the current implementation. Furthermore a control implementation in C would demand less computational power.

Commercial solutions delivering the described functionality exist. One of the systems which might be adequate is the The MathWorks, Inc [2010] real-time workshop extension to MATLAB. This software offers generation and execution of stand-alone C code, for development and testing of algorithms. The generated C code can be loaded into the OBC, and interacted with using Simulink or other application of choice. This solution enables the control system to run with a higher bandwidth closer to the low level controllers. This would likely remove the possible network error, provide faster signal flow between the

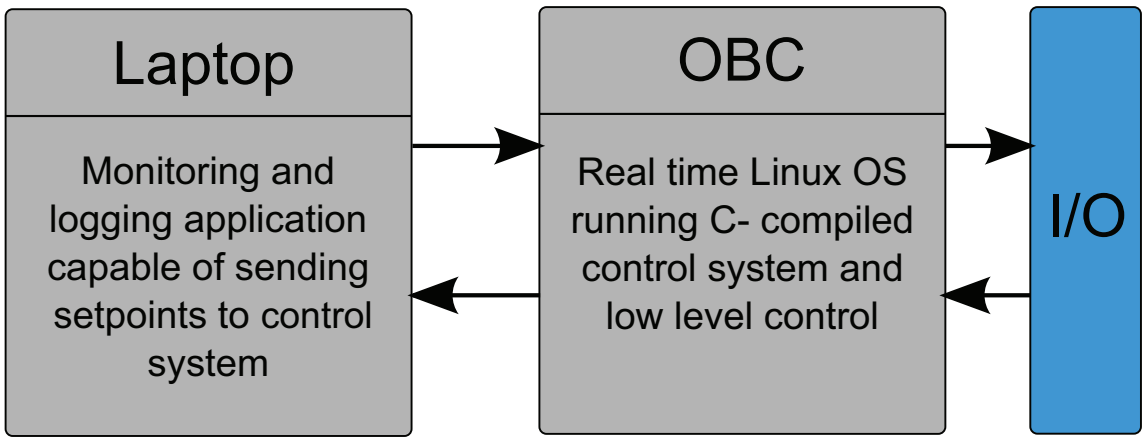

Figure 7.11: Proposed alternative control hierarchy

controllers and ensure better timing when interacting with the actuators. This would also remove the uncertainty of running the control algorithms in an ordinary Simulink setup.

However it is not solely the control hierarchy that should be changed to obtain a reliable and versatile development platform. Upgrading the signal handling system to encompass gyros and accelerometers could prove advantageous. The output from these implementations along with the data from the Furuno GPS system then could be implemented in a Kalman filter. This incorporates the vessel dynamics and reduces the phase problems of other filtering techniques. Additional benefits of a Kalman filter would be the improved signal quality from using separate sensor systems, and it is further reason to believe that this could also improve the delay problems. In Furuno SC-50 Specifications [2010] it is stated that it contains a 3-axis vibrating-gyro rate sensor and that it should be possible to setup this device to deliver yaw-rate with 40 [Hz] update rate. Maybe the yaw-rate problem could be as simple as a badly setup Furuno system.

Another aspect of obtaining a reliable and easy-to-use development platform is the OBC location which in the current configuration is placed in an outside storage compartment in the rear of the vessel. Even though this compartment offers a seal on the hatch, it is more susceptible to moist and corrosion which might lead to indeterministic and unstable behavior of certain modules as the hatch is opened several times during experiments in all sorts of weather. As much of the electronic systems as possible should be placed inside the wheelhouse where the environment is dryer and placed readily accessible for the developer.

All of the proposals to upgrade the Viknes 830 USV include economical investment, either in equipment or in working hours, and it is not in the scope of this thesis to decide or suggest what should or should not be done to resolve the problems encountered, on the other hand, if suggested installations are executed, the Viknes 830 USV will appear much more adequate to similar system development tasks as presented in this thesis.

Chapter 8

Conclusions and future work

A positioning controller based on the simple and intuitive pendulum principle was derived. This weather optimal heading strategy can be used both by fully actuated and underactuated vessels, delivering good positioning capabilities to heading independent operations. The convergence rate towards the weather optimal position is directly linked to the pendulum length. Utilizing this, further fuel efficiency might be gained. The control system consist of two separate controllers, the first creates the pendulum analogy by keeping distance and heading towards a given suspension point and the second moves the suspension point to coincide vessel and desired position. Conventional reference filters can be removed by applying the mathematical properties of sigmoid functions. These functions might define a velocity profile dependent on the deviation from the desired position, in turn resulting in bounded control inputs for the virtual line controllers. This approach also removes the need for conventional proportional terms.

A 6 DOF vessel model using parameters derived by hydrodynamic software with actuator dynamics and environmental disturbances was developed to simulate the underactuated Viknes 830 USV behaviour, and further study the performance of the control system. The simulations clearly demonstrate system capabilities of handling both calm and harsh weather, consisting of waves, wind and currents. Simulations also revealed the significance of the structural vessel design to have paramount importance in terms of actuator usage. A weather optimal heading stable vessel will use less yaw moment to maintain its heading compared to an unstable one. Successful sea trials indicate that high performance of the real-world implementation should be obtainable if the position and velocity signals have appropriate real-time capabilities.

WOPC schemes yield greater freedom in USV design, enabling greater diversity in propulsion configurations, which is convenient for utilizing the removal of the human factor in radical hull designs. Fully actuated or not, to enhance its performance and subsequently increase the endurance, the design should take advantage of the environmental disturbances using them to its benefit. As future work several aspects should be considered:

- **Complete Lyapunov proof**
  The Lyapunov proof should be completed to mathematically demonstrate combined system convergence.
- **Verify and enhance simulator accuracy**
  Deviating simulator parameters should be verified and updated through high precision data recorded at sea trials and other experiments. Additionally more advanced wind and current models should also be considered.
- **C code implementation of WOPC system**
  To provide better real-time capabilities the control system should be implemented in C/C++ as this could be run on the on-board computer.
- **Pendulum length control**
  Pendulum length control should be applied to enhance the control system performance. By using a short pendulum with rapid convergence when far from the desired position, and changing to optimized pendulum length according to operational position accuracy and fuel consumption criteria after convergence.
- **Kalman filter**
  A Kalman filter should be implemented to enable the use of increased sensor diversity to enhance the total signal quality.
- **Performance verifying sea trials**
  When the signal issues have been resolved, sea trials further documenting the system performance should be conducted.
- **Wave management**
  To enhance the control system performance and decrease fuel consumption, a wave management and filtering scheme could be a feasible implementation. This would aid the controllers to determine when to counteract the waves and when not to.

Appendix A

Data used in ShipX/Veres

Ship name: Viknes
Loading condition description: Design waterline

ShipX exported data
Main dimensions (from input):

Length between perpendiculars	(m)	7.200
Breadth	(m)	2.573
Draught, midship	(m)	0.760
Sinkage	(m)	0.000
Trim, + = aft	(deg)	0.000

Coefficients for data check etc:	Type	Specified	Calculated
Displacement	tonnes	5	5
Vertical center of buoyancy	KB		0.562*
Vertical center of gravity	VCG	1.012*	
Longitudinal center of buoyancy	LCB		2.837*
Longitudinal center of gravity	LCG	2.850	2.837*
Block coefficient	Cb	0.349	0.347
Water plane area coefficient	Cw	0.884	0.785
Prismatic coefficient	Cp		0.753
Mid section area coefficient	Cm	0.483	0.460*
Longitudinal metacentric height	GMl		8.623*
Transverse metacentric height	GMt		0.971*
Roll radius of gyration	r44	0.890*	
Pitch radius of gyration	r55	1.960*	
Yaw radius of gyration	r66	1.960*	
Roll-yaw radius of gyration	r46	0.000*	

* - Applied in the hydrodynamic calculations

ShipX - 10.02.2010 - 15:32:05 - Licensed to: TIF CeSOS (NTNU)

Appendix B

Experimental data

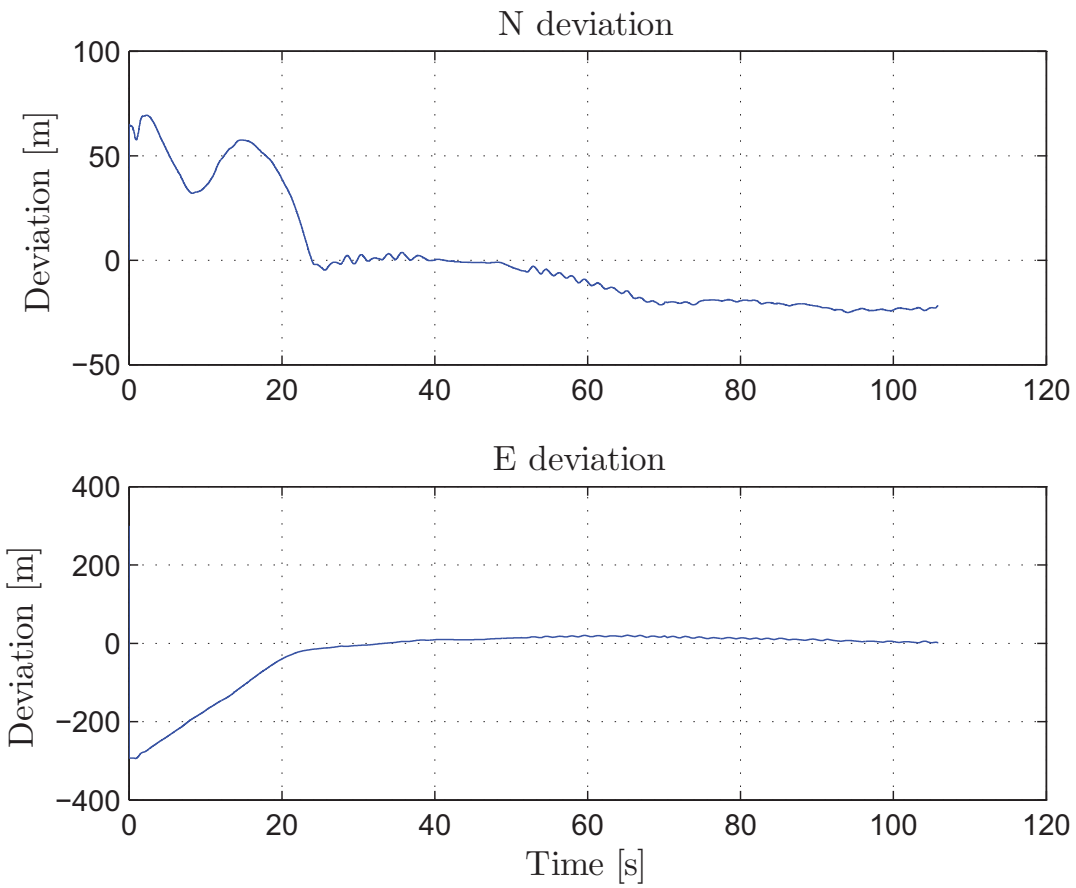

Figure B.1: Second WOPC sea trial deviations from desired position.

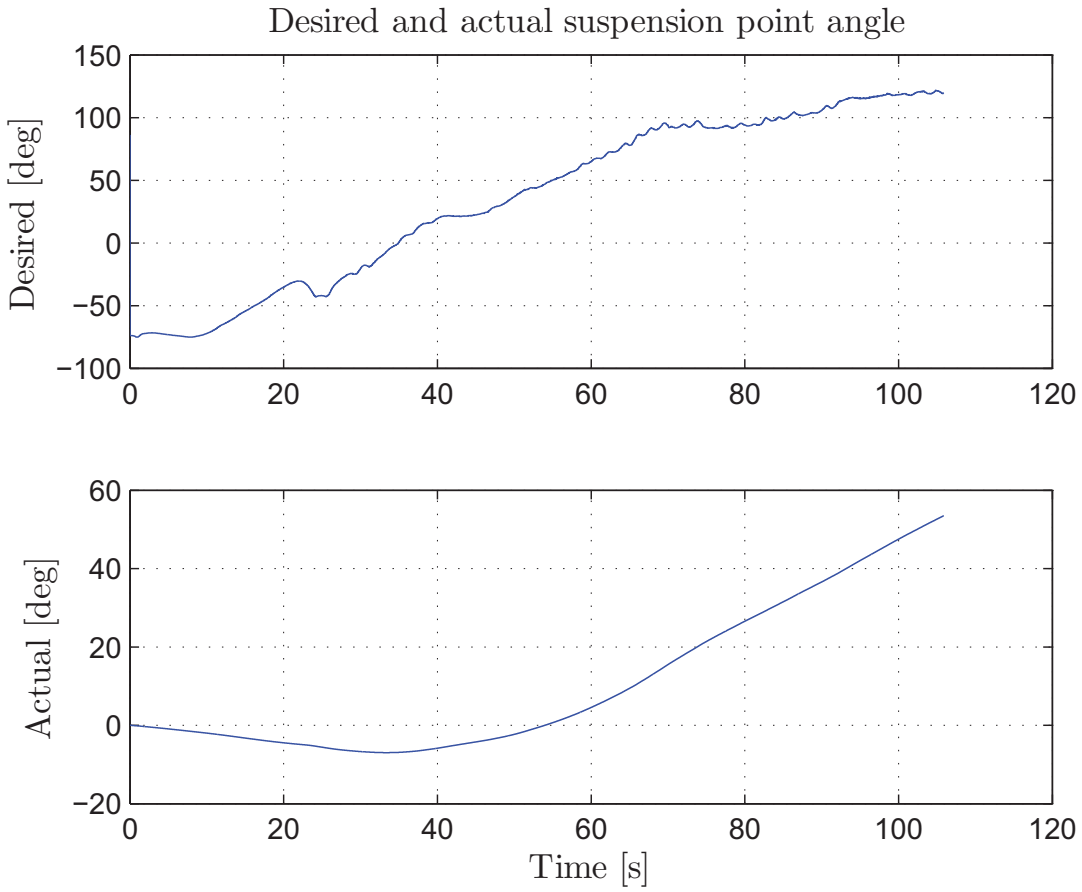

Figure B.2: Second WOPC sea trial desired and actual suspension point angles.

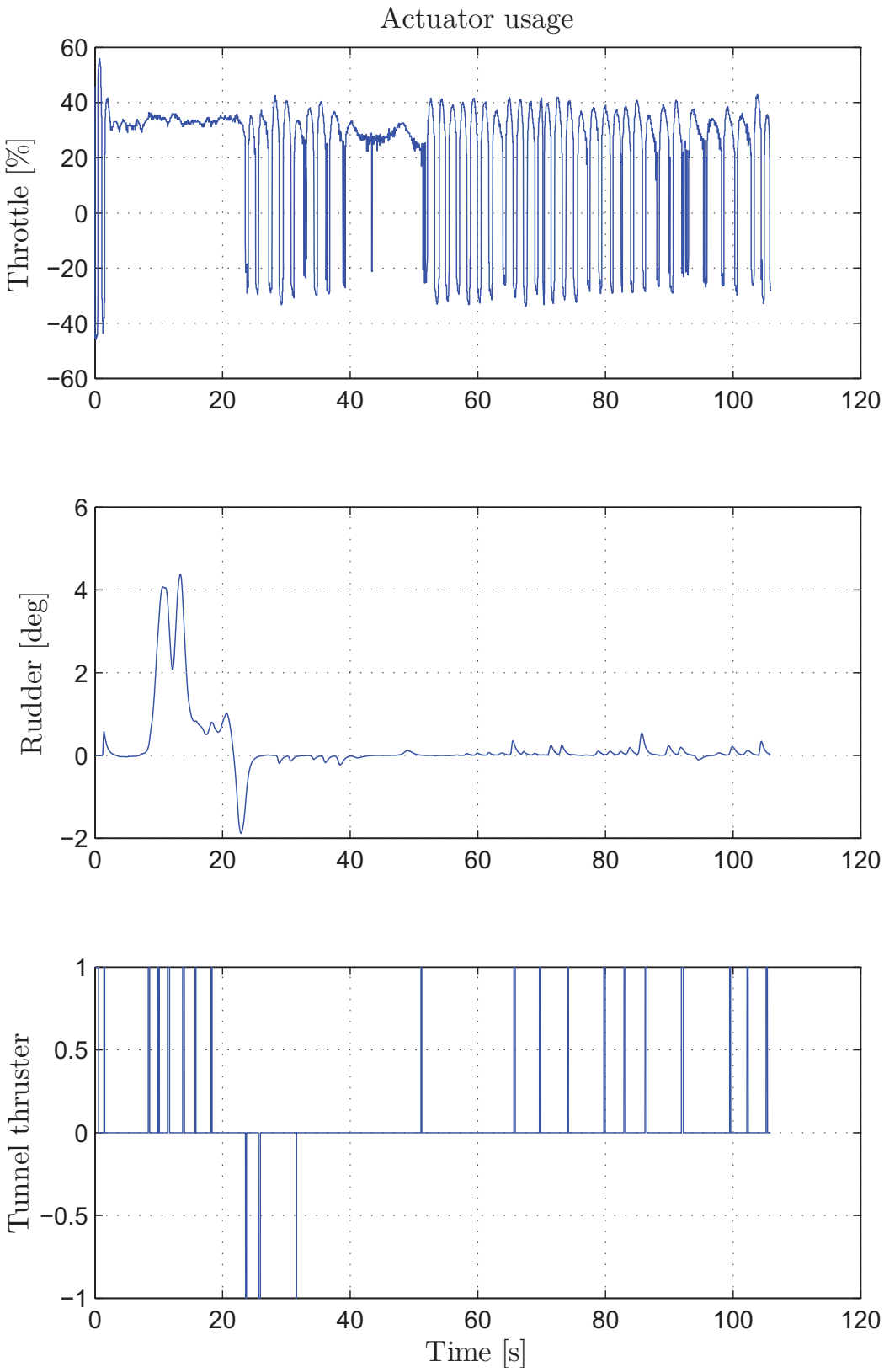

Figure B.3: Second WOPC sea trial suspension actuator usage.

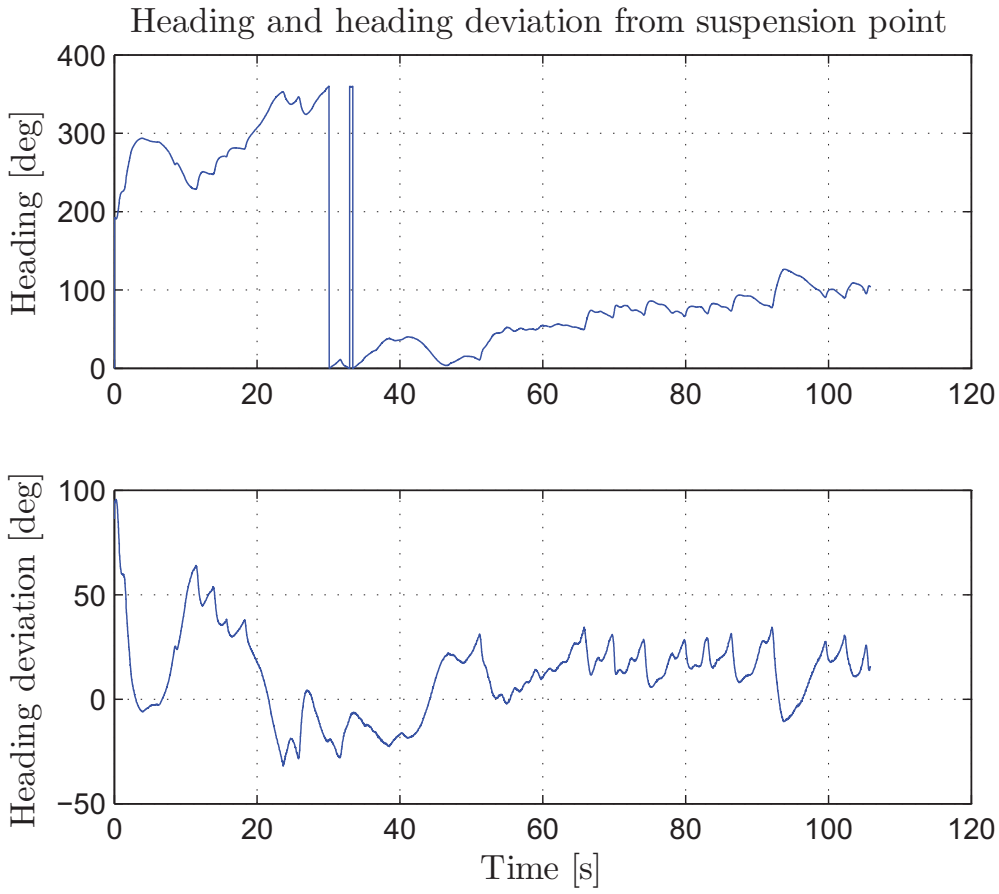

Figure B.4: Second WOPC sea trial heading and heading deviation from suspension point.

Appendix C

CD content

A CD is attached on the inside of the back-cover of this thesis which contains the following folders:

- **Thesis** Contains this thesis as PDF.
- **Matlab** Contains the MATLAB files needed to run the experiments presented in this thesis along with instructions.
- **References** Contains the available references in PDF format.

References

V. Bertram. *Practical Ship Hydrodynamics*. Butterworth-Heinemann, 2000. ISBN 0750648511.

V. Bertram. Unmanned surface vehicles, a survey. *In Skibsteknisk Selskab*, 2008.

W. Blendermann. Parameter identification of wind loads on ships. *Wind engineering and industrial aerodynamics*, 51:339 – 351, 1994.

D. Bray. *Dynamic Positioning (Oilfield Seamanship)*. Oilfield Publications Ltd, 2003. ISBN 1902157443.

M. Breivik. Nonlinear maneuvering control of underactuated ships. Master's thesis, Norwegian University of Science and Technology, Trondheim, Norway, June 2003.

M. Breivik, V. E. Hovstein, and T. I. Fossen. Straight-line target tracking for unmanned surface vehicles. *Modeling, Identification and Control*, 29(4):131 – 149, 2008.

Cummins MerCruiser Diesel. Zeus web page, May 2010. URL `http://www.cmdmarine.com/prop/zeus.html`.

O. Doucy and F. Ghozlan. Advanced functions for USV. In *Proceedings of the ATMA International Autonomous Surface Ship Symposium, Paris, France*, 2008.

O. Faltinsen. *Sea Loads on Ships and Offshore Structures (Cambridge Ocean Technology Series)*. Cambridge University Press, 1993. ISBN 0521458706.

T. I. Fossen. *Marine Control Systems: Guidance, Navigation and Control of Ships, Rigs, and Underwater Vehicles*. Marine Cybernetics, 2002. ISBN 82-92356-00-2.

T. I. Fossen and J. P. Strand. Nonlinear passive weather optimal positioning control (WOPC) system for ships and rigs: Experimental results. *Automatica*, 37(5):701 – 715, 2001.

Furuno SC-50 Specifications, 2010.

M. Greytak and F. Hover. Exponentially stable underactuated dynamic positioning of marine vehicle. In *Dynamic Positioning Conference, Houston, Texas, USA*, 2007.

H. Halvorsen. Dynamic positioning for unmanned surface vehicles. Master's thesis, Norwegian University of Science and Technology, Trondheim, Norway, June 2008.

HamiltonJet. blue arrow web page, May 2010. URL `http://www.hamjet.co.nz/blue_arrow`.

S. F. Hoerner. *Fluid Dynamic Drag*. Hoerner Fluid Dynamics, 1965.

J. Holvik. Basics of dynamic positioning. In *Dynamic Positioning Conference, Houston, Texas, USA*, October 1998.

M. Kaltschmitt, W. Streicher, and A. Wiese. *Renewable Energy: Technology, Economics and Environment*. Springer, 2007. ISBN 3540709479.

H. K. Khalil. *Nonlinear Systems (3rd Edition)*. Prentice Hall, 2001. ISBN 0130673897.

K.-P. W. Lindegaard. *Acceleration Feedback in Dynamic Positioning*. PhD thesis, Norwegian University of Science and Technology, 2003.

Marine Systems Simulator. Marine systems simulator, Sept. 2009. URL `http://www.marinecontrol.org/download.html`.

A. Matos and N. Cruz. Positioning control of an underactuated surface vessel. In *OCEANS 2008, Quebec, Canada*, Sept 2008.

J. E. Oliver. *The Encyclopedia of World Climatology (Encyclopedia of Earth Sciences Series)*. Springer, 2005. ISBN 1402032641.

T. Perez. *Ship Motion Control: Course Keeping and Roll Stabilisation Using Rudder and Fins (Advances in Industrial Control)*. Springer, 2005. ISBN 1852339594.

T. Perez, T. I. Fossen, and A. J. Sørensen. A discussion about seakeeping and manoeuvring models for surface vessels. Technical report, Centre for Ships and Ocean Structures, NTNU, Trondheim, Norway, 2004.

K. Y. Pettersen and T. I. Fossen. Underactuated dynamic positioning of a ship - experimental results. *IEEE transactions on control systems technology*, 8(5):856 – 863, 2000.

J. A. Pinkster and U. Nienhuis. Dynamic positioning of large tankers at sea. In *Offshore Technology Conference Houston, Texas, USA*, 1986.

L. Pivano. *Thrust Estimation and Control of Marine Propellers in Four-Quadrant Operations*. PhD thesis, Norwegian University of Science and Technology, 2008.

P. W. Singer. *Wired for War: The Robotics Revolution and Conflict in the 21st Century*. Penguin Press HC, The, 2009. ISBN 1594201986.

Sleipner Motor AS Product Specifications SP 55 Si.

A. J. Sørensen. *Lecture Notes Marine Cybernetics: Modeling and Control*. Faculty of Engineering Science and Technology, NTNU, Trondheim, Norway, 2005.

The MathWorks, Inc. Real-time workshop 7.5, June 2010. URL http://www.mathworks.com/products/rtw/.

Viknes. Viknes baat og service as, May 2010. URL http://www.viknes.no.

Volvo Penta. Volvo Penta IPS web page, May 2010. URL http://www.volvopenta.com/volvopenta/norway/no-no/marine_leisure_engines/volvo_penta_ips/Pages/volvo_penta_ips.aspx.